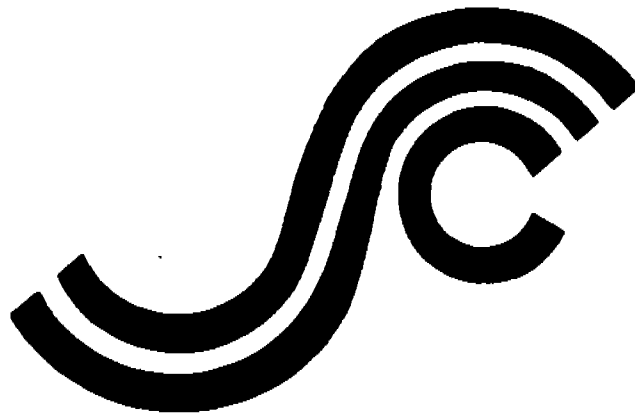


**SSC-362**

**SHIPBOARD WAVE HEIGHT  
SENSOR**



This document has been approved  
for public release and sale; its  
distribution is unlimited

**SHIP STRUCTURE COMMITTEE**

**1990**

## SHIP STRUCTURE COMMITTEE

The SHIP STRUCTURE COMMITTEE is constituted to prosecute a research program to improve the hull structures of ships and other marine structures by an extension of knowledge pertaining to design, materials, and methods of construction.

RADM J. D. Sipes, USCG, (Chairman)  
Chief, Office of Marine Safety, Security  
and Environmental Protection  
U. S. Coast Guard

Mr. Alexander Malakhoff  
Director, Structural Integrity  
Subgroup (SEA 55Y)  
Naval Sea Systems Command

Dr. Donald Liu  
Senior Vice President  
American Bureau of Shipping

Mr. H. T. Haller  
Associate Administrator for Ship-  
building and Ship Operations  
Maritime Administration

Mr. Thomas W. Allen  
Engineering Officer (N7)  
Military Sealift Command

CDR Michael K. Parmelee, USCG,  
Secretary, Ship Structure Committee  
U. S. Coast Guard

## CONTRACTING OFFICER TECHNICAL REPRESENTATIVES

Mr. William J. Siekierka  
SEA 55Y3  
Naval Sea Systems Command

Mr. Greg D. Woods  
SEA 55Y3  
Naval Sea Systems Command

## SHIP STRUCTURE SUBCOMMITTEE

The SHIP STRUCTURE SUBCOMMITTEE acts for the Ship Structure Committee on technical matters by providing technical coordination for determining the goals and objectives of the program and by evaluating and interpreting the results in terms of structural design, construction, and operation.

### AMERICAN BUREAU OF SHIPPING

Mr. Stephen G. Arntson (Chairman)  
Mr. John F. Conlon  
Mr. William Hanzalek  
Mr. Philip G. Rynn

### MILITARY SEALIFT COMMAND

Mr. Albert J. Attermeyer  
Mr. Michael W. Touma  
Mr. Jeffery E. Beach

### MARITIME ADMINISTRATION

Mr. Frederick Seibold  
Mr. Norman O. Hammer  
Mr. Chao H. Lin  
Dr. Walter M. Maclean

### NAVAL SEA SYSTEMS COMMAND

Mr. Robert A. Sielski  
Mr. Charles L. Null  
Mr. W. Thomas Packard  
Mr. Allen H. Engle

### U. S. COAST GUARD

CAPT T. E. Thompson  
CAPT Donald S. Jensen  
CDR Mark E. Noll

## SHIP STRUCTURE SUBCOMMITTEE LIAISON MEMBERS

### U. S. COAST GUARD ACADEMY

LT Bruce Mustain

### U. S. MERCHANT MARINE ACADEMY

Dr. C. B. Kim

### U. S. NAVAL ACADEMY

Dr. Ramswar Bhattacharyya

### STATE UNIVERSITY OF NEW YORK MARITIME COLLEGE

Dr. W. R. Porter

### WELDING RESEARCH COUNCIL

Dr. Martin Prager

### NATIONAL ACADEMY OF SCIENCES - MARINE BOARD

Mr. Alexander B. Stavovy

### NATIONAL ACADEMY OF SCIENCES - COMMITTEE ON MARINE STRUCTURES

Mr. Stanley G. Stiansen

### SOCIETY OF NAVAL ARCHITECTS AND MARINE ENGINEERS - HYDRODYNAMICS COMMITTEE

Dr. William Sandberg

### AMERICAN IRON AND STEEL INSTITUTE

Mr. Alexander D. Wilson

**Member Agencies:**

*United States Coast Guard  
Naval Sea Systems Command  
Maritime Administration  
American Bureau of Shipping  
Military Sealift Command*



**Ship  
Structure  
Committee**

**An Interagency Advisory Committee  
Dedicated to the Improvement of Marine Structures**

**Address Correspondence to:**

**Secretary, Ship Structure Committee  
U.S. Coast Guard (G-MTH)  
2100 Second Street S.W.  
Washington, D.C. 20593-0001  
PH: (202) 267-0003  
FAX: (202) 267-0025**

December 3, 1990

SSC-362  
SR-1314

**SHIPBOARD WAVE HEIGHT SENSOR**

The ability to obtain accurate ship motion information and to correlate these data with local sea conditions are necessary for advanced ship and ship motion research. This report describes the development, testing, and assessment of a prototype system designed to simultaneously acquire ship motion and wave height data. The integrated system includes a pulsed laser wave height sensor, vertical accelerometers, motion sensors for roll and pitch, and a data acquisition computer. The system was installed on an ocean going vessel for testing and evaluation. The reliability and accuracy of the prototype system were considered as well as the robustness or survivability of the unit under adverse sea conditions.

A handwritten signature in black ink, appearing to read 'J. D. Sipes', written over a circular stamp or mark.

**J. D. SIPES  
Rear Admiral, U.S. Coast Guard  
Chairman, Ship Structure Committee**



1. Report No. SSC-362		2. Government Accession No.		3. Recipient's Catalog No.	
4. Title and Subtitle SHIPBOARD WAVE HEIGHT SENSOR				5. Report Date November 1990	
				6. Performing Organization Code	
				8. Performing Organization Report No. SR 1314	
7. Author(s) R. Atwater				10. Work Unit No. (TRAIS)	
9. Performing Organization Name and Address Scientific Applications International Corporation 1522 Cook Place Goleta, CA 93117				11. Contract or Grant No. DTCG23-87-20033	
				13. Type of Report and Period Covered Final Report	
12. Sponsoring Agency Name and Address Ship Structure Committee U. S. Coast Guard 2100 Second Street, SW Washington, DC 20593				14. Sponsoring Agency Code G-M	
				15. Supplementary Notes This work was sponsored by the Ship Structure Committee and its member agencies.	
16. Abstract <p>This report summarizes the results of an effort to develop, test and evaluate a Pulsed Laser Based, Shipboard Mounted, Ship Motion Compensated Wave Height Sensor. This system was used in a North Atlantic run to measure sea surface waves at normal sea speed. The wave height sensor utilizes an infrared wave surface range sensor coupled with a vertical accelerometer and pitch and roll sensors. The prototype system was evaluated for measurement accuracy and reliability as well as ruggedness and survivability in elevated sea state conditions. Lack of ground truth precluded a comprehensive qualitative evaluation of overall performance. Data drop outs were experienced when operating in elevated seas thereby making further work necessary on the sensor and on the data processing software. Prototype system characteristics, signal processing flow chart and analyzed data are presented.</p> <p>As an adjunct to the development of the wave height sensor, the Ship Structure Committee and the Society of Naval Architects and Marine Engineers cosponsored a project at the University of Michigan to investigate through model testing the influence of ship generated waves in front of the bow. The report of this study is included as Appendix D.</p>					
17. Key Words Ship Motion                      Sea State Measure Ship Response                    Ship Accelerations Wave Height                      Roll Pulsed Laser Sensor          Pitch Bow Displacement              Heave			18. Distribution Statement Available to the public from: National Technical Information Service, Springfield, VA 22161 or Marine Technical Information Facility, National Maritime Research Center, Kings Point, NY 10024-1699		
19. Security Classif. (of this report) UNCLASSIFIED		20. Security Classif. (of this page) UNCLASSIFIED		21. No. of Pages 98	22. Price

# METRIC CONVERSION FACTORS

## Approximate Conversions to Metric Measures

Symbol	When You Know	Multiply by	To Find	Symbol
--------	---------------	-------------	---------	--------

### LENGTH

in	inches	2.5	centimeters	cm
ft	feet	30	centimeters	cm
yd	yards	0.9	meters	m
mi	miles	1.6	kilometers	km

### AREA

in <sup>2</sup>	square inches	6.5	square centimeters	cm <sup>2</sup>
ft <sup>2</sup>	square feet	0.09	square meters	m <sup>2</sup>
yd <sup>2</sup>	square yards	0.8	square meters	m <sup>2</sup>
mi <sup>2</sup>	square miles	2.6	square kilometers	km <sup>2</sup>
	acres	0.4	hectares	ha

### MASS (weight)

oz	ounces	28	grams	g
lb	pounds	0.45	kilograms	kg
	short tons (2000 lb)	0.9	tonnes	t

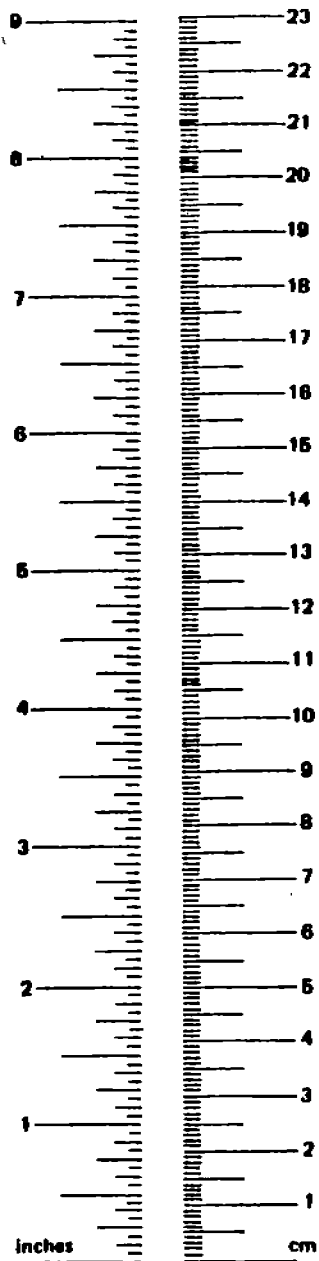
### VOLUME

tp	teaspoons	5	milliliters	ml
Tbsp	tablespoons	15	milliliters	ml
fl oz	fluid ounces	30	milliliters	ml
c	cups	0.24	liters	l
pt	pints	0.47	liters	l
qt	quarts	0.96	liters	l
gal	gallons	3.8	liters	l
ft <sup>3</sup>	cubic feet	0.03	cubic meters	m <sup>3</sup>
yd <sup>3</sup>	cubic yards	0.76	cubic meters	m <sup>3</sup>

### TEMPERATURE (exact)

°F	Fahrenheit temperature	5/9 (after subtracting 32)	Celsius temperature	°C
----	------------------------	----------------------------	---------------------	----

\* 1 in. = 2.54 cm (exactly). For other exact conversions and more detail tables see NBS Misc. Publ. 286, Units of Weight and Measure. Price \$2.25 SD Catalog No. C13 10 286.



## Approximate Conversions from Metric Measures

Symbol	When You Know	Multiply by	To Find	Symbol
--------	---------------	-------------	---------	--------

### LENGTH

mm	millimeters	0.04	inches	in
cm	centimeters	0.4	inches	in
m	meters	3.3	feet	ft
m	meters	1.1	yards	yd
km	kilometers	0.6	miles	mi

### AREA

cm <sup>2</sup>	square centimeters	0.16	square inches	in <sup>2</sup>
m <sup>2</sup>	square meters	1.2	square yards	yd <sup>2</sup>
km <sup>2</sup>	square kilometers	0.4	square miles	mi <sup>2</sup>
ha	hectares (10,000 m <sup>2</sup> )	2.5	acres	

### MASS (weight)

g	grams	0.035	ounces	oz
kg	kilograms	2.2	pounds	lb
t	tonnes (1000 kg)	1.1	short tons	

### VOLUME

ml	milliliters	0.03	fluid ounces	fl oz
l	liters	2.1	pints	pt
l	liters	1.06	quarts	qt
l	liters	0.26	gallons	gal
m <sup>3</sup>	cubic meters	36	cubic feet	ft <sup>3</sup>
m <sup>3</sup>	cubic meters	1.3	cubic yards	yd <sup>3</sup>

### TEMPERATURE (exact)

°C	Celsius temperature	9/5 (then add 32)	Fahrenheit temperature	°F
----	---------------------	-------------------	------------------------	----

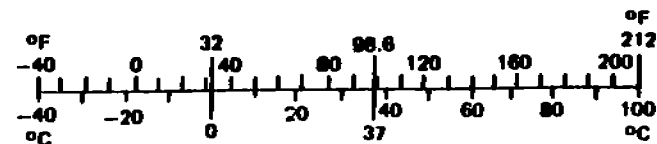


## TABLE OF CONTENTS

<u>SECTION</u>	<u>TITLE</u>	<u>PAGE</u>
1.0	SUMMARY . . . . .	1
1.1	Measurement Reliability/Accuracy . . . . .	1
1.2	System Ruggedness/Survivability . . . . .	4
2.0	BACKGROUND . . . . .	5
3.0	PROGRAM OVERVIEW . . . . .	5
3.1	Phase I . . . . .	6
3.2	Phase II . . . . .	7
4.0	PROTOTYPE SYSTEM . . . . .	9
4.1	Bow Mounted Sensors . . . . .	11
4.2	Gyro Pitch/Roll Sensors . . . . .	11
4.3	A/D Conversion System . . . . .	11
4.4	Computer System and Software . . . . .	14
5.0	PERFORMANCE EVALUATION . . . . .	14
5.1	Angle Measurement Subsystem Performance . . . . .	16
5.2	Vertical Acceleration Sensor Subsystem Performance . . . . .	24
5.3	Wave Surface Range Sensor Performance Evaluation . . . . .	27
	5.3.1 Data Drop Out Detection Algorithm . . . . .	29
	5.3.2 Wave Surface Range Reconstruction Algorithm . . . . .	57
5.4	Overall Performance . . . . .	59
6.0	RECOMMENDATIONS . . . . .	61

REFERENCES

APPENDICES

## LIST OF TABLES

<u>TABLE #</u>	<u>TITLE</u>	<u>PAGE</u>
1	Gyro/Pendulum Pitch Roll Sensor Comparison . . . . .	17
2	Drop Out Detection Statistics . . . . .	36
3	Comparison with NOAA Buoy #41002 Data . . . . .	60

## LIST OF FIGURES

<u>FIGURE #</u>	<u>TITLE</u>	<u>PAGE</u>
1	USNS DENEbola	2
2	Wave Sensor Installed on USNS DENEbola	8
3	Block Diagram - Prototype Shipboard Waveheight System	10
4	EMI Wave Gauge Sensor Assembly	11
5	SSC Sea Trial Vessel - USNS DENEbola (SL-7)	13
6	Overall Flowchart for Signal Processing	15
7	Gyro/Pendulum Comparison File: 131800.DAT	18
8	Gyro/Pendulum Comparison File: 16220.DAT	19
9	Gyro/Pendulum Comparison File: 083801.DAT	20
10	Gyro/Pendulum Comparison File: @16Hz0.DAT	21
11	Gyro/Pendulum Comparison File: 17550.DAT	22
12	Parameter Data Using Pendulum Sensors File: 080301.DAT	25
13	Parameter Data Using Pendulum Sensors File: 083801.DAT	26
14	Flat Spot Detection/Reconstruction	30
15	Pitch and EMI Range File: 083801.DAT	31
16	Pitch and EMI Range File: @16Hz0.DAT	32
17	Pitch and EMI Range File: 12590.DAT	33
18	Pitch and EMI Range File: 134200.DAT	34
19	Drop Out Severity vs. Pitch	37
20	Sea Trial Data File: 131800.DAT	38
21	Sea Trial Data File: 16220.DAT	39
22	Sea Trial Data File: 13110.DAT	40
23	Sea Trial Data File: 165800.DAT	41
24	Sea Trial Data File: 17480.DAT	42
25	Sea Trial Data File: 12050.DAT	43
26	Sea Trial Data File: 12590.DAT	44
27	Sea Trial Data File: 17180.DAT	45
28	Sea Trial Data File: 134200.DAT	46
29	Sea Trial Data File: 14030.DAT	47
30	Sea Trial Data File: 083801.DAT	48
31	Sea Trial Data File: 08220.DAT	49
32	Sea Trial Data File: @16Hz0.DAT	50
33	Sea Trial Data File: 08380.DAT	51
34	Sea Trial Data File: 17550.DAT	52
35	Parameter Time Series (Non-Flat Spot Reconstructed) File: 131800.DAT	53
36	Parameter Time Series (Non-Flat Spot Reconstructed) File: 083801.DAT	54
37	Parameter Time Series (Non-Flat Spot Reconstructed) File: @16Hz0.DAT	55
38	Parameter Time Series (Non-Flat Spot Reconstructed) File: 17550.DAT	56

## 1.0 SUMMARY

This report summarizes the development and evaluation of a pulsed laser wave height sensor suitable for use on an underway vessel operating in an elevated seaway. A prototype measurement system based on an infrared wave surface range sensor, coupled with a vertical accelerometer and pitch and roll sensors was evaluated while the system was mounted on the bow of the USNS DENEbola (SL-7) en route from Bremerhaven, Germany to Savannah, Georgia during October 1988. Figure 1 shows the sensor and DENEbola operating in sea state 4 on October 23rd. Data obtained during this sea trial are discussed and provide the foundation for recommended future work.

The prototype system was evaluated from two points of view: (1) accuracy and reliability of wave height measurements; and (2) ruggedness/survivability under elevated sea state conditions. The issue of wave field contamination from vessel-generated waves was considered analytically during the initial design phase.

### 1.1 Measurement Reliability/Accuracy

System performance was evaluated in terms of three major subsystems: (1) the gyro and pendulum pitch and roll sensors; (2) the vertical acceleration sensor and vertical bow displacement calculations; and (3) the infrared wave surface range sensor. The pendulum pitch and roll sensor data were found to contain a significant response to the vertical acceleration of the vessel. For larger accelerations, as much as a degree or two was added to the measured pendulum pitch and roll angles when compared with the more accurate gyro sensor data. The effects of the errors in angle measurements, while not significant for the encountered sea states, will be more severe for higher seas (larger vertical accelerations) and may compromise the calculated wave heights when pitch and roll angles are more extreme.

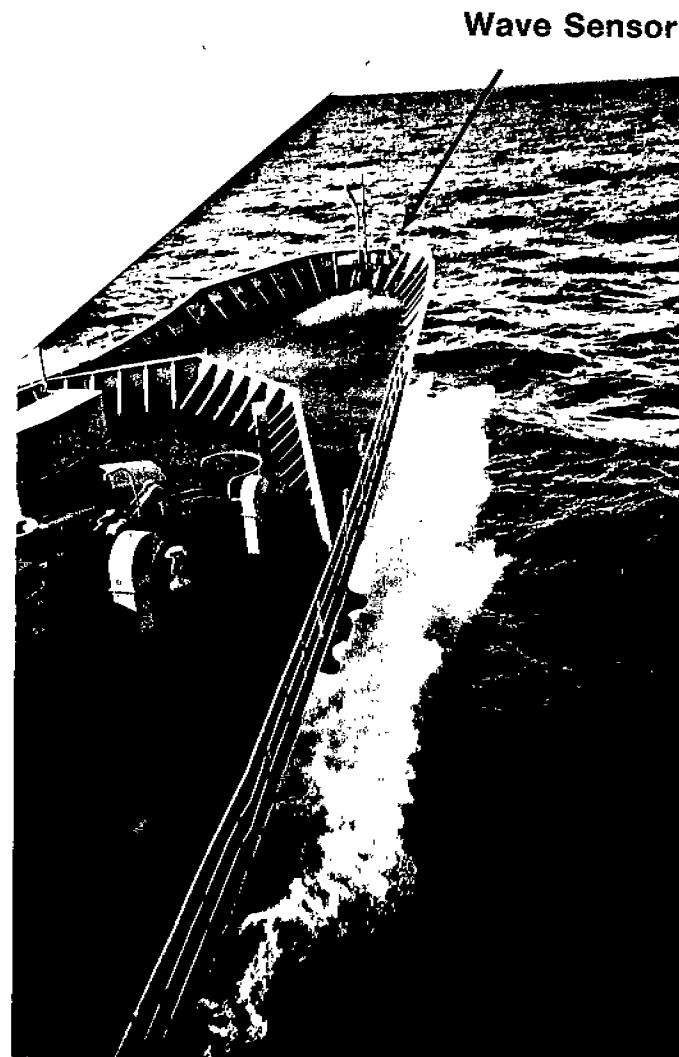
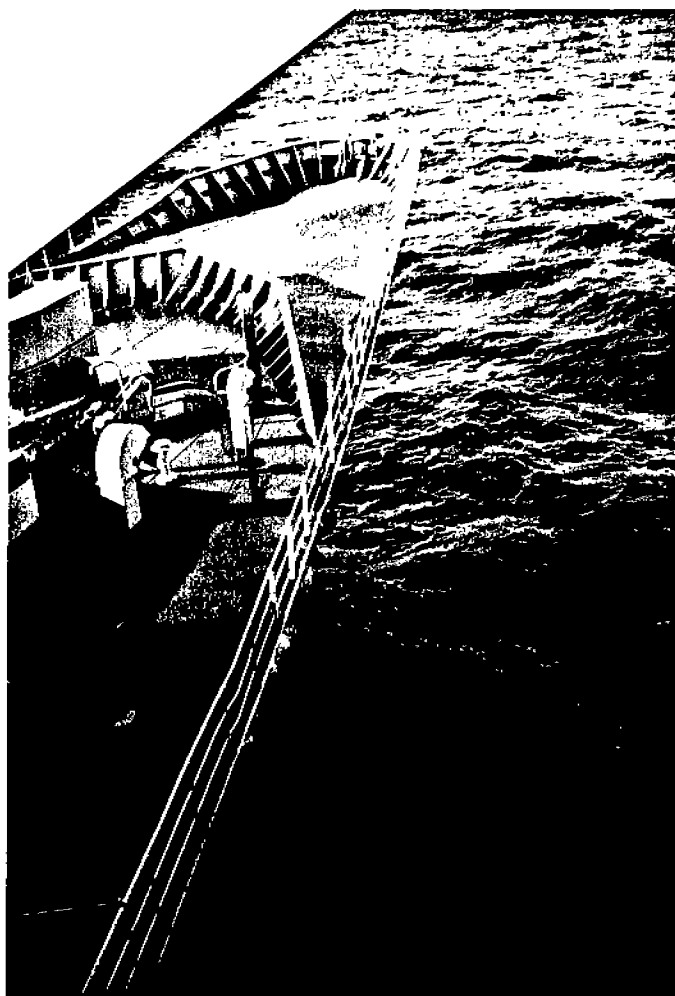


**Figure 1**  
**USNS DENEbola**  
**1346 October 23, 1988**  
**7.3 feet Significant Wave Height**

The vertical accelerometer and bow displacement calculation algorithm performed well; no significant errors related to data sampling, filtering or integration were evident in the computed bow displacement data.

The infrared laser wave sensor exhibited a response problem under certain sea state conditions. As discussed in Section 5.3, the signal from this sensor would intermittently "hold" at a constant value for intervals of a few seconds during conditions of high pitch motion. The onset of these "data drop outs" occurred shortly after the minimums and maximums of the pitch signal. Examination of the data indicates that the severity of the drop out problem is dependent on both the amplitude and period of the pitch motion. A data reconstruction algorithm was developed that appears to adequately interpolate through the data drop out intervals. By eliminating the drop outs, the reconstructed time series, associated spectra, and computed statistics are consistent with visual observations, model data and buoy measurements.

The "Recommendations" section of this report provides suggestions for further evaluation and possibly limiting the effects of the data drop outs. Such possibilities include (1) sensor malfunction under the more extreme sea-states; (2) acquiring "raw" sensor data instead of data which has been screened by the logic circuitry of the wave gauge; and (3) further investigating whether the cause of the drop outs is "bow splash" by obtaining data while the sensor is temporarily mounted away from the bow.

The lack of ground truth information for the prototype sea trials precludes a comprehensive quantitative evaluation of overall performance of the wave height measurement system. In this regard, the results of the sea trials must be considered somewhat inconclusive, particularly with respect to the ability of the infrared laser to operate in the presence of vessel induced waves or spray. The data drop outs limit the reliable performance envelope of the prototype. However, revisions and improvements to the electronic signal rejection logic and data reconstruction algorithms may overcome these limitations.

An improved understanding of the drop out phenomena combined with a more rigorous ground truth experiment will provide a definitive evaluation of the operational utility of the pulsed laser wave height system for underway measurements.

## 1.2 System Ruggedness/Survivability

The prototype system consists of three physically separated groups of components:

1. The wave gauge, vertical accelerometer and pendulum sensors were packaged in an explosion proof housing mounted at the bow of the DENEbola. No damage occurred to any of these sensors or their mountings during either leg of the voyage. The system was installed but not operating during the eastward crossing, and was operating continuously during the westward crossing. Elevated sea states, including "green water" over the bow, were encountered during the eastward crossing. Sea states were milder during the westward crossing.
2. The gyro-type angle sensors were installed in the wheel house. No problems were experienced by these sensors throughout the sea trials.
3. The data acquisition computer system performed without any major problems. The system operator's notes report occasional questionable computer performance, and a jammed printer ribbon, but these are deemed minor "inconveniences" rather than ruggedness/survivability problems. The uninterruptable power supply (UPS) for the computer was not functional during the sea trials. The UPS was stored in the wheelhouse near an open door during the eastward leg of the voyage and may have been damaged by exposure to salt air during this time.

## 2.0 BACKGROUND

An accurate analysis of full scale ship performance is dependent upon a reliable measure of the encountered seaway. Researchers have repeatedly been frustrated by the lack of a reliable and accurate sensor suitable for underway measurements. As part of the SL-7 and the STEWART J. CORT research programs, the Ship Structure Committee (SSC) and the US Coast Guard have evaluated a variety of shipboard wave height sensors. Based upon the results of these evaluations, Dalzell (Ref 1, 2) concluded that neither the Tucker pressure meter nor the OWHS radar system were suitable for reliable measurements in an elevated seaway. The recommendations presented in SSC Report #313 (Ref 3) indicated that the development of an improved shipboard wave height measurement system was critical to future full scale vessel research. Subsequently, the NMRC (Ref 4) analyzed the system requirements and application of a pulsed laser for underway measurements. The results of the NMRC work provided the impetus and direction for the current shipboard wave height sensor development program.

A variety of problems have been encountered with previous shipboard wave measurement systems. The Tucker wave meter has been used relatively successfully on stationary weather ships; however, because of non-linearities related to vessel speed, it is not suitable for underway measurements. Narrow beam radar altimeters have suffered structural damage when mounted on exposed bow locations. Moving the sensor to more protected locations compounds the problem of removing the ship motion effects. Also, radar, microwave and sonic sensors are relatively wide aperture sensors that loose definition of the individual encountered wave shape. Previous investigators also reported considerable difficulty eliminating noise and drift errors from the double integration of accelerometer data used to compensate for vessel motions.

## 3.0 PROGRAM OVERVIEW

The objective of this program was to develop, test and evaluate a pulsed laser wave height system suitable for installation on the bow of an ocean-going vessel. The program consisted of two phases as shown below:

## PHASE I

- o Analyze Sources of Error
- o Simulate System Performance
- o Breadboard System
- o Breadboard Sea Trial
- o Develop Prototype Design

## PHASE II

- o Prototypes System Development
- o Ocean Test
- o Data Analysis

### 3.1 Phase I

The Phase I objectives were satisfied through a combination of analytical studies, computer simulations and breadboard experiment. The primary issues considered during Phase I were the effect of wave contamination, laser inclination, sensor stabilization and accelerometer integration errors. The results of these investigations were used to configure a breadboard system demonstration and refine the prototype system design. A complete discussion of the Phase I, work is presented in the SAIC Phase I report (Ref 5). The significant conclusions derived from Phase I are summarized below.

- o Wave contamination is a potential problem for any shipboard sensor. At elevated sea states, vessel generated waves may reduce the measurement accuracy.
- o Based upon breadboard experiments, the pulsed laser sensor should operate satisfactorily at inclinations up to 15 degrees from vertical.

- o For the vessel motions typical of the SL-7 in sea states  $\leq 7$  a gimbaled sensor platform is not required.
- o The acceleration should be sampled at  $\geq 16$  Hz and digitally integrated to minimize integration errors and preserve phase coherence.

### 3.2 Phase II

The prototype wave measurement system design developed during Phase I was built and tested during Phase II. The system includes a pulsed laser wave height sensor combined with appropriate vessel motion sensors and a real time computer data acquisition and display system. An EMI pulsed laser wave height sensor mounted in a ruggedized explosion proof housing was selected for the prototype. This sensor has been successfully used on fixed offshore platforms since 1982. Selecting an existing and proven sensor sub-system minimized the development effort required to validate the application of infrared laser technology to the shipboard wave measurement requirement.

Upon completion of laboratory testing, the prototype system was installed on the bow of the USNS DENEbola (Figure 2) for test and evaluation during the October 1988 Atlantic Crossings. The ruggedness of the wave sensor and installation were verified on the east bound crossing when "green water" was taken over the bow. Data acquisition was successfully conducted during the west bound trip.

Approximately 60 wave measurement data sets were acquired during the voyage from Bremerhaven, Germany to Savannah, Georgia. Each data set included measurements of wave height along with vessel motions. Visual observations of wind and wave conditions were also recorded. Measured ground truth data was limited to a NOAA weather buoy located approximately 250 miles east of Charleston, SC.

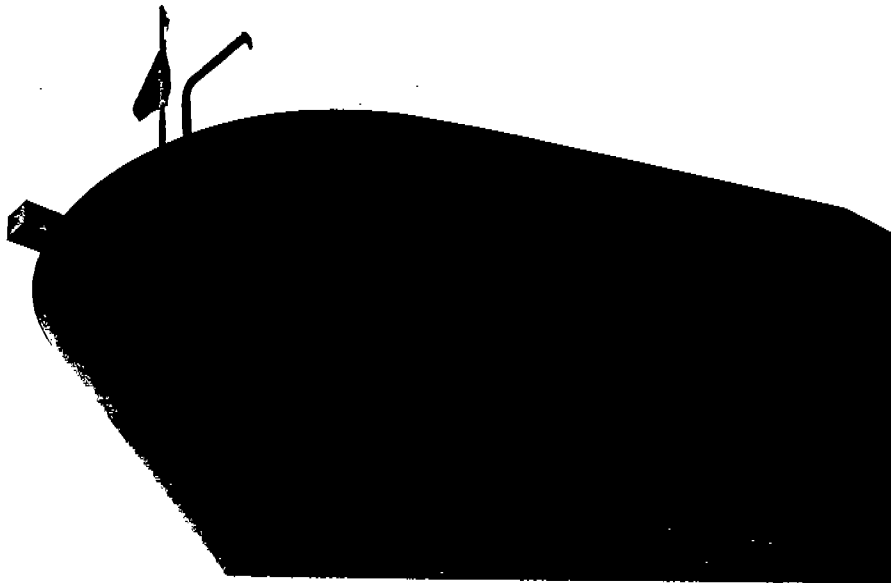
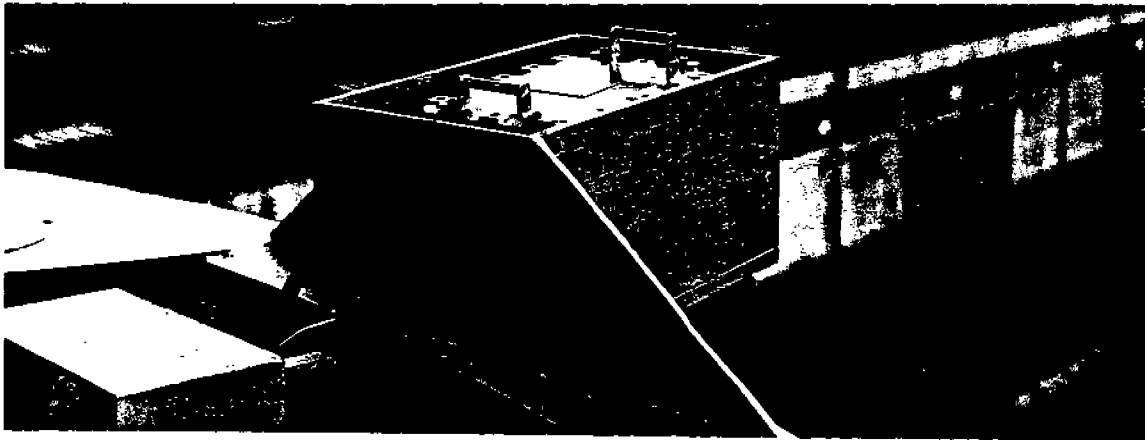
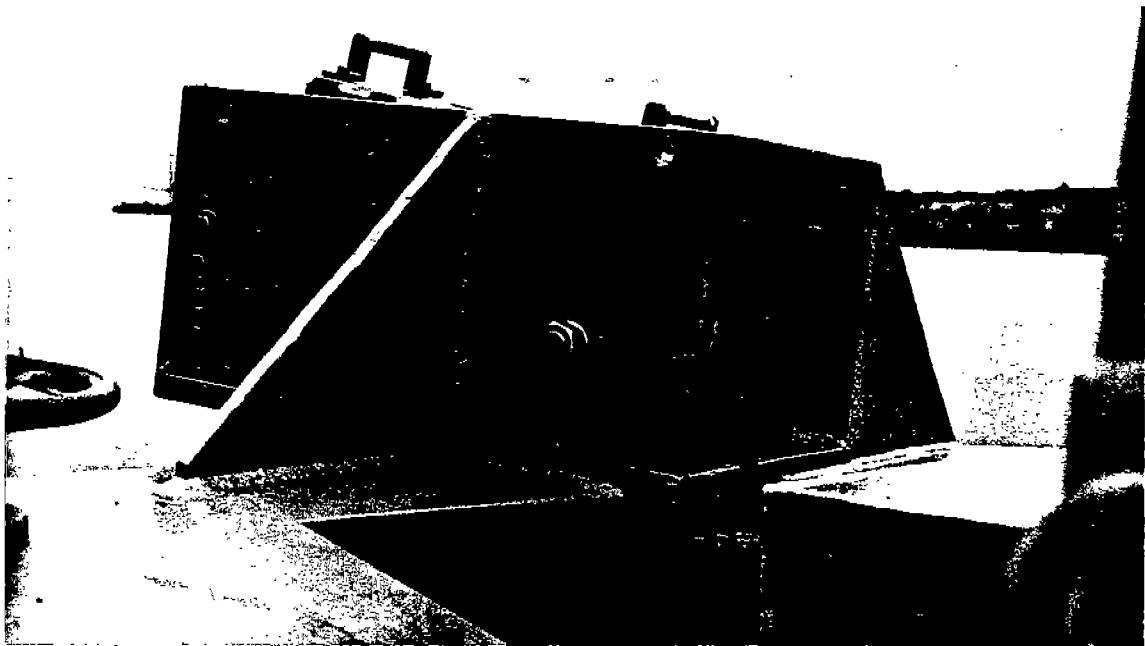


**Figure 2**  
**Wave Sensor Installed on USNS DENEbola**

Data obtained during the October sea-trials from the underway wave measurement system has been analyzed relative to sub-system performance and overall wave measurement capability. Because of the limited ground truth, and relatively mild conditions, the sea trial results are not totally conclusive. As anticipated, wave spray adversely effect the laser beam. Data drop outs from spray or excessive sensor inclinations are partially overcome with an adaptive data recovery algorithm. The processed data with or without occasional drop outs compares favorably with the observed wave conditions.

With additional work to minimize data dropouts and/or adaptively interpret between good data, the pulsed infrared laser will provide a robust sensor for underway wave measurements in an elevated seaway. The following sections of this report discuss the prototype wave measuring system and the results of the October 1988 sea trials.

#### 4.0 PROTOTYPE SYSTEM

The initial proof-of-concept "breadboard" system design was tested in the Santa Barbara channel as described in the SAIC "Phase I Report, Shipboard Wave Height Sensor" (Ref 5). The Phase I Report summarized the objectives and environment considerations for the system, and described the breadboard system used to test the sensor and processing components of the to-be-built prototype system. The results of the breadboard system trial were judged encouraging, within the limitations of the low sea state in effect when the test was conducted.

The prototype system block diagram is presented in Figure 3. This system can be divided into four major subsystems: (1) a sensor subsystem containing the EMI infrared laser wave surface range sensor, vertical accelerometer, and pendulum-type pitch and roll sensors; (2) separately positioned gyro-type pitch and roll sensors; (3) an analog-to-digital conversion subsystem; and (4) a PC/AT compatible computer system with attached monochrome display and hardcopy printer. These subsystems are described in the following sections.

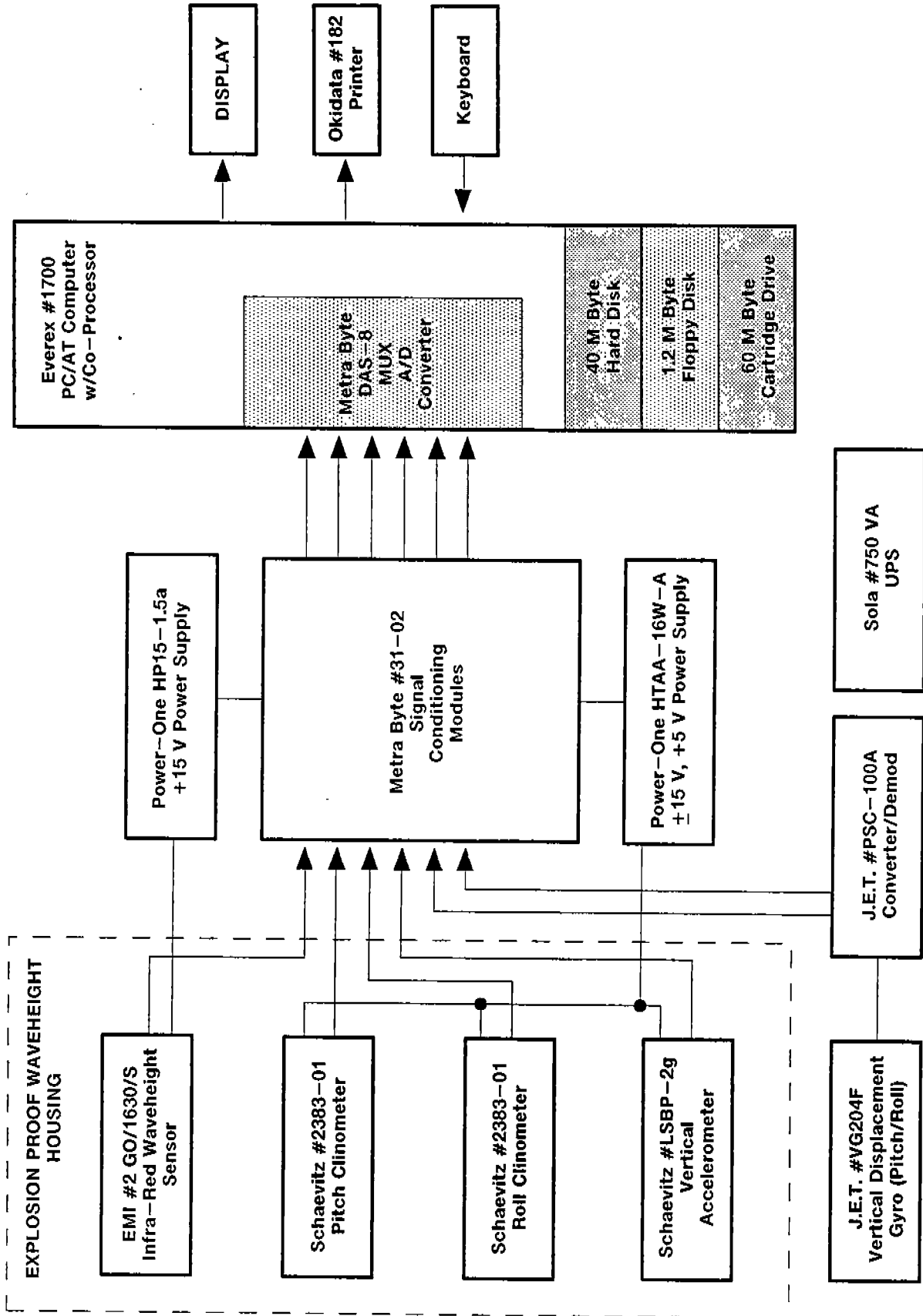


Figure 3  
 Block Diagram - Prototype Shipboard Waveheight System

#### 4.1 Bow Mounted Sensors

Figure 4 shows the EMI wave gauge sensor assembly. The pitch/roll vertical accelerometer and pendulum sensors were mounted inside the wave sensor an explosion proof steel housing. The explosion proof housing was bolted to a steel mounting tray and the mounting tray was bolted to a steel housing "box". At installation, the housing box was welded to the bow plate of the USNS DENEbola. The downward look angle of the wave sensor was variable by adjustment of the bolts fastening the mounting tray to the housing box. The initial angle was set at 12 degrees and was not changed during the sea trials. The USNS DENEbola geometry installation is shown in Figure 5.

A waterproof cable provided power to the EMI wave sensor and vertical accelerometer from DC power supplies in the wheelhouse , and returned the sensor signals to the A/D conversion system mounted on the backplane of the computer.

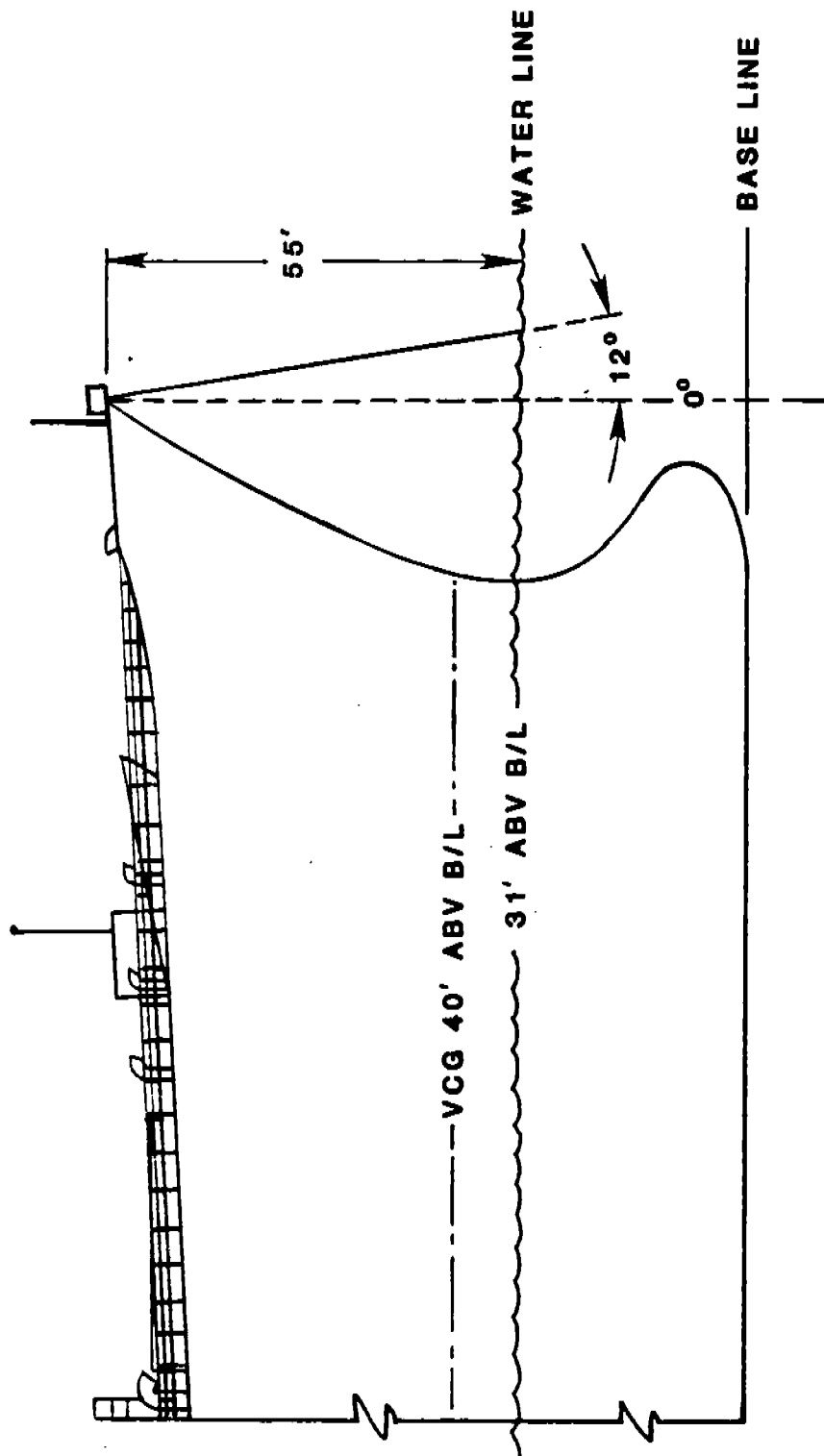
#### 4.2 Gyro Pitch/Roll Sensors

The gyro pitch/roll sensors were mounted in the wheelhouse in a vibration damped housing; signals from these sensors were cabled to the A/D converter.

#### 4.3 A/D Conversion System

The analog sensor signals were converted to digital form by a 12 bit A/D converter mounted on the backplane of the computer. Signal conversions were rapidly clocked and multiplexed by the A/D subsystem so that inter-channel timing skew was minimized. The interval between A/D scans was set to an operator-determined sample rate controlled by a software timing loop in the data acquisition program. Scan intervals of 8 and 16 Hz were used during the sea trials.





LENGTH OVERALL 948'



Figure 5  
 SSC Sea Trial Vessel  
 USNS DENEbola (SL-7)

#### 4.4 Computer System and Software

The real time sensor data acquired by the A/D conversion system was processed by a computer program running on the Everex 1700 PC/AT compatible computer system. This computer has dual clock frequency capability, switchable to 8 or 12 MHz. The 12 MHz setting was used during the sea trials.

The overall logic of the real time processing program is shown in Figure 6. As shown by this figure, the processing sequence consisted of several steps: (1) A/D conversion and scaling to physical units; (2) correction of measured acceleration and wave surface range to the vertical; (3) double integration of the corrected acceleration to calculate bow displacement; (4) decimation from the 8 or 16 Hz sample frequency to the 2 Hz processing frequency; (5) wave height computation (wave range less bow elevation); (6) statistics computation (min, max, mean, RMS, zero crossing period and max peak-to-peak cycle); and (6) data display (raw time series, processed time series, spectra, and statistics time histories). Appendix A lists the processing modules which perform the functions described above and details the double integration/filtering scheme ('TRANSFORM' flowchart) used to compute bow displacement from vertical acceleration.

In addition to the real time processing and display sequence listed above, at the operator's discretion both raw and/or processed data could be stored on the hard disc for subsequent re-processing. A tabulation of data recorded during the October 1988 sea trials is found in Appendix B; this appendix also describes the format of the data records.

#### 5.0 PERFORMANCE EVALUATION

This section of the report discusses the performance of the prototype wave height measurement system in terms of the three major subsystems: the angular position subsystems; the heave measurement subsystem; and the wave surface range measurement subsystem. The overall performance of the system in terms of the accuracy and reliability of the under way wave height measurements is discussed in paragraph 5.4.

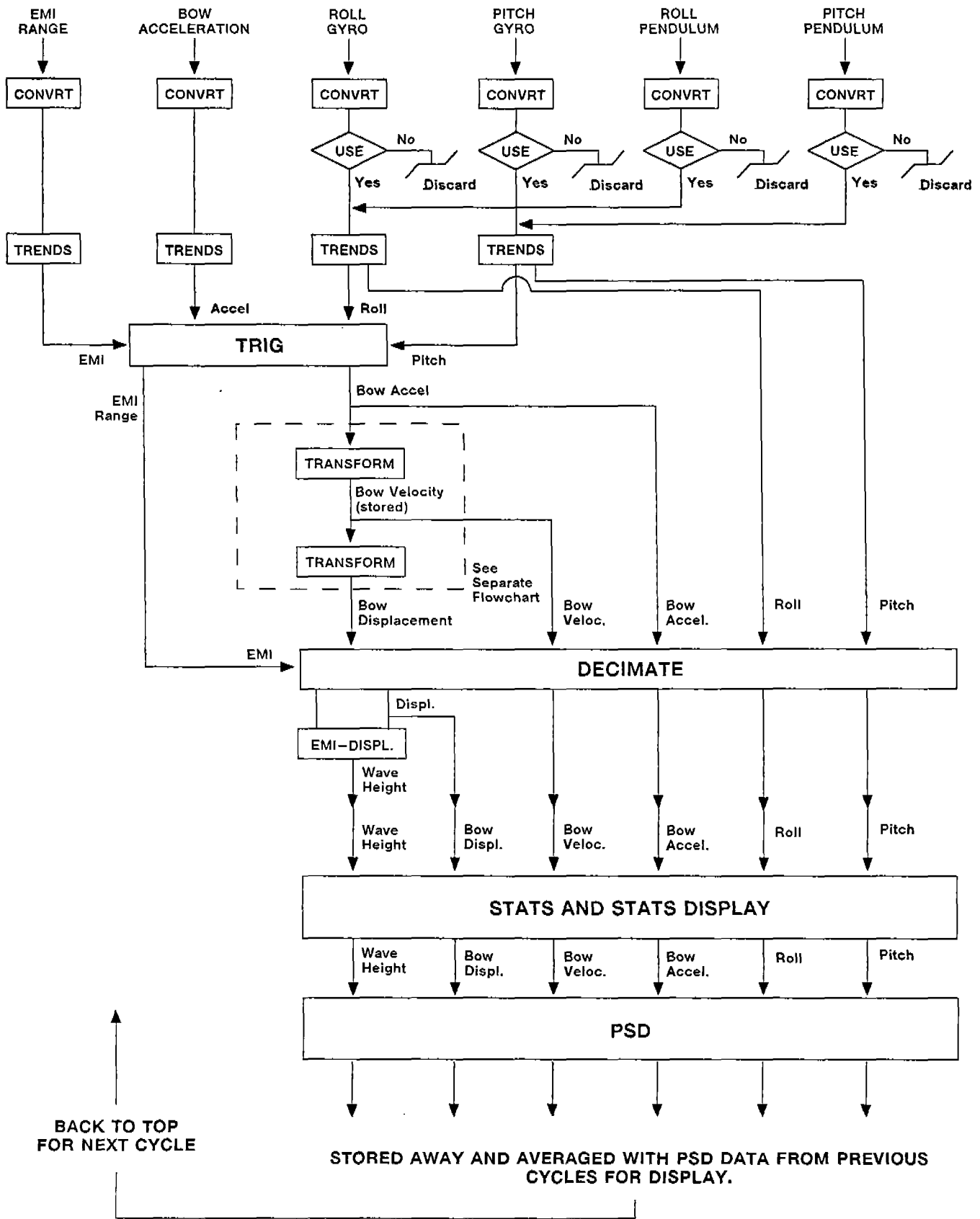


Figure 6  
Overall Flowchart for Signal Processing

The data discussed in this section were obtained over the time period from 19-25 October, 1988 the USNS DENEbola (SL-7), was en route from Bremerhaven, Germany to Savannah, Georgia, crossing the Atlantic at a heading of about 230-265 degrees at speeds ranging from under 10 knots to over 20 knots. Over 60 data files containing the raw sensor data were recorded during the sea trials. Each file contains the unprocessed output of the A/D converter for the pendulum and gyro pitch and roll sensors, the vertical accelerometer, and the EMI wave gauge. These files are listed in Appendix B. A representative sample of the sea trial data, covering the range of pitch, roll, acceleration, and wave height measurements was reviewed while preparing this section of the report. Selected records were re-processed from the recorded raw data using a modified version of the real time software. As discussed below, the modifications included: (1) a geometric correction for the tilt of the laser/accelerometer sensor; and (2) an algorithm to detect "data drop-outs" in the wave gauge signal and to estimate the true wave surface range during periods of missing range data.

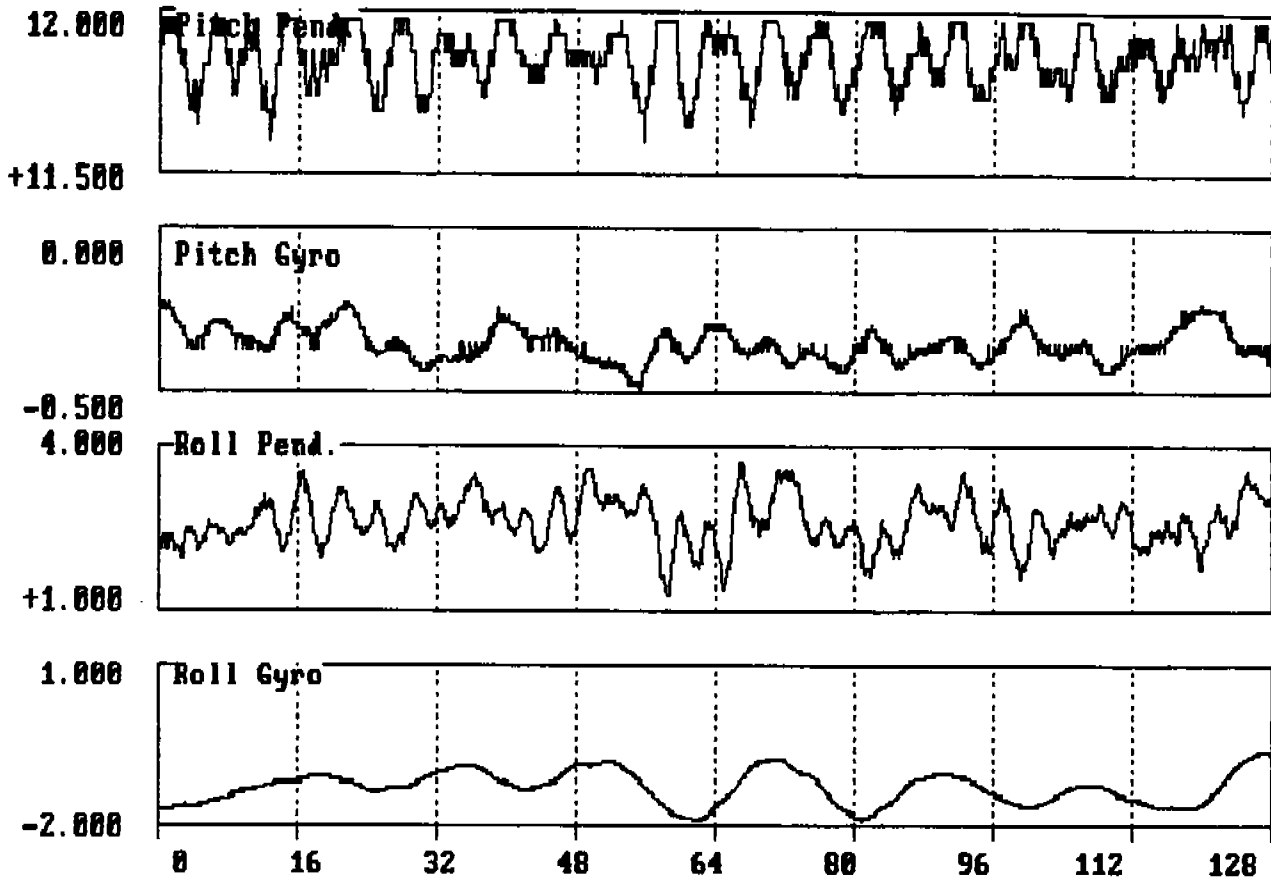
### 5.1 Angle Measurement Subsystem Performance

Pitch and roll angles were measured by two subsystems: (1) a gyro vertical reference unit mounted in the wheel house; and (2) pendulum-type sensors mounted at the bow the EMI wave gauge housing. Comparison time series and spectra are included for these two sensors at several pitch and roll magnitudes, representative of the range of values encountered during the sea trials.

The data presented in Table 1 and in Figures 7 through 11, summarizes the gyro/pendulum sensor comparisons. Table 1 is a tabulation of the roll and pitch amplitudes and periods for five data records. In Figures 7 through 11, a 128 second time series of the corresponding data is plotted along with the associated frequency spectra (Hz).

**TABLE 1**  
**GYRO/PENDULUM PITCH ROLL SENSOR COMPARISON**

Sensor	RMS Double Amplitude (degrees)	Significant Period (seconds)	Data File ID	Reference Data Plots
Roll gyro Roll pend Pitch gyro Pitch pend Bow accel	0.6 0.6 0.2 0.1 <0.05 g	15.7 4.7 10.2 3.9 7.2	131800 10/25/88 13:21:51	Figure 7
Roll gyro Roll pend Pitch gyro Pitch pend Bow accel	4.0 4.2 0.5 0.4 0.05 g	19.7 18.5 16.0 7.9 10.5	16220 10/23/88 16:22:34	Figure 8
Roll gyro Roll pend Pitch gyro Pitch pend Bow accel	1.5 3.4 0.7 1.4 0.15 g	15.3 9.3 8.1 7.1 7.4	083801 10/20/88 14:54:47	Figure 9
Roll gyro Roll pend Pitch gyro Pitch pend Bow accel	2.3 4.3 1.1 2.3 0.25 g	15.6 8.5 8.0 7.1 7.4	@16Hz0 10/20/88 14:54:47	Figure 10
Roll gyro Roll pend Pitch gyro Pitch pend Bow accel	1.3 2.6 1.4 2.1 0.20 g	15.5 8.8 9.3 8.3 8.3	17550 10/19/88 17:55:31	Figure 11



GYRO

PENDULUM

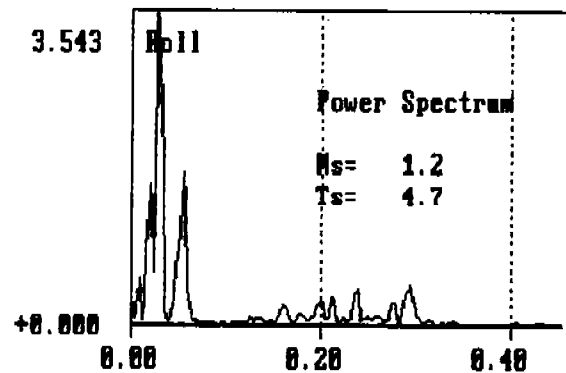
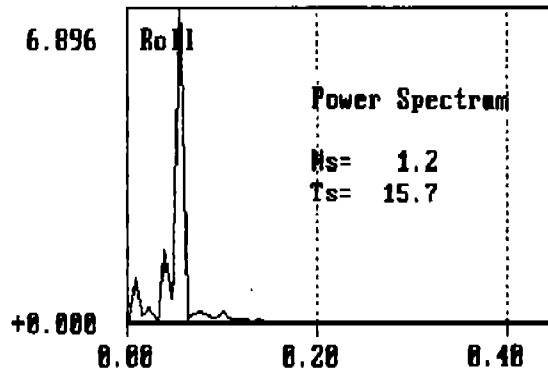
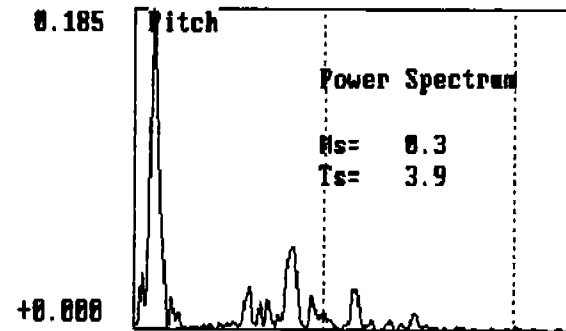
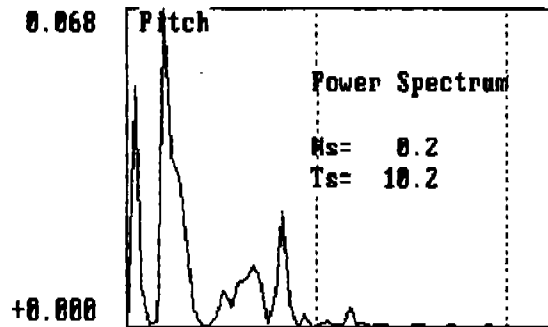
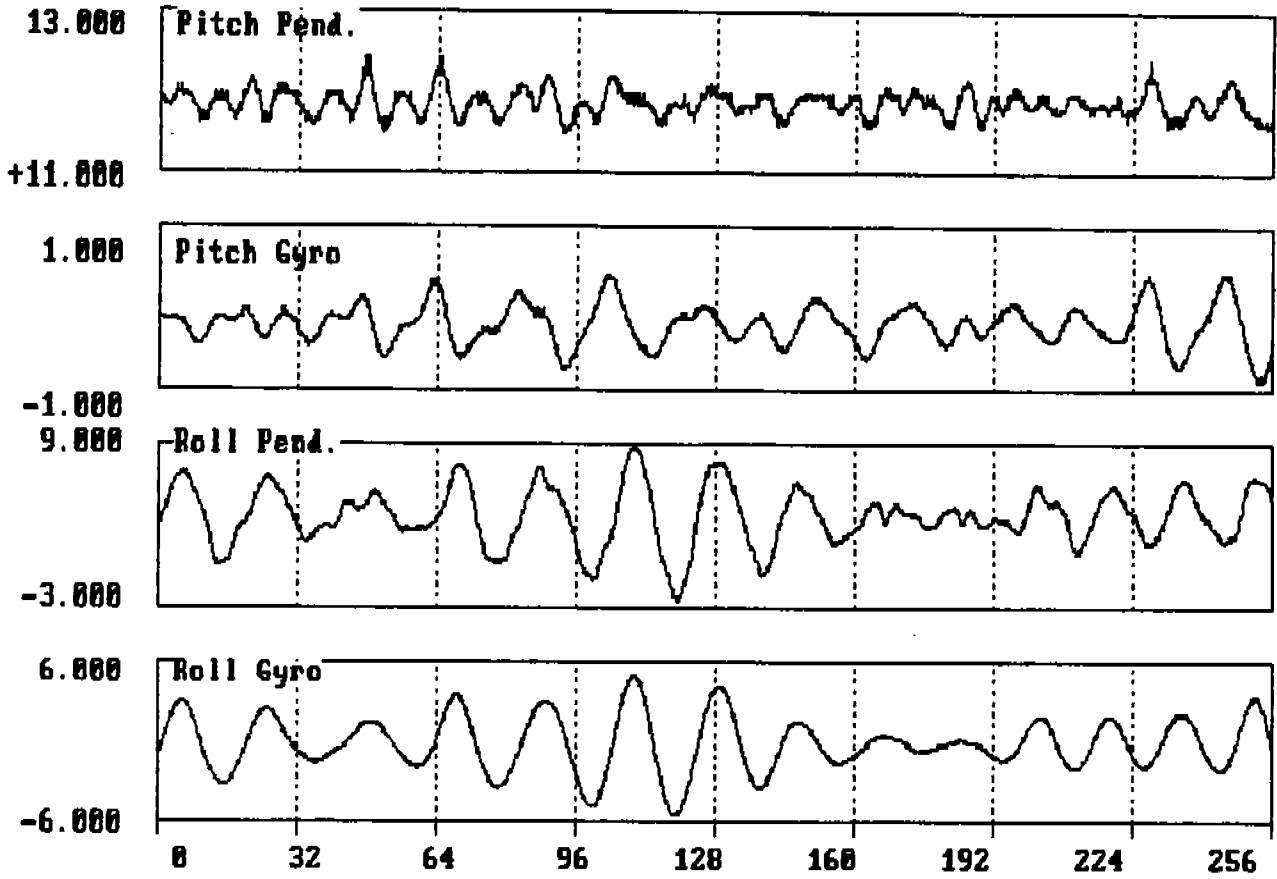


Figure 7  
GYRO/PENDULUM COMPARISON  
File: 131800.DAT  
Time: 25 OCT 88 - 13:21:51



GYRO

PENDULUM

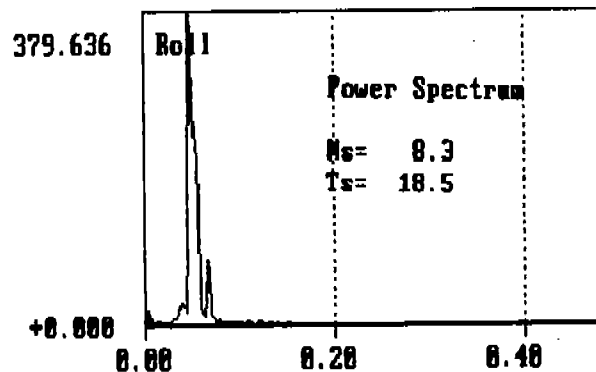
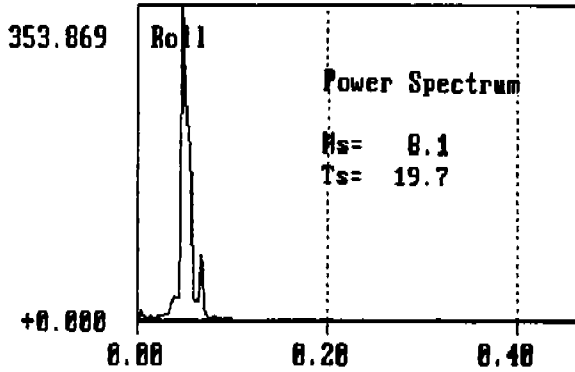
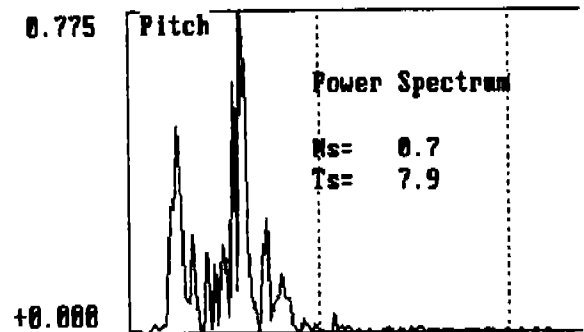
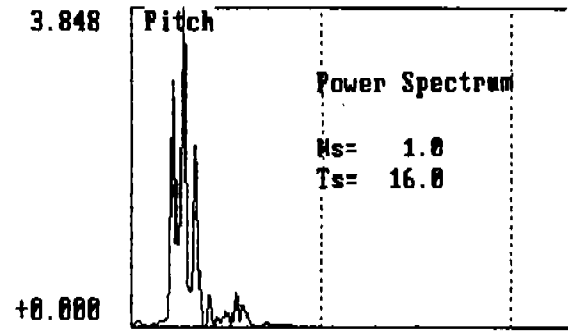
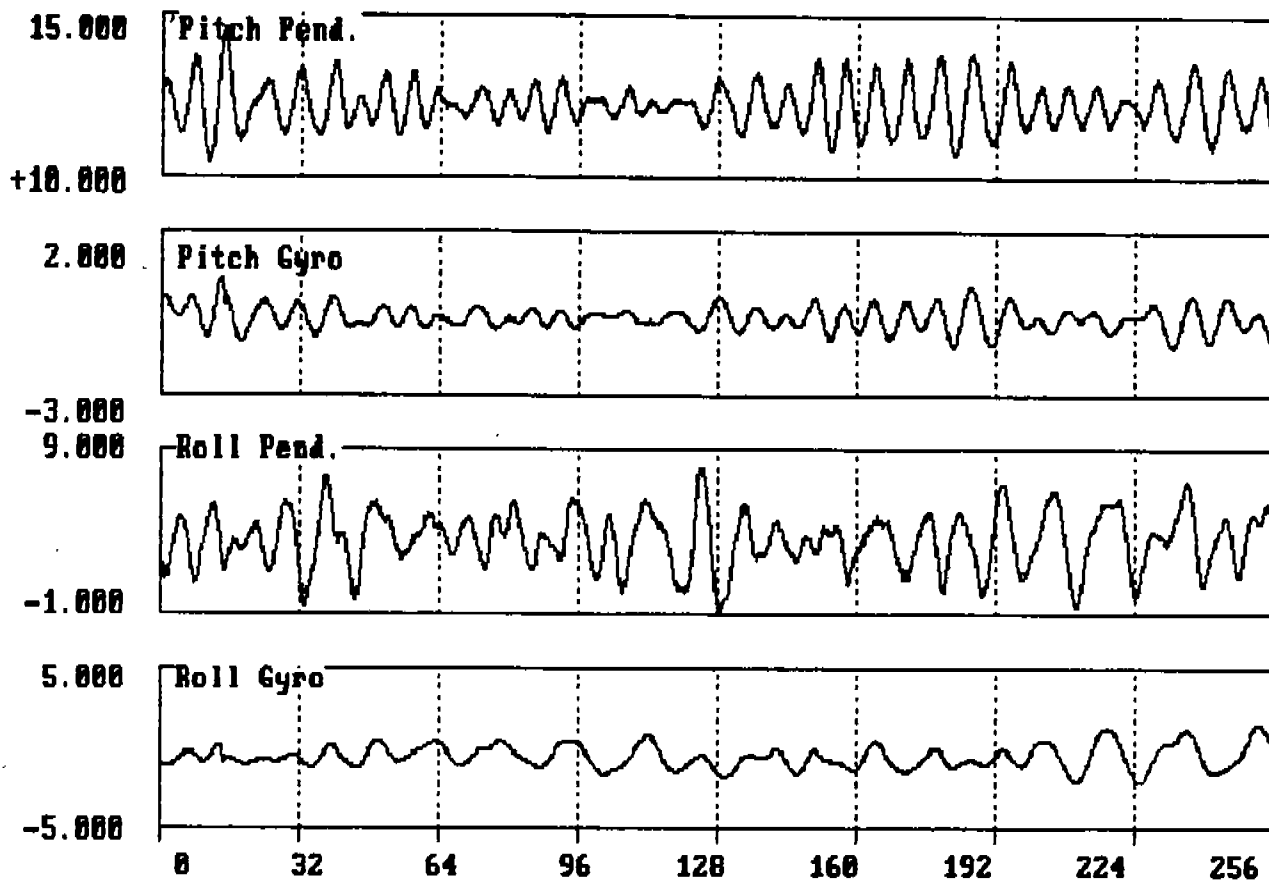


Figure 8  
GYRO/PENDULUM DATA  
File: 16220.DAT  
Time: 23 OCT 88 - 16:22:34



GYRO

PENDULUM

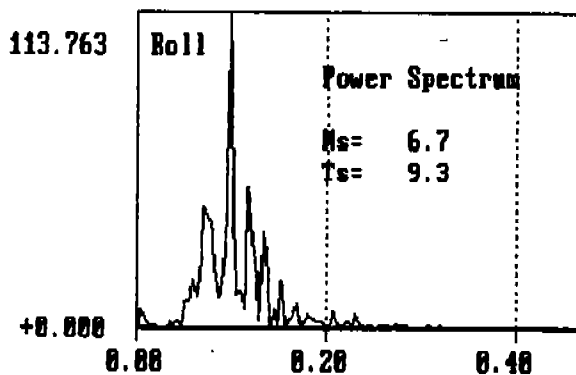
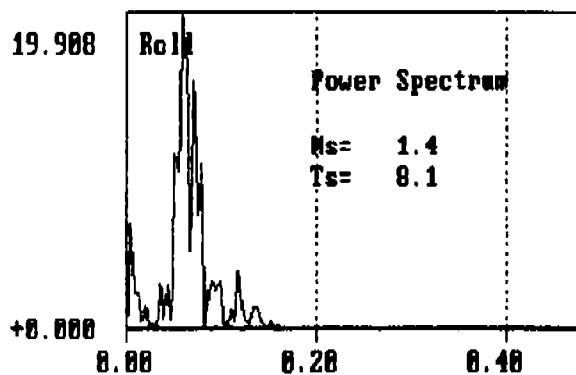
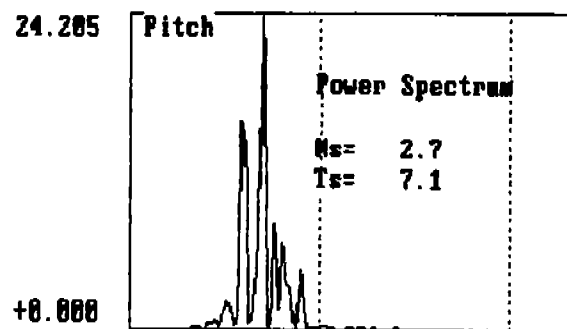
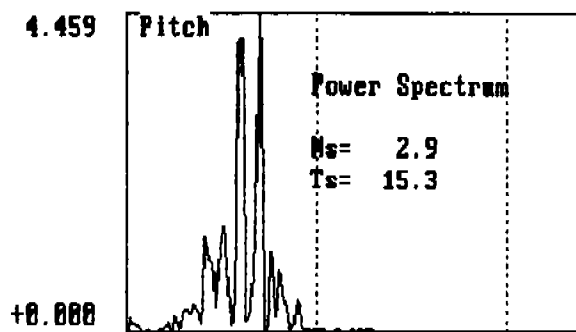
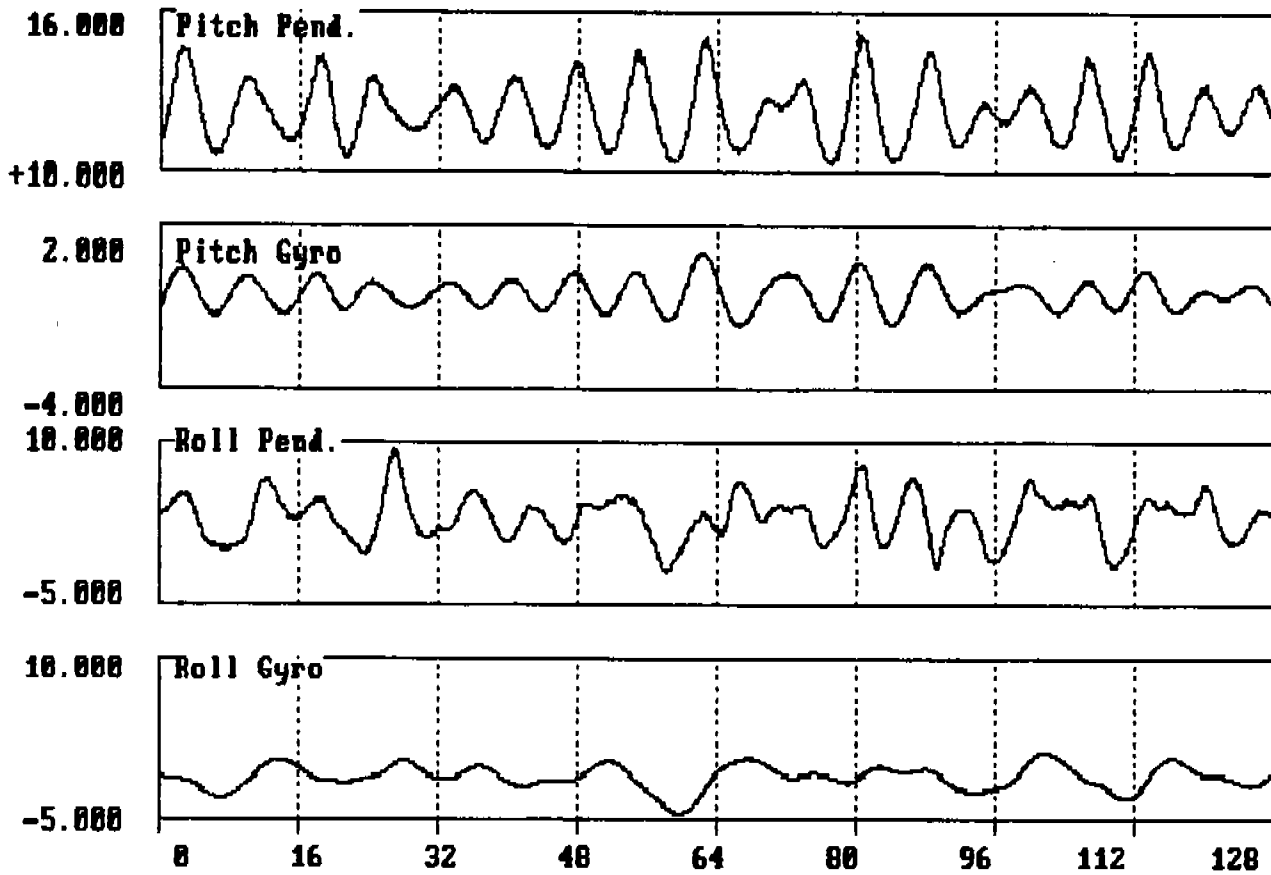


Figure 9  
GYRO/PENDULUM DATA  
File: 083801.DAT  
Time: 20 OCT 88 - 09:15:10



GYRO

PENDULUM

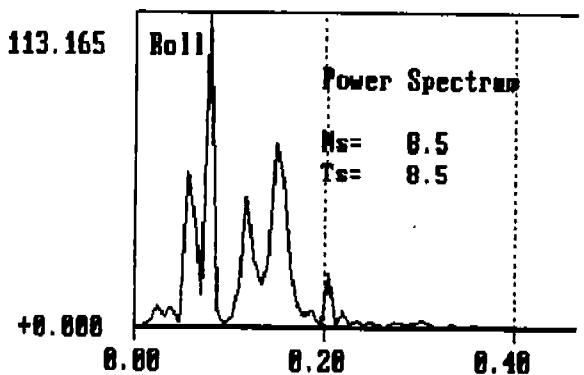
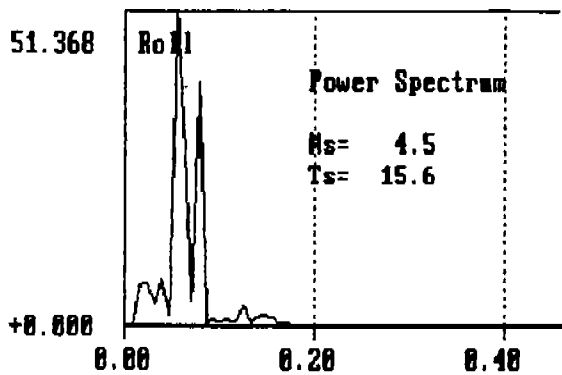
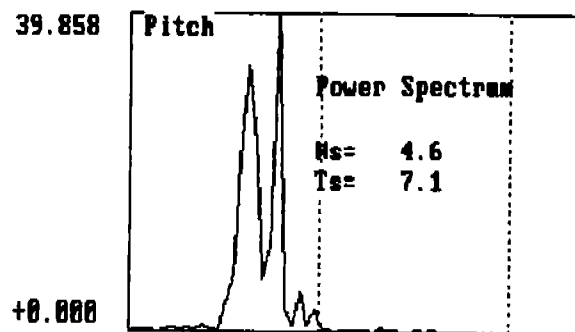
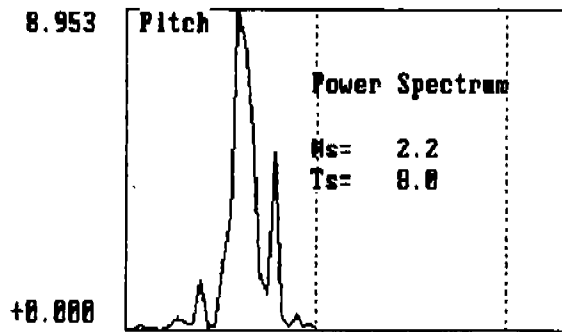
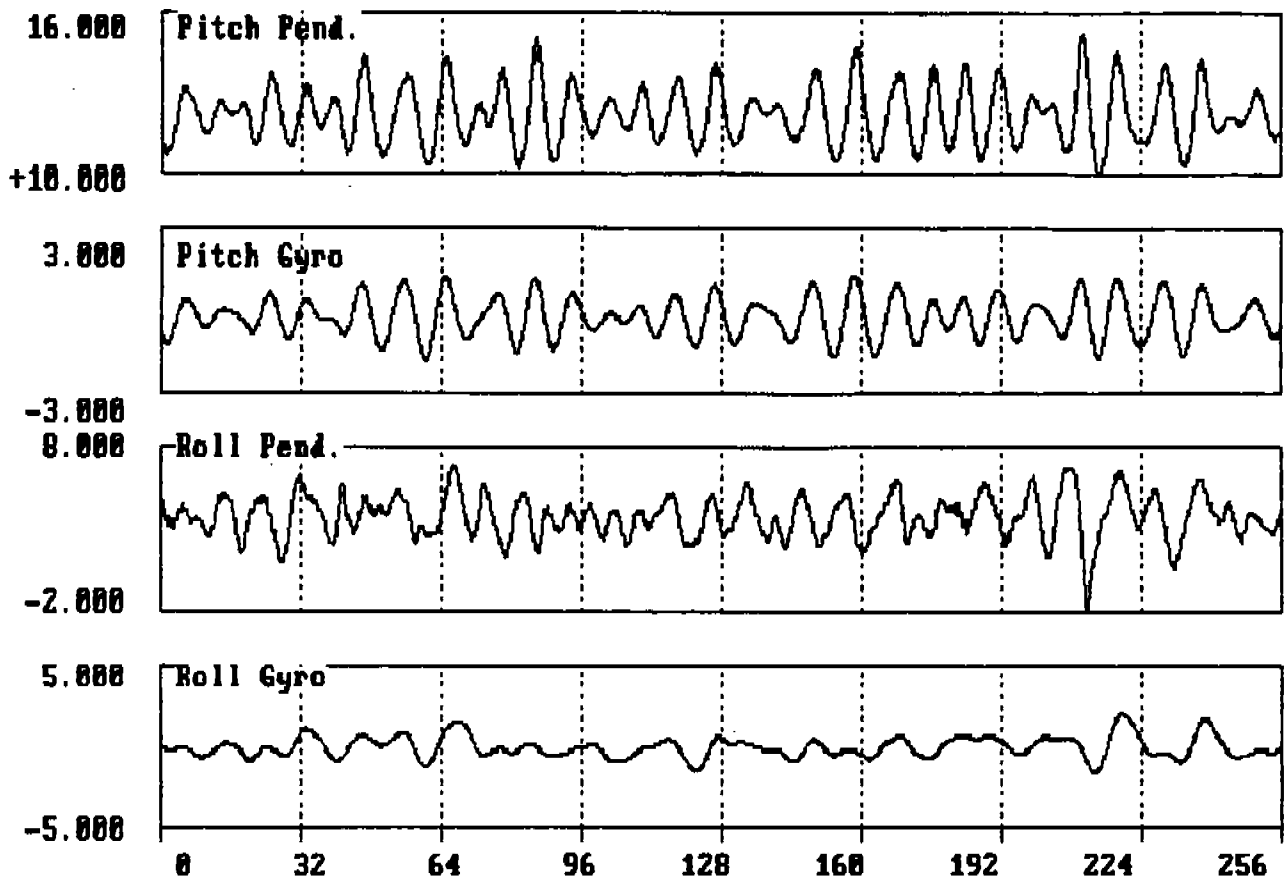


Figure 10  
GYRO/PENDULUM DATA  
File: @16Hz0.DAT  
Time: 20 OCT 88 - 14:54:47



GYRO

PENDULUM

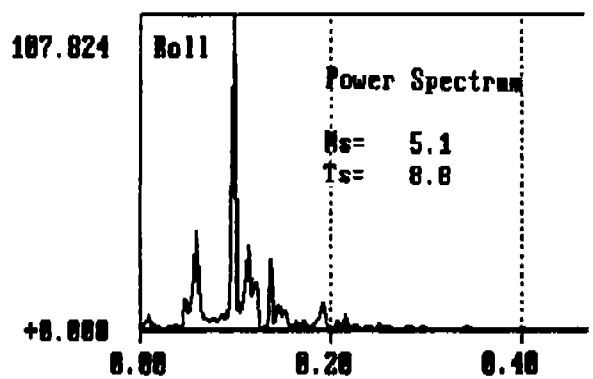
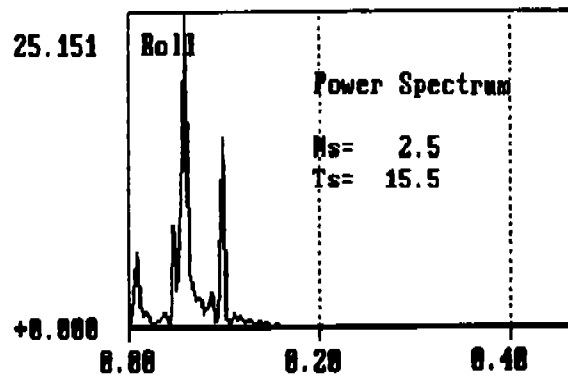
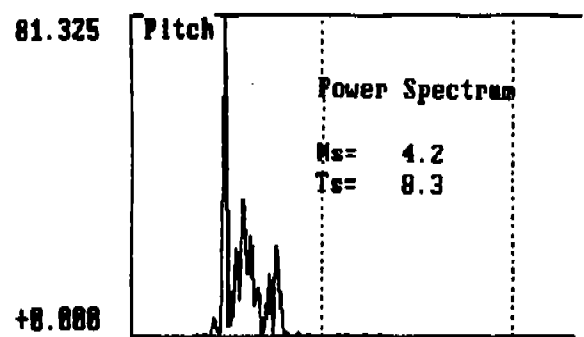
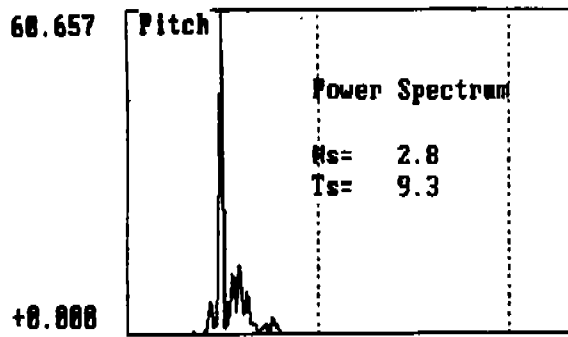


Figure 11  
GYRO/PENDULUM COMPARISON

File: 17550.DAT

Time: 19 OCT 88 - 17:55:31

As shown by this table and Figures 7 through 11, there are several differences between the gyro and pendulum sensor data:

1. For pitch angles above about 1 degree, both the pitch and roll pendulum RMS double amplitudes are higher (by nearly a factor of two) than the gyro amplitudes.
2. The pendulum sensor data (especially roll) generally contains more high frequency energy (and thus has lower significant periods) than does the gyro data.

The presented data indicate that the pendulum sensors were responding to translational accelerations as well as the angular vessel attitude. The pitch spectra for both the gyro and pendulum sensors have "shapes" that are similar to each other as well as to the acceleration spectrum; spectral peaks among these sensors are well aligned on the frequency axis. Spectral power, however, is significantly higher for the pendulum sensor, which also tends to have somewhat more energy at higher frequencies. The additional energy in the pendulum spectrum appears to be due to the vertical (heave) acceleration which adds energy at essentially the same frequencies as the true pitch spectrum.

The data for the pendulum roll sensor clearly shows the vertical acceleration coupling. Comparison of the gyro roll, pendulum roll and acceleration sensor spectra shows that the acceleration energy has, in effect, been "added" to the pendulum roll spectrum. The higher frequency content of the acceleration-induced "roll" results in the much lower significant periods of the pendulum roll versus the more accurate gyro roll. The data in Figure 10 show this effect particularly clearly. The comparison of measured data demonstrates that the gyro sensors measure the angular attitude of the vessel more accurately than do the pendulum sensors even at relatively low accelerations.

Figures 12 and 13 show the corrected wave heights, vertical acceleration and vertical bow displacement obtained using the pendulum angles and gyro angles respectively for geometric correction. These figures include a 256 second time series and the corresponding spectra for each parameter. For the low range of pitch and roll values encountered during the sea trials, the differences are small. However, for higher sea states with correspondingly higher accelerations and larger pitch and roll angle errors, the gyro sensors are clearly preferable.

## 5.2 Vertical Acceleration Sensor Subsystem Performance

Vertical acceleration was measured by a Schaevitz Vertical Accelerometer. The vertical bow displacement was computed from the vertical acceleration and gyro pitch and roll data as described below:

1. Compute the true vertical component ( $A_v$ ) of the measured vertical acceleration ( $A_z$ )

$$\begin{aligned} \text{define: } r1 &= \sin \delta \cos \gamma \cos \beta + \sin \delta \sin \beta \\ r2 &= -\sin \delta \cos \gamma \sin \beta + \sin \delta \cos \beta \\ q1 &= -\cos \gamma \cos \delta \sin \theta \\ q2 &= r1 (\cos \theta \sin \phi) \\ q3 &= r2 (\cos \theta \cos \phi) \end{aligned}$$

where:

- $\delta$  = vertical dip angle (from horizontal) = 78.0
- $\gamma$  = sensor azimuth (from forward) = 0.0 deg
- $\beta$  = transverse tilt (from horizontal) = 4.1 deg
- $\theta$  = pitch angle (positive when bow is up)
- $\phi$  = roll angle (positive when starboard side is down)

then:  $A_v = A_z (q1 + q2 + q3)$

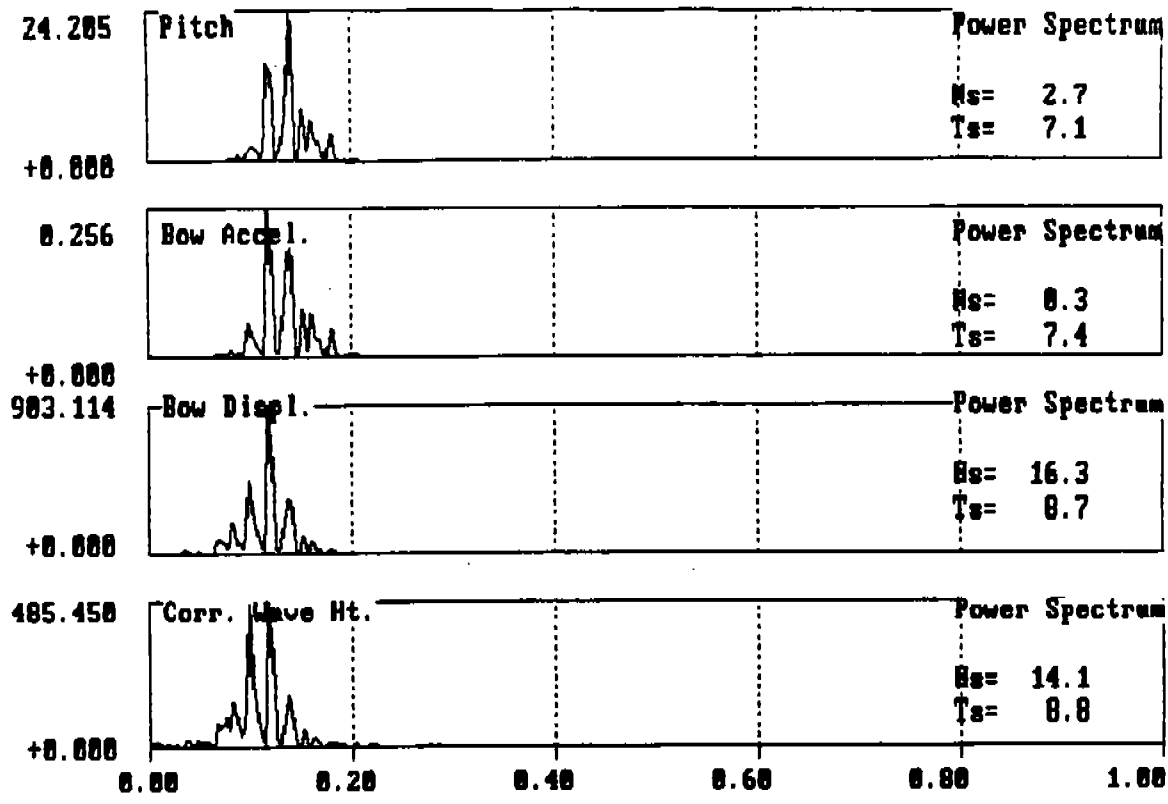
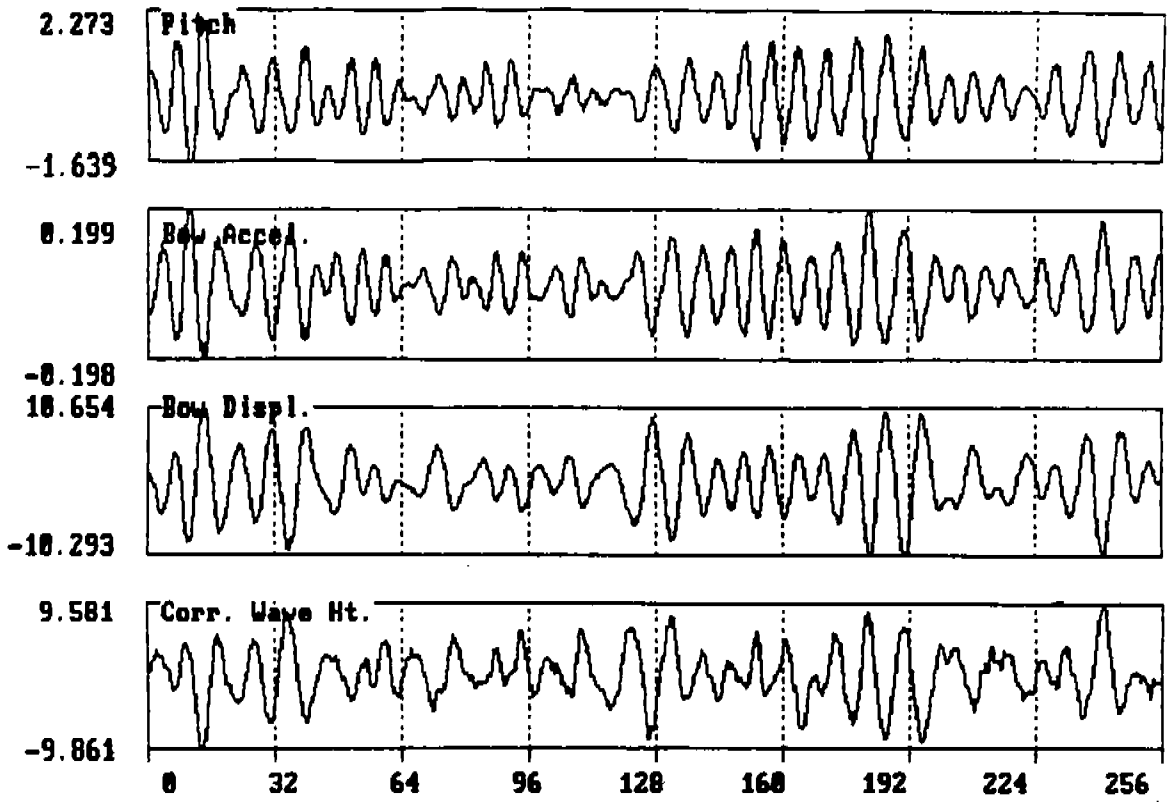


Figure 12  
 PARAMETER DATA USING PENDULUM SENSORS

File: 080301.DAT  
 Time: 20 OCT 88 - 09:15:10

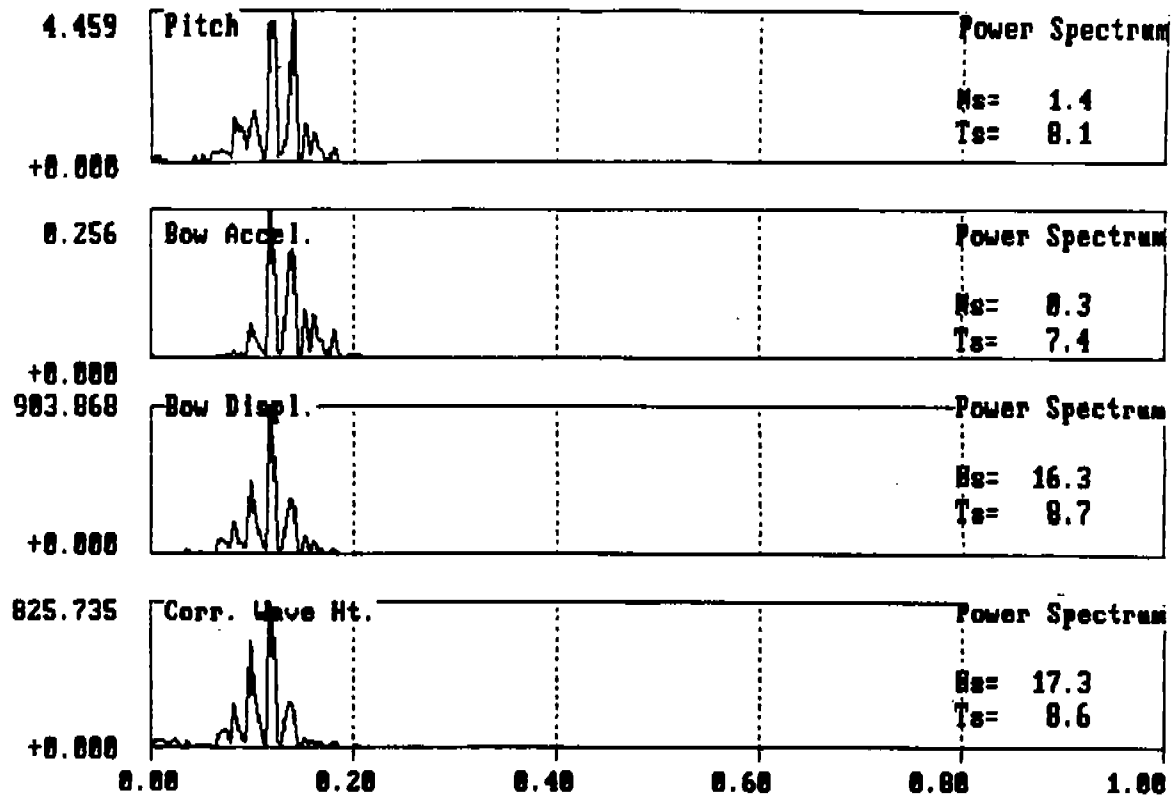
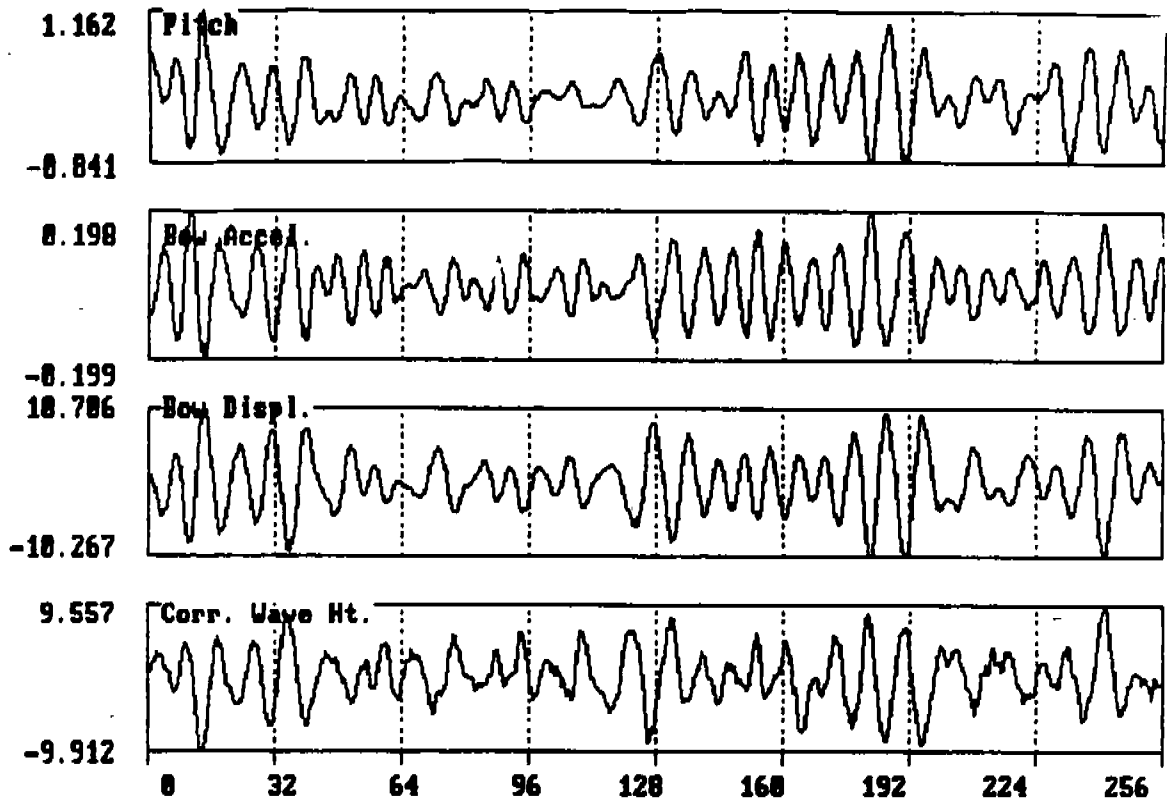


Figure 13  
PARAMETER DATA USING GYRO SENSORS

File: 083801.DAT

Time: 20 OCT 88 - 09:15:10

2. Remove the trend from the time series.
3. Band pass filter the series in the frequency domain by applying a rectangular window (perfect filter) to the FFT coefficients. The window (W) has  $W(f) = 1$  for frequency (f) between  $f_1$  and  $f_2$ ;  $W(f) = 0$  for all other frequencies. For the data presented in this report,  $f_1 = 2$  Hz and  $f_2 = 30$  Hz.
4. Inverse-FFT the filtered FFT back to the time domain; then integrate the filtered series using trapezoidal integration to compute the velocity time series.
5. Repeat steps (2) through (4) on the velocity data; compute the vertical bow displacement time series =  $g * (\text{integrated velocity})$ , where  $g$  = gravity acceleration.

The acceleration measurement and vertical bow displacement computation functioned well for the sea trial data. Integration accuracy on the order of 1 or 2 percent was obtained using calibrated inputs at the frequencies of interest. Additionally, comparison of the acceleration time series and bow displacement time series as illustrated in Figure 13 shows the expected phase reversal but similar shape of the two traces with no indication of integration artifacts such as excessive low frequency modulation or drift. Finally, using the acceleration significant periods from the acceleration spectrum plots and the amplitudes on the time series plots, the amplitudes on the bow displacement plots are found to be in good agreement with the expected values derived from the approximation:

$$\text{bow displacement} = 1/2 g (\text{acceleration}) (\text{period}/4)^2$$

### 5.3 Wave Surface Range Sensor Performance Evaluation

The slant distance range to the wave surface was measured by an EMI infrared wave gauge. This sensor measures the time for an infrared light pulse to be reflected from the sea surface

back to the sensor. By transmitting a series of pulses, a continuous measure of the distance to the wave surface is obtained. Electronic filters and signal processing circuits integral to the EMI sensor minimizes the effect of spurious reflections from sunlight, rain and spray (Ref 6). The optical system consists of a concentric transmitter/receiver and the transmitting lens collimates the emitted radiation to a 0.6 degree beam width. At a range of 75 feet this results in a 1 ft diameter illumination spot.

The EMI laser sensor operated without problem during the sea trial. On the eastward crossing, it survived "green water" submersion and the associated wave impact loads, thus demonstrating its robustness. However, many of the EMI wave gauge data records contain periods of what are termed "data drop outs" - periods of 1 to 3 seconds when the wave surface range values reported by the sensor remain essentially constant. These data drop outs distort both the raw range data statistics as well as the encountered wave height spectra and statistics.

Three questions relative to the wave range data are discussed below:

1. What is the envelope of pitch conditions within which the EMI sensor data is acceptable or recoverable?
2. What is the result of the distorted wave surface range time series on the calculated wave height spectrum and statistics?
3. Can the distorted data be sufficiently recovered to provide usable wave height information?

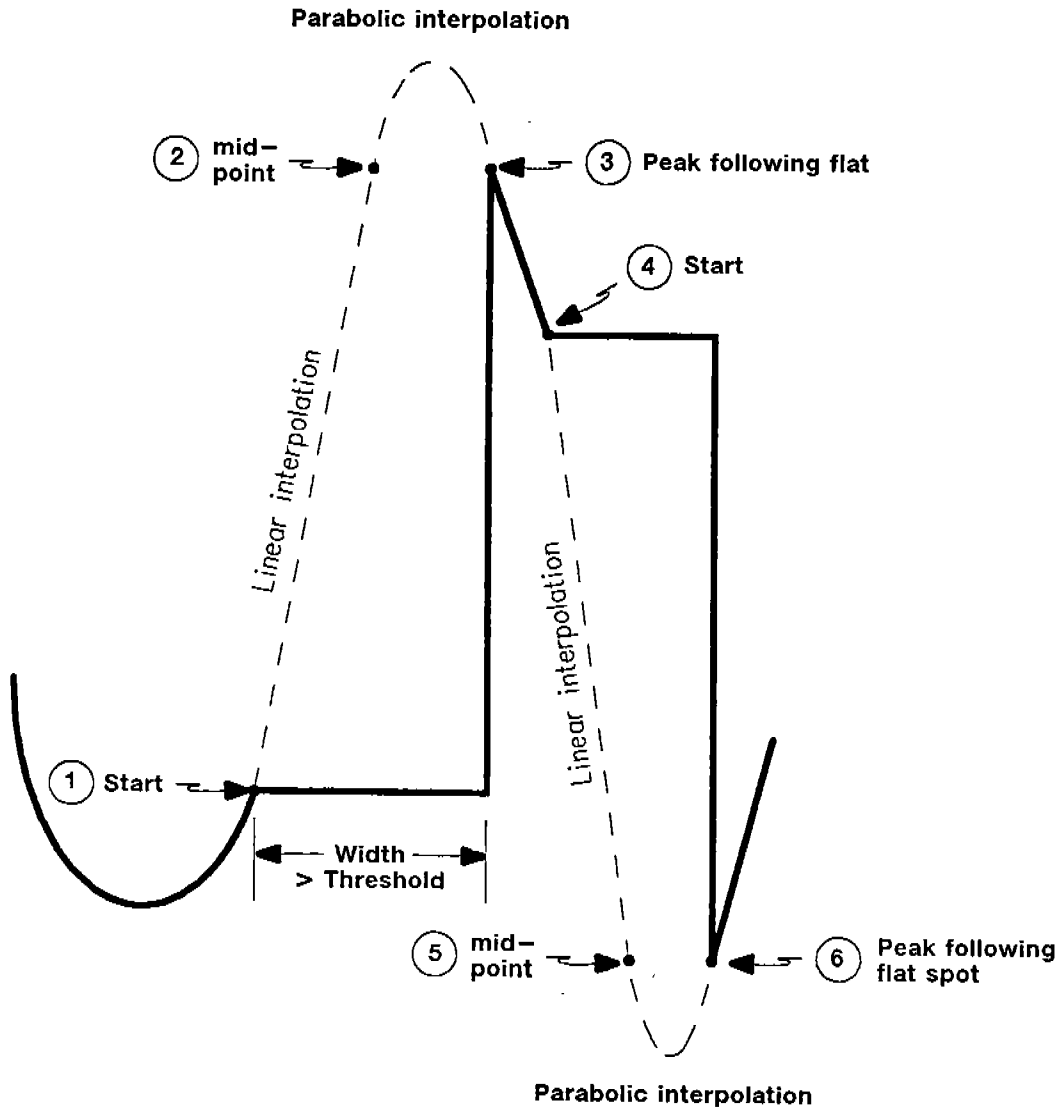
To answer these questions, approximately 20 percent of the data records, representing the full range of sea states encountered during the sea trials, were re-processed to: (1) compute drop out statistics as a basis for comparison; (2) relate sea state conditions to drop out severity; and (3) evaluate the effectiveness of algorithms which attempt to reconstruct the wave range data during drop outs.

### 5.3.1 Data Drop Out Detection Algorithm

Referring to Figure 14, the wave surface slant range data record is scanned and each point is compared with the preceding point. If the difference in values is less than a preset limit (currently 0.5 feet), a "sequential flat point" counter is incremented. If the counter reaches one second or more, AND the difference between the last "flat" value and the first "flat" value is still less than the point-to-point difference limit (0.5 feet), a potential drop out is flagged in the algorithm logic. A "true" drop out is detected if the potential drop out is followed within a preset time by local maximum or minimum of sufficient "height" above or below the drop out. Details of the drop out detection and range data reconstruction algorithm are presented in Appendix C.

This peak detection algorithm is essentially empirical and to some extent arbitrary. It evolved by means of trial and error in an attempt to duplicate the drop out "detection" performed by eye, but with a consistent definition which could be applied to all data records. Comparison of the raw uncorrected EMI wave gauge data against the reconstructed EMI data in Figures 15 through 18 indicates that the algorithm is generally in good agreement with visual judgements. It should be noted, however, that the quantitative results, in terms of number of drop-outs and drop out percentage are sensitive to the threshold parameters used by the algorithm. The "drop out percentage" can vary by 10-20% depending on the choice of threshold values. Nonetheless, the algorithm was applied consistently to the data presented in this report, and the results are considered at least qualitatively correct.

Heavy line = measured data  
Dotted line = reconstructed range



Parabola fit through points ① ② ③ for upward peak  
Parabola fit through points ④ ⑤ ⑥ for downward peak

Figure 14  
Flat Spot Detection/Reconstruction

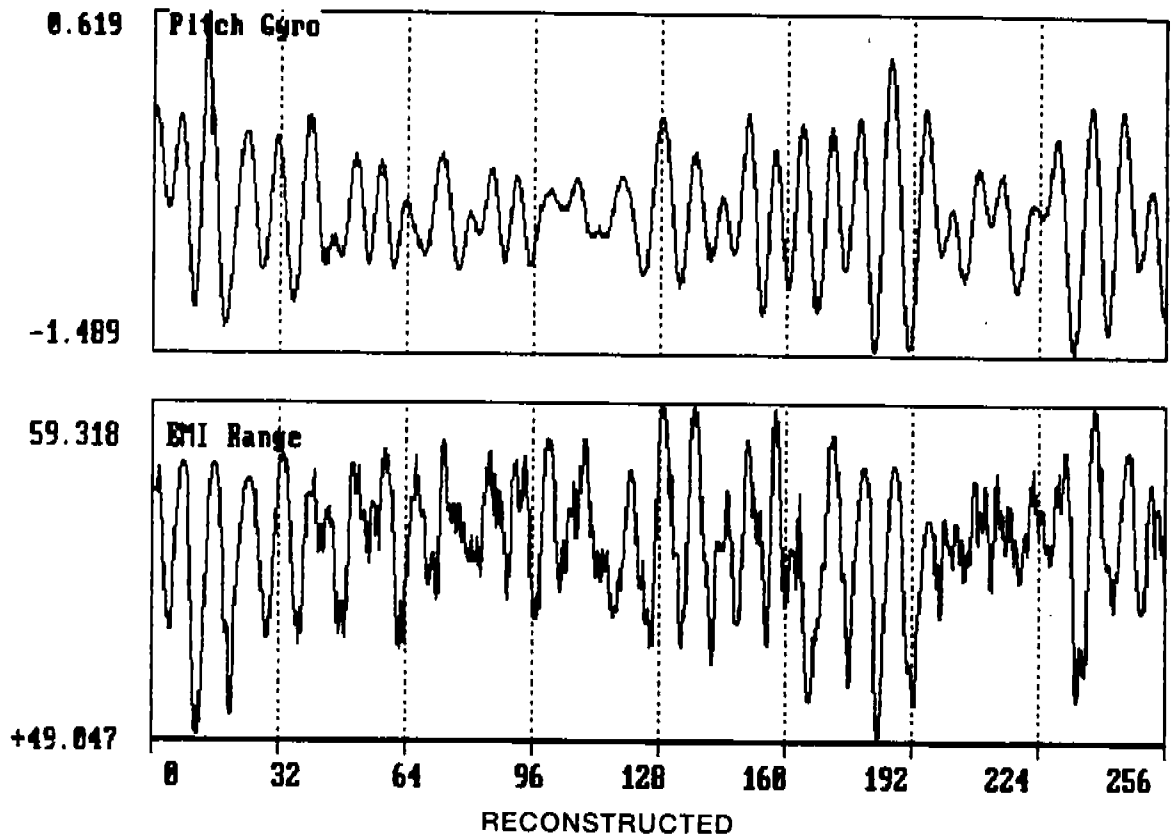
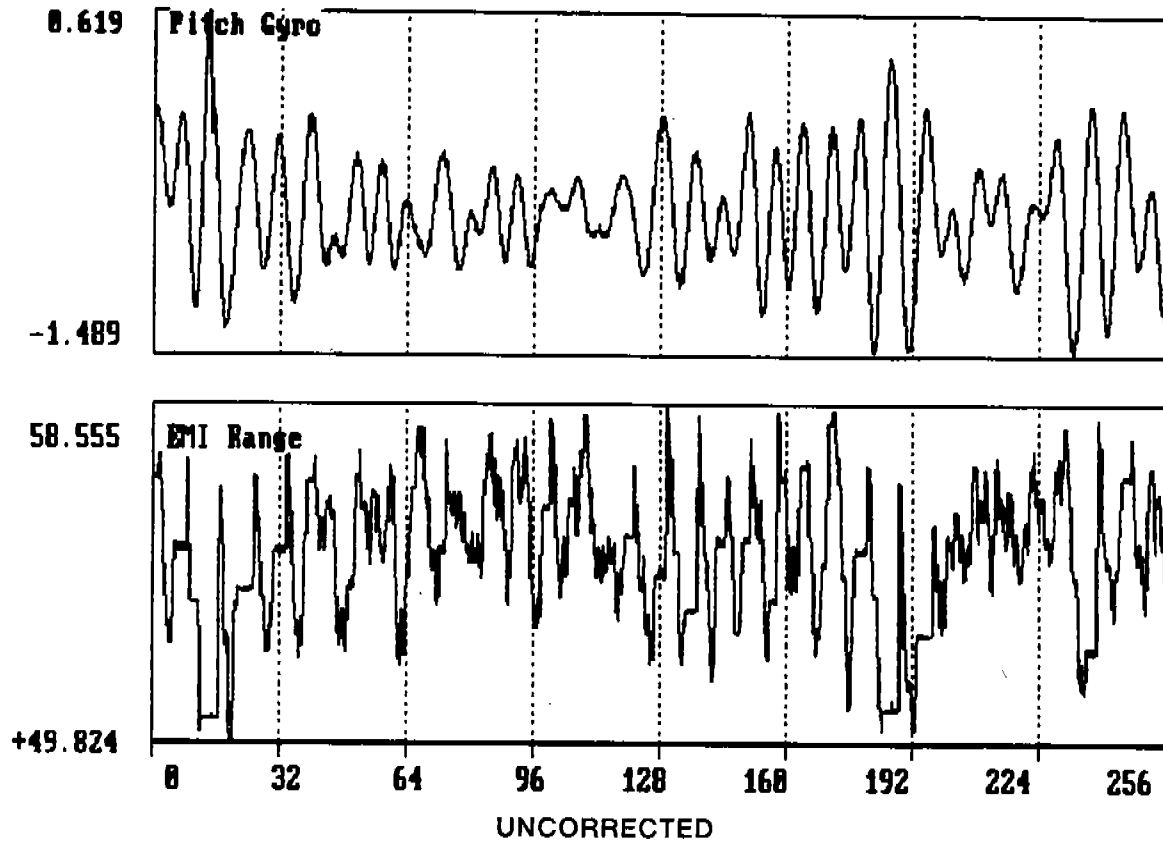


Figure 15  
 PITCH AND EMI RANGE  
 File: 083801.DAT  
 Time: 20 OCT 88 - 09:15:10

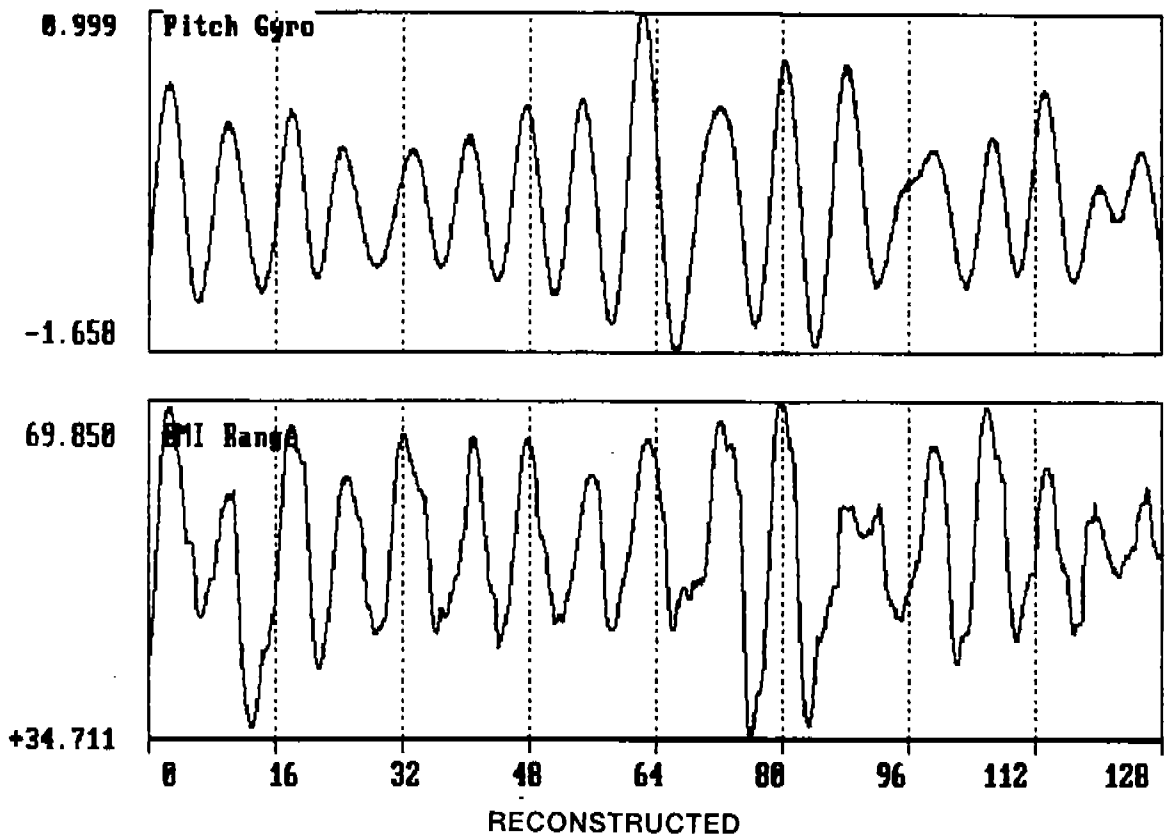
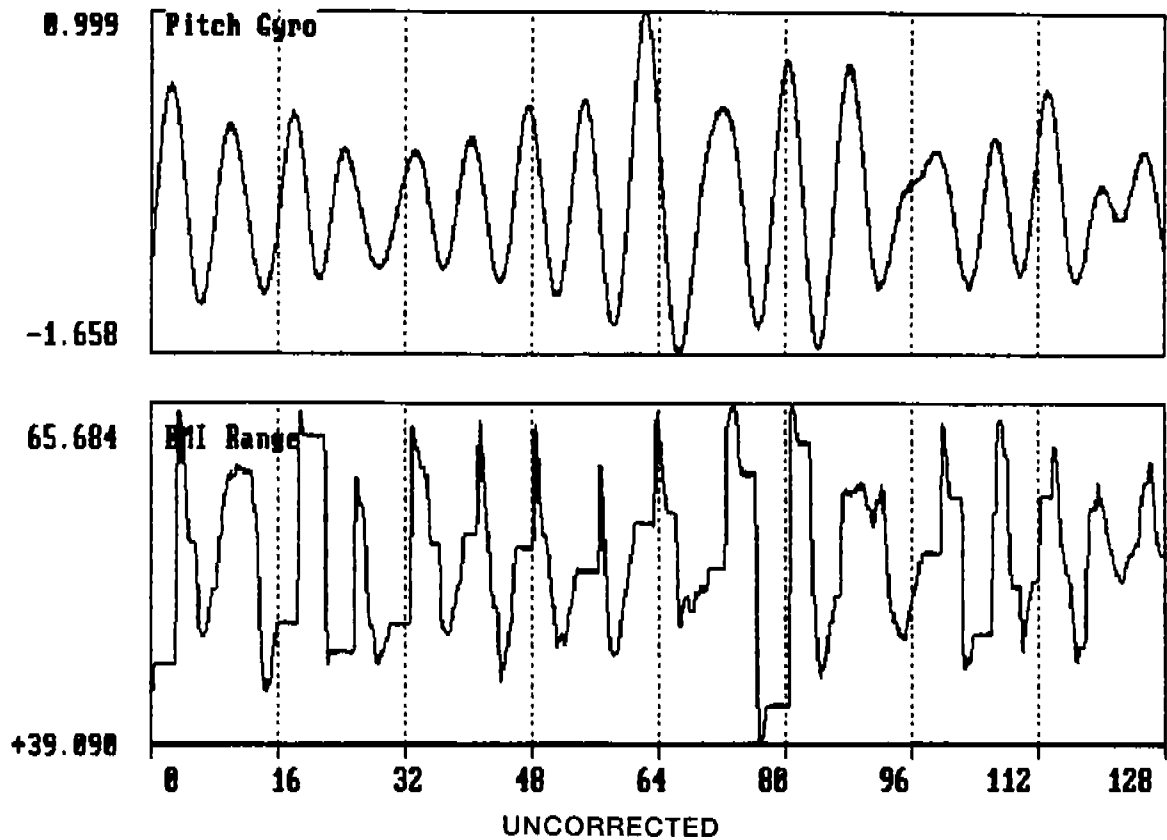


Figure 16  
 PITCH AND EMI RANGE  
 File: @16Hz0.DAT  
 Time: 20 OCT 88 - 14:54:47

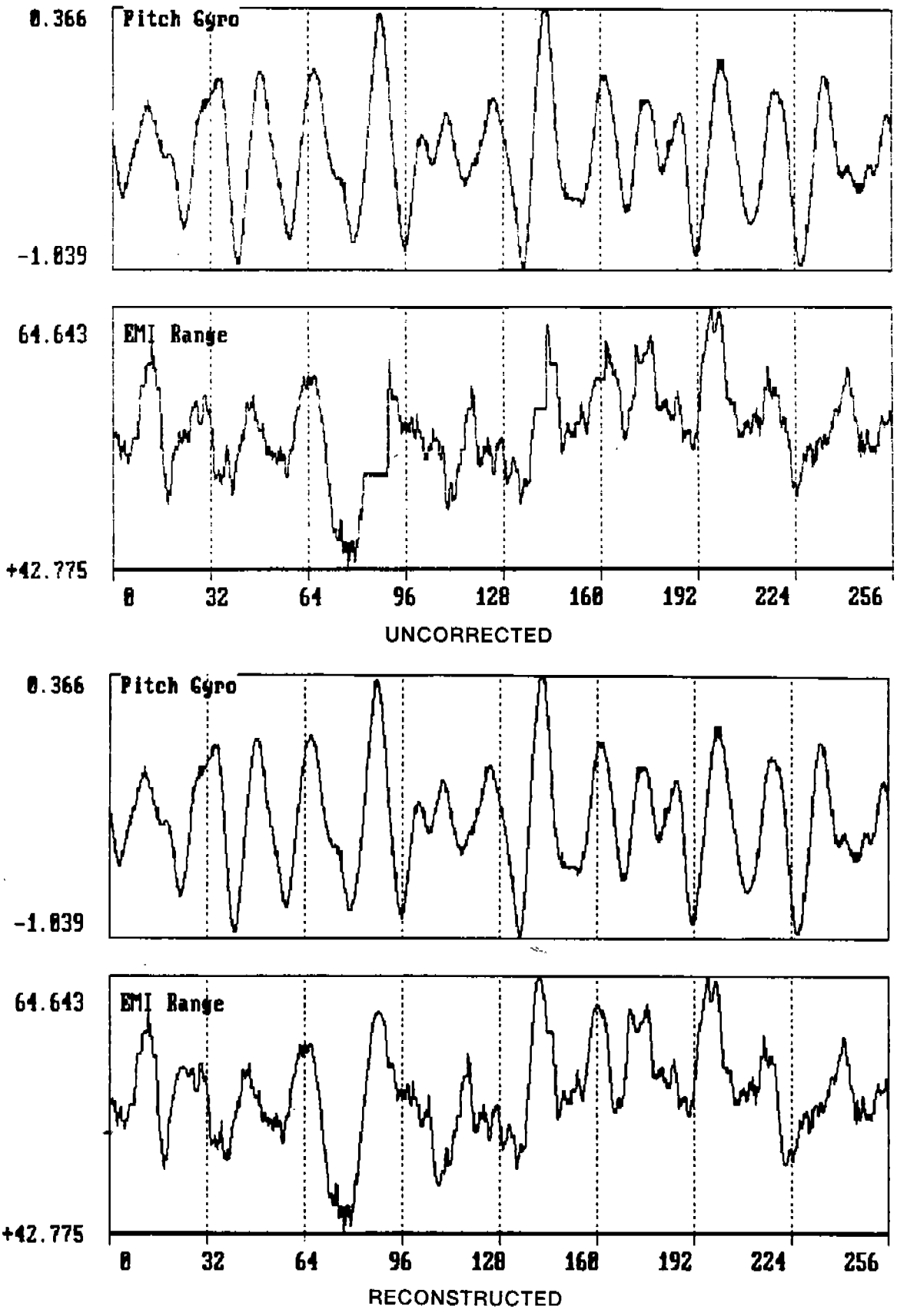


Figure 17  
 PITCH AND EMI RANGE  
 File: 12590.DAT  
 Time: 22 OCT 88 - 12:59:24

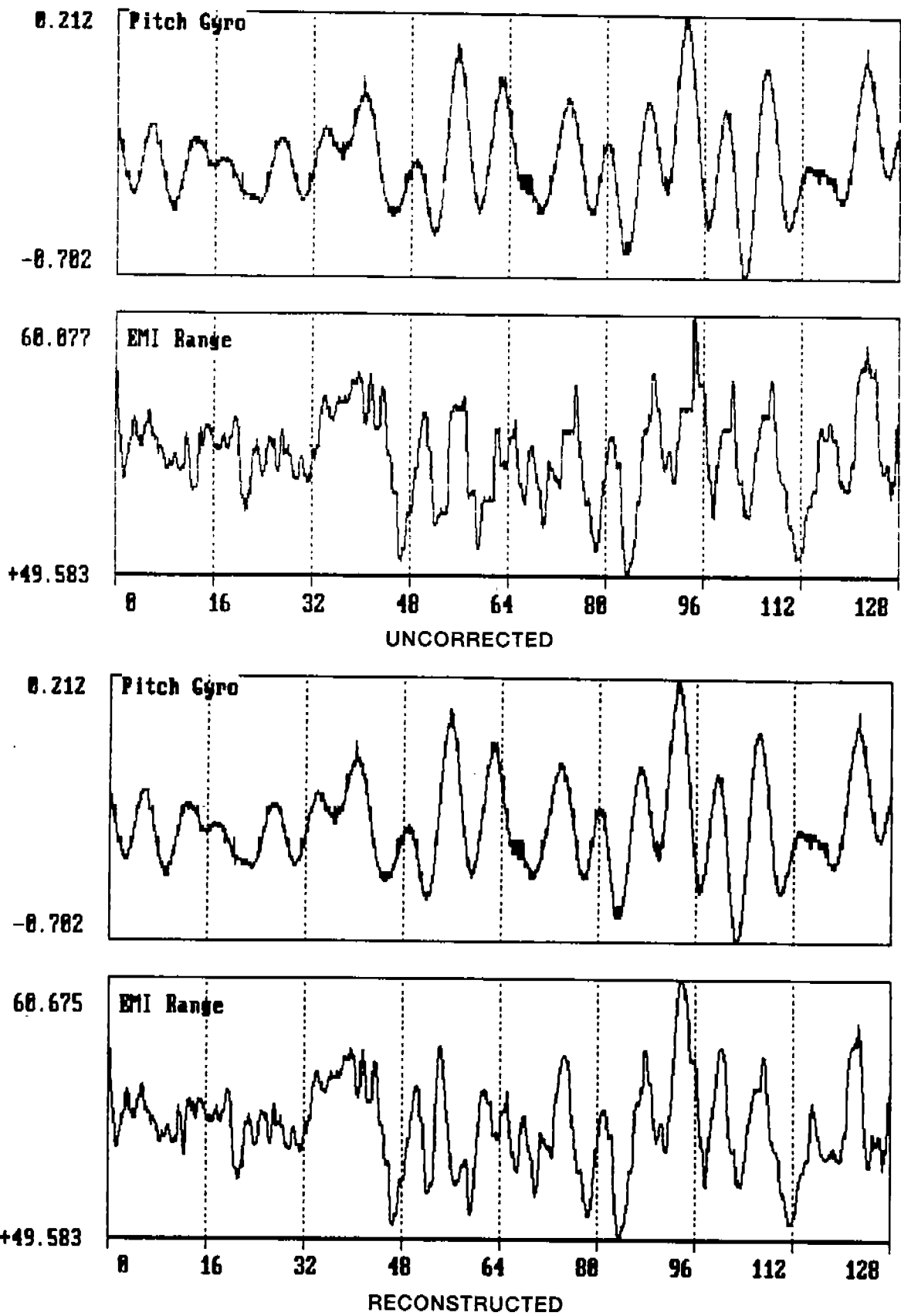


Figure 18  
 PITCH AND EMI RANGE  
 File: 134200.DAT  
 Time: 24 OCT 88 - 13:44:43

Table 2 and Figure 19 present the results of the drop out analysis of 15 data records representative of the range of sea state conditions encountered during the sea trials. The data are presented in two segments: records with pitch periods less than 9.5 seconds; and data with pitch periods greater than 9.5 seconds. Figures 20 through 27 present the data, in order of increasing drop out severity, for pitch periods under 9.5 seconds; Figures 28 through 34 present the data for periods greater than 10 seconds. The wave height time series and spectra in all figures represent "drop out reconstructed data". Each of these figures show the raw wave range time series and spectrum; the "drop out reconstructed" range time series and spectrum; and time series and spectra for gyro pitch, vertical acceleration, bow displacement and wave height. Figures 35 to 38 present, selected time series and spectra derived from the as-measured (non "reconstructed") data. These plots correspond to the plots of reconstructed data presented in Figures 20, 30, 32 and 38. All angle data used in the processing of the presented data was measured by the gyro sensors.

Within each segment, the Table 2 data entries are ordered by increasing "drop out percentage", defined as the ratio of the number of points in all detected data drop outs compared to the total number of points (2048) in the data record. The table also lists the number of different data drop out (#) segments in the record, and the gyro pitch double amplitude and period. The filename of the data record and the corresponding data figures are included for reference.

Although there is a fair amount of scatter in the drop out statistics due to the sensitivity to the threshold used in the algorithm, a qualitative relationship of the drop out severity to the sea state, specifically to the pitch amplitude and period, is evident. Drop out severity is generally proportional to pitch amplitude. To a lesser degree, the number of drop outs is also a function of pitch period. The drop out percentage at lower periods (higher frequency) is relatively greater than for those same pitch amplitudes at longer periods. Figure 19, based on the data in Table 2, clearly shows this dependence.

**TABLE 2**  
**DROP OUT DETECTION STATISTICS**

Filename	RMS Pitch Double Amplitude (deg)	Significant Pitch (seconds)	Dropouts		Reference Figure #
			#	%	
131800	0.1	10.2	3	2.6	20 & 35
16220	0.5	16.0	13	7.6	21
13110	0.4	16.8	4	7.9	22
165800	0.4	14.9	8	8.6	23
17480	0.2	11.7	18	10.2	24
12050	0.8	13.4	17	12.1	25
12590	0.6	16.4	9	14.8	26
17180	0.1	14.6	21	16.6	27
134200	0.3	8.7	9	12.1	28
14030	0.7	8.8	25	20.5	29
083801	0.7	8.1	29	25.7	30 & 36
08220	1.0	8.3	21	27.1	31
@16Hz0	1.1	8.0	22	34.1	32 & 37
08380	0.8	8.5	38	46.1	33
17550	1.4	9.3	43	56.1	34 & 38

Examination of the unprocessed wave range data in Figures 20 through 34 shows that a qualitative difference exists between the drop outs at lower pitch periods compared with higher periods: At the lower periods, the wave range data drop outs occur shortly after both pitch minimums (bow down) as well as pitch maximums (bow up); for the higher periods the data drop outs occur only after pitch minimums.

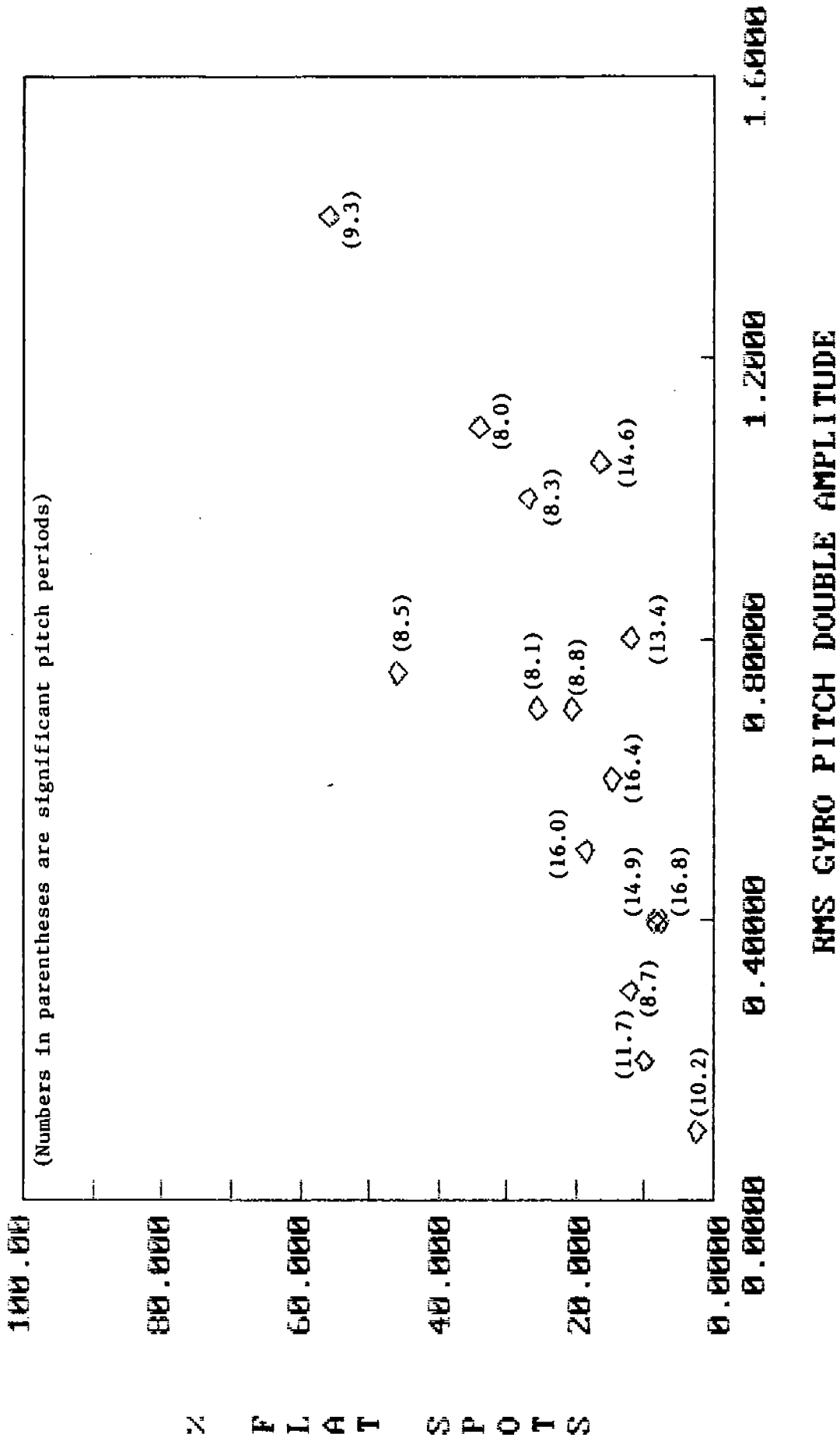
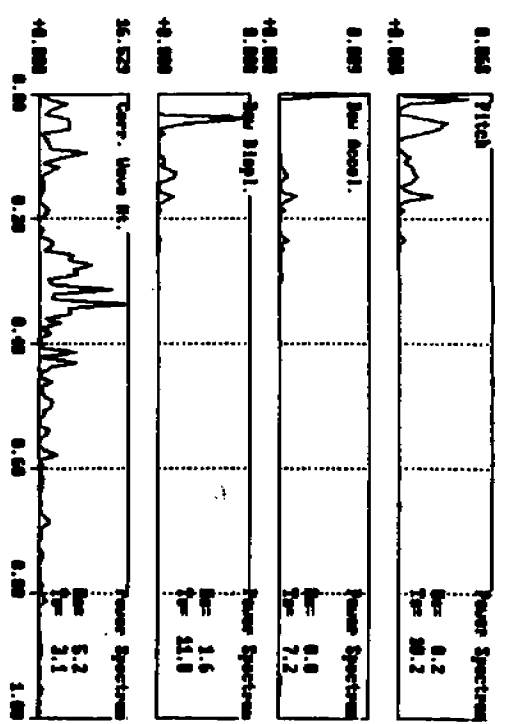
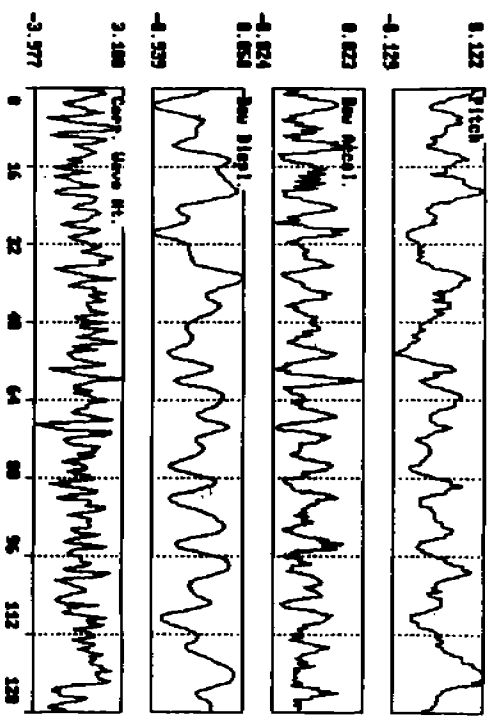
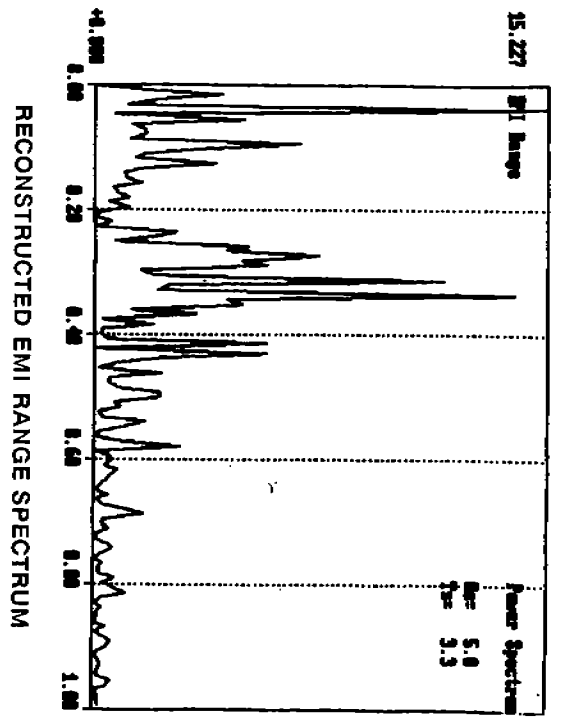
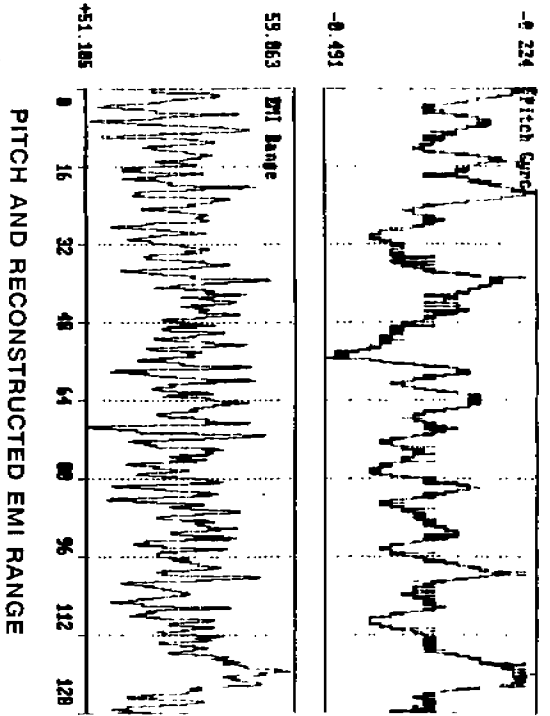
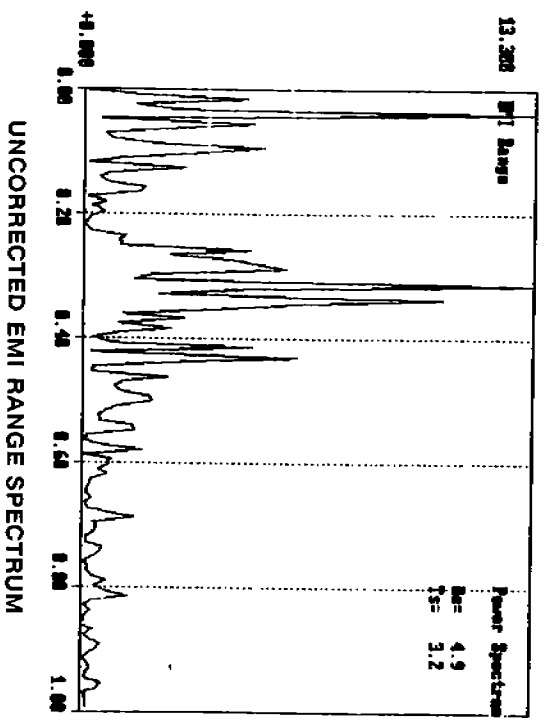
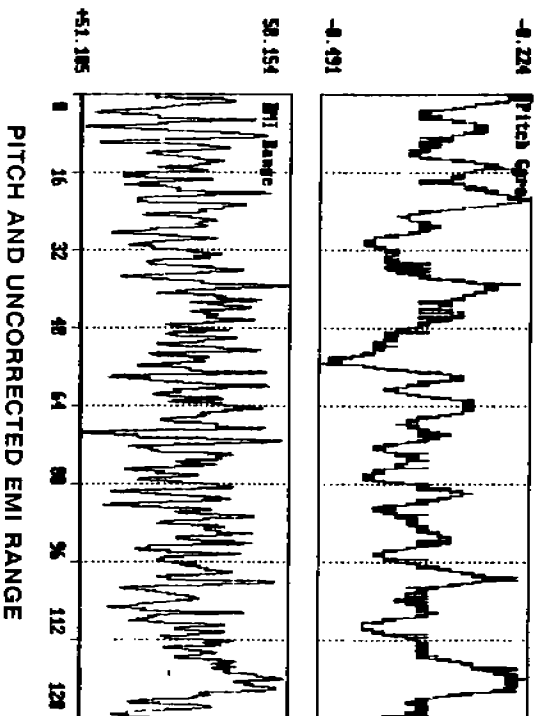
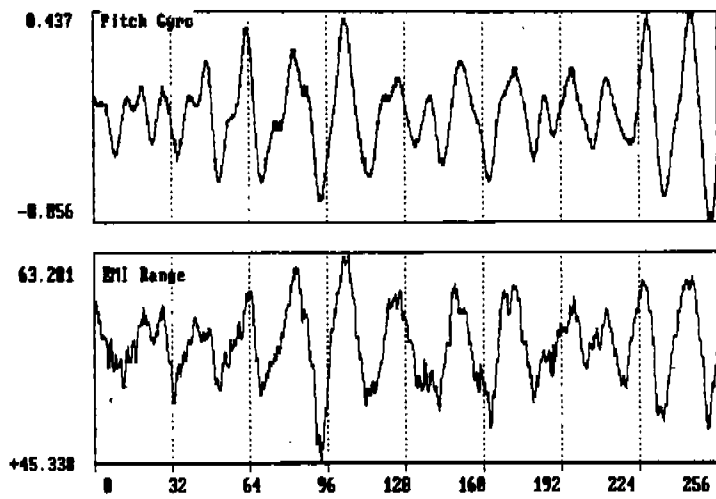


Figure 19  
Drop Out Severity vs Pitch

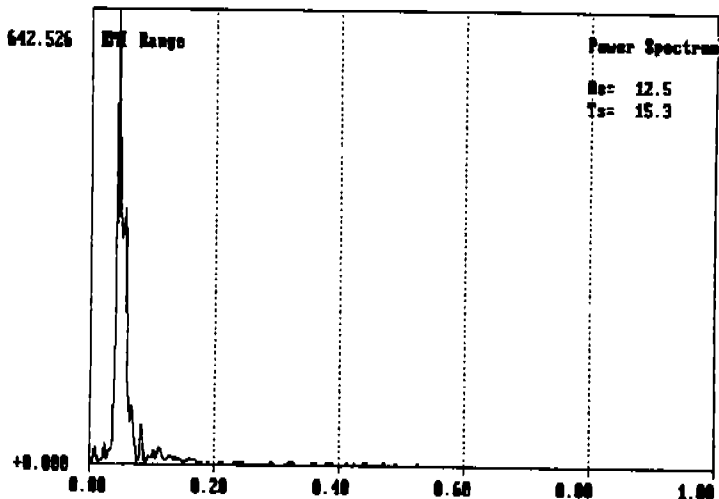


PARAMETER TIME SERIES

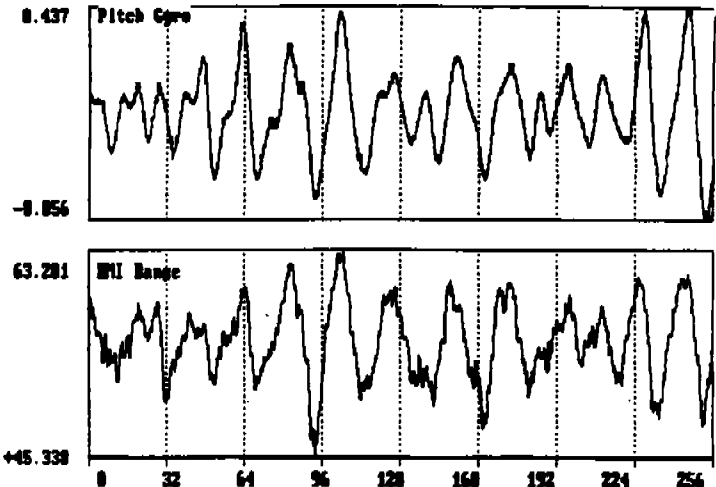
PARAMETER SPECTRA



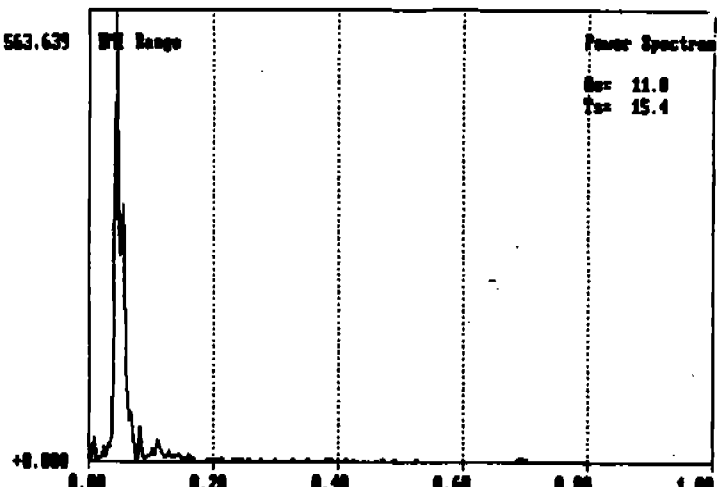
PITCH AND UNCORRECTED EMI RANGE



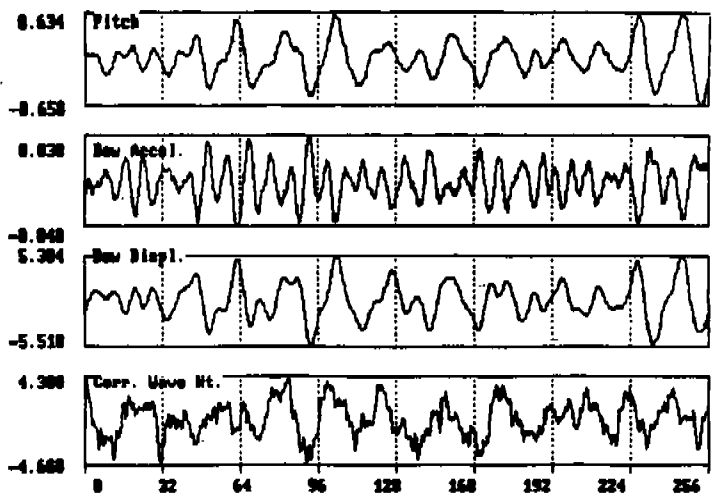
UNCORRECTED EMI RANGE SPECTRUM



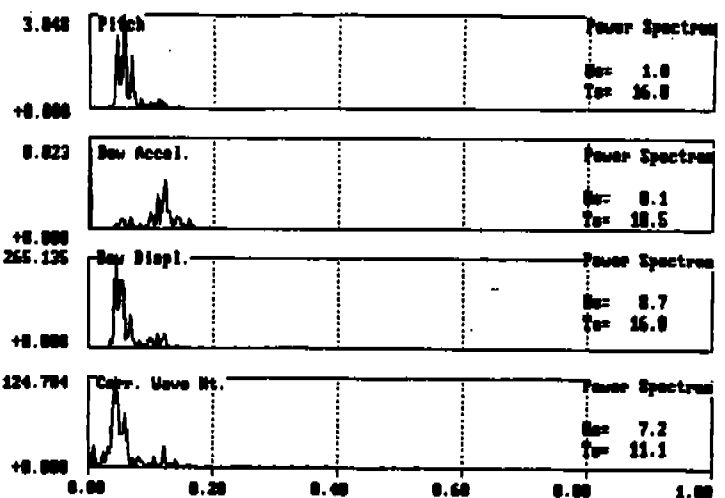
PITCH AND RECONSTRUCTED EMI RANGE



RECONSTRUCTED EMI RANGE SPECTRUM

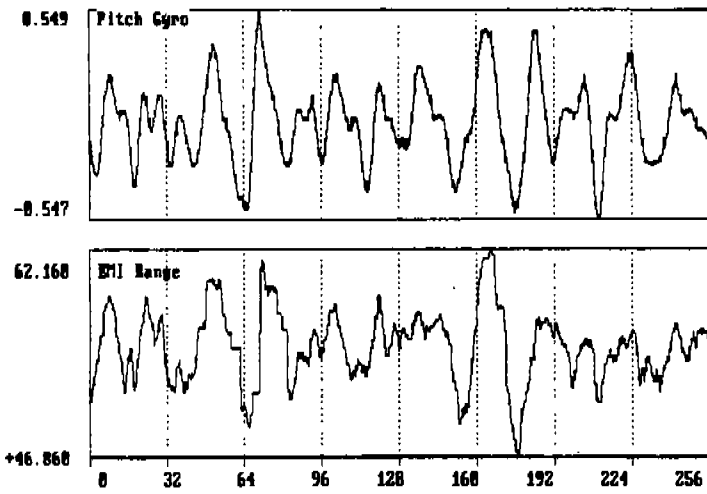


PARAMETER TIME SERIES

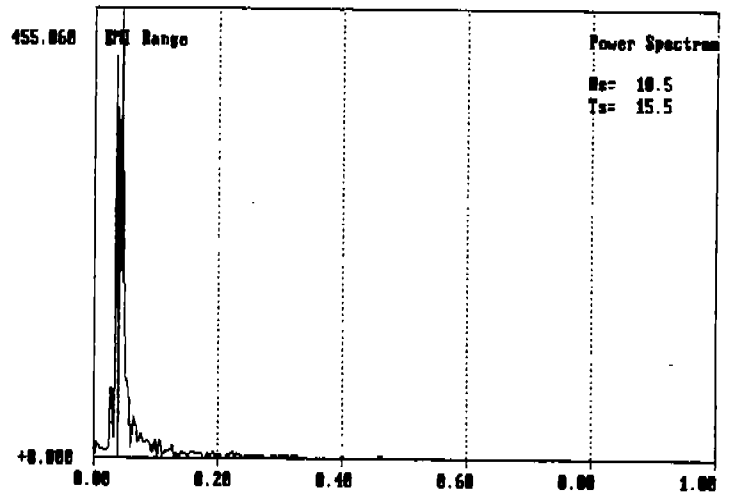


PARAMETER SPECTRA

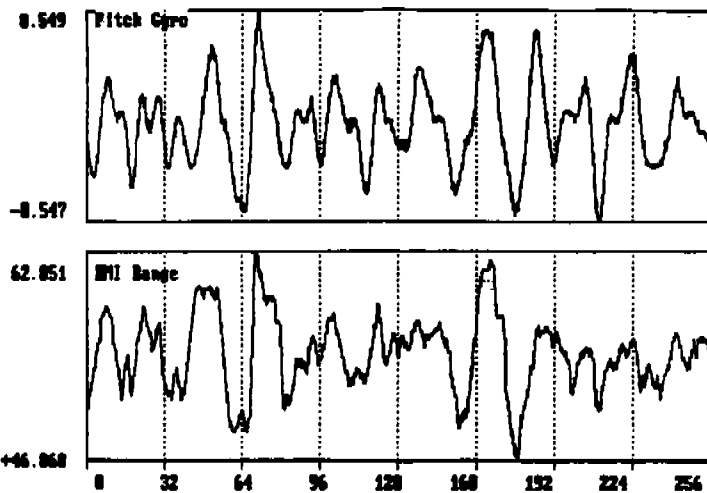
Figure 21  
SEA TRIAL DATA  
File: 16220.DAT  
Time: 23 OCT 88 - 16:22:34



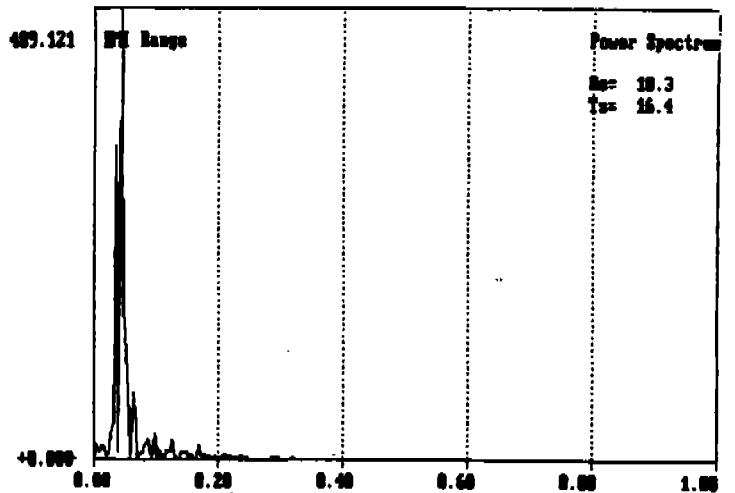
PITCH AND UNCORRECTED EMI RANGE



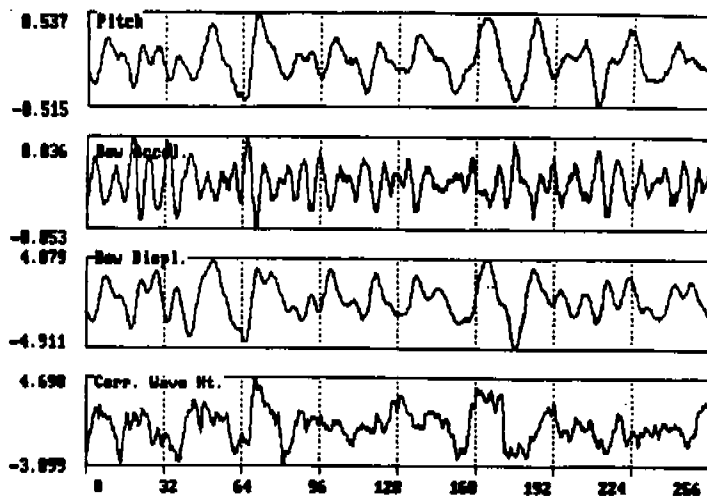
UNCORRECTED EMI RANGE SPECTRUM



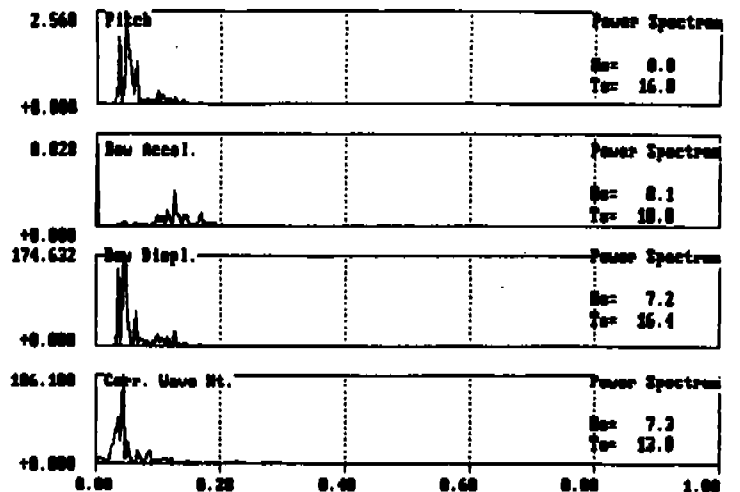
PITCH AND RECONSTRUCTED EMI RANGE



RECONSTRUCTED EMI RANGE SPECTRUM



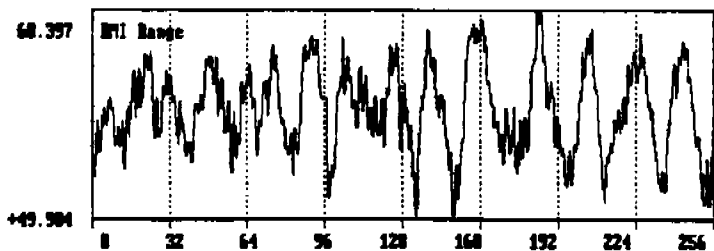
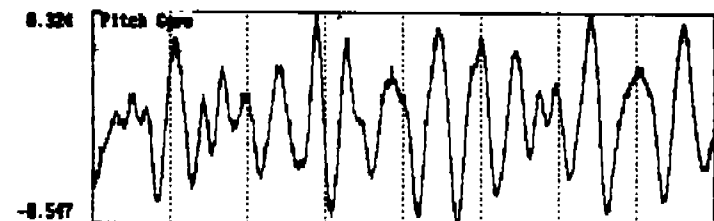
PARAMETER TIME SERIES



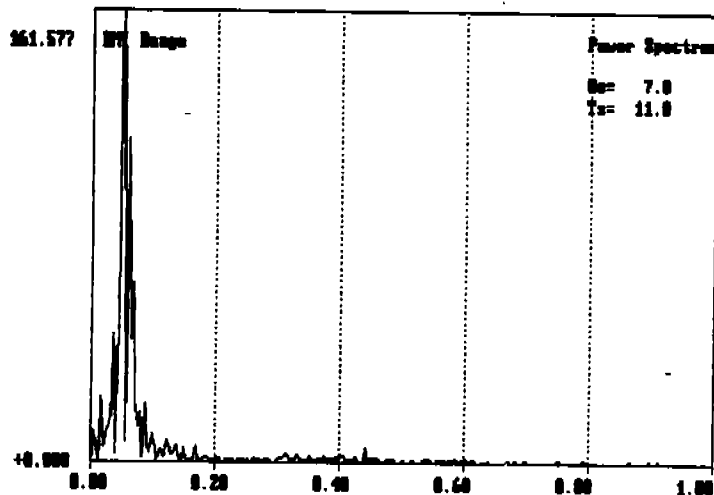
PARAMETER SPECTRA

Figure 22  
SEA TRIAL DATA

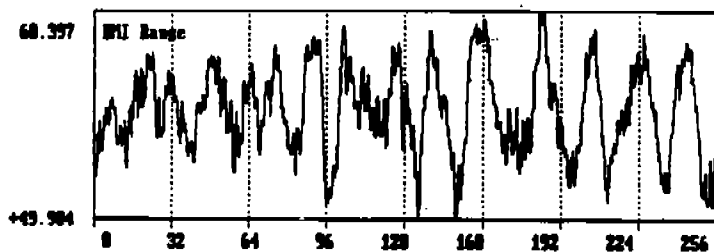
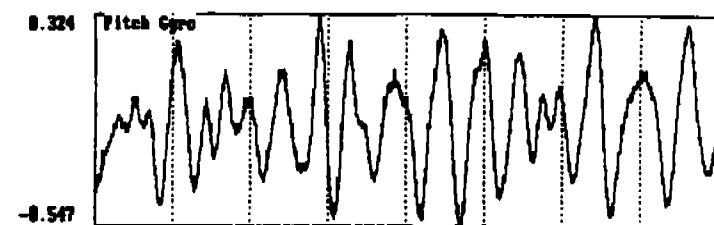
File: 13110.DAT  
Time: 23 OCT 88 - 13:11:41



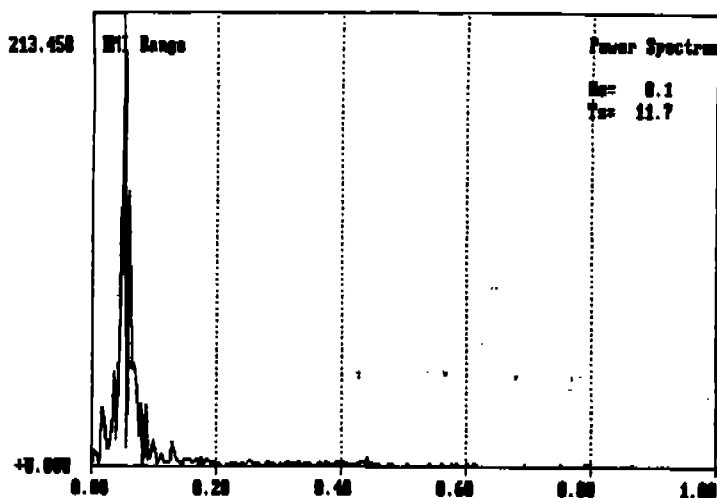
PITCH AND UNCORRECTED EMI RANGE



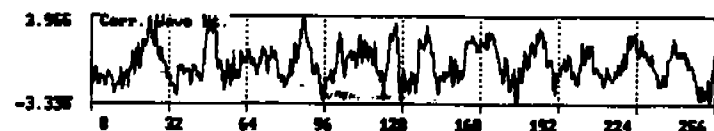
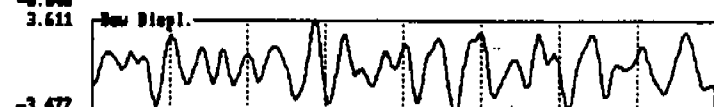
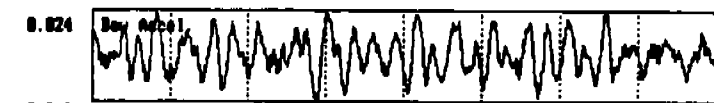
UNCORRECTED EMI RANGE SPECTRUM



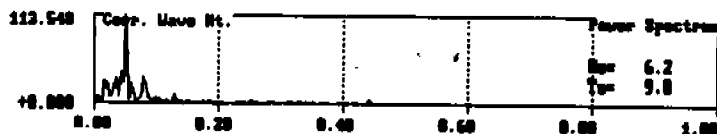
PITCH AND RECONSTRUCTED EMI RANGE



RECONSTRUCTED EMI RANGE SPECTRUM

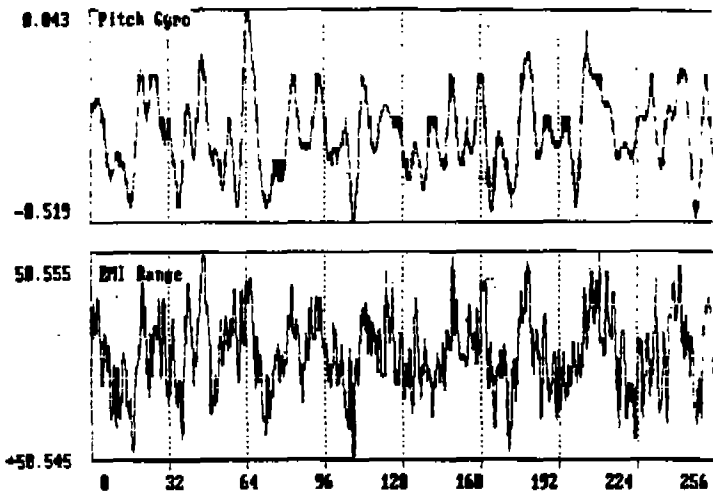


PARAMETER TIME SERIES

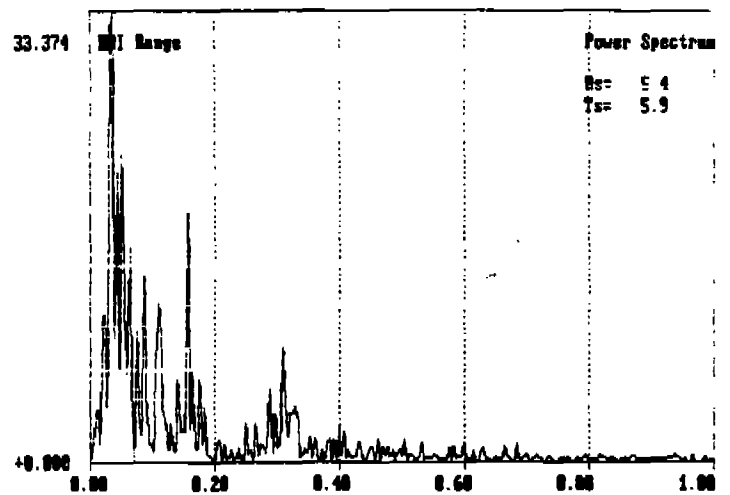


PARAMETER SPECTRA

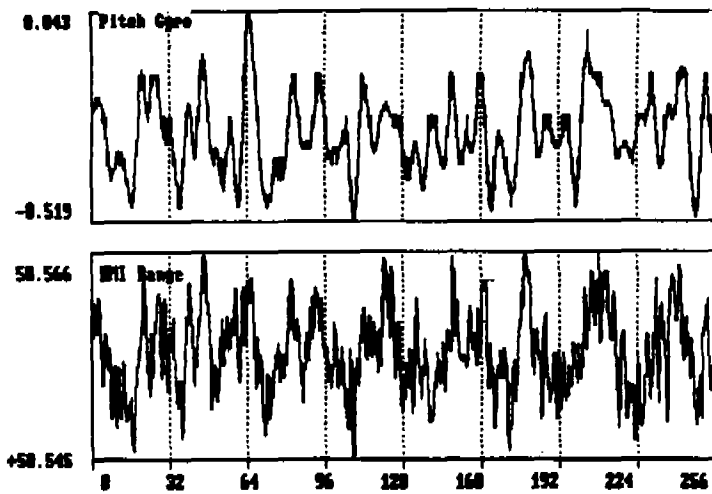
Figure 23  
SEA TRIAL DATA  
File: 165800.DAT  
Time: 23 OCT 88 - 17:03:47



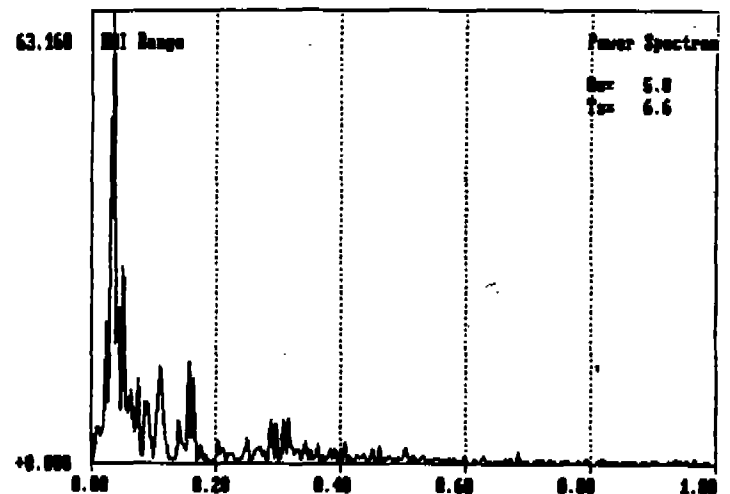
PITCH AND UNCORRECTED EMI RANGE



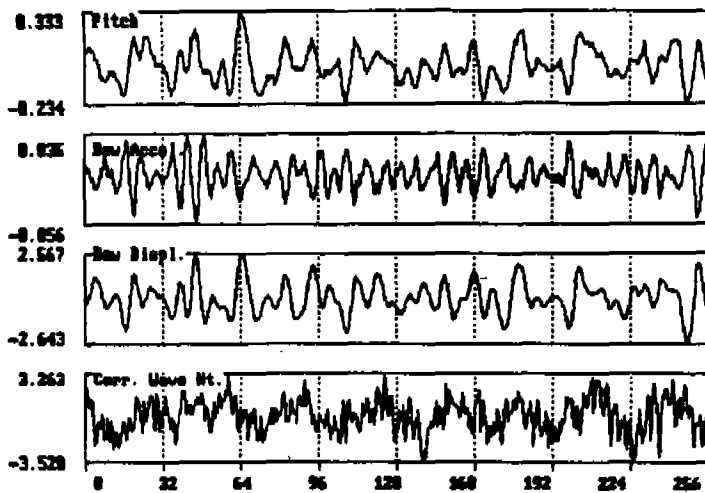
UNCORRECTED EMI RANGE SPECTRUM



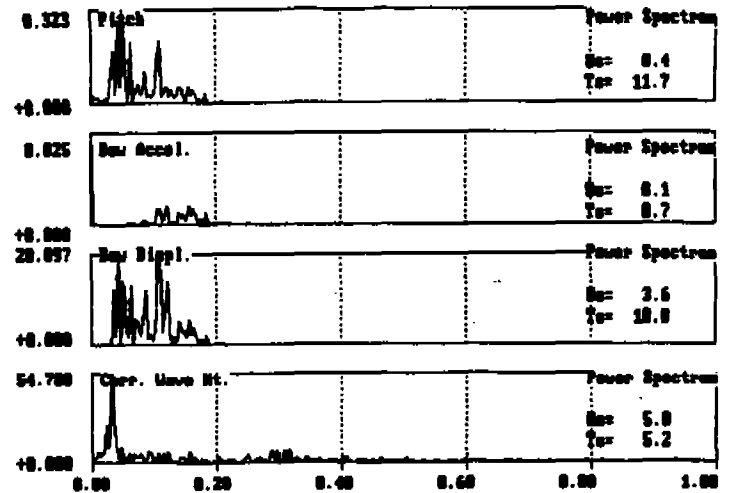
PITCH AND RECONSTRUCTED EMI RANGE



RECONSTRUCTED EMI RANGE SPECTRUM



PARAMETER TIME SERIES



PARAMETER SPECTRA

Figure 24  
SEA TRIAL DATA

File: 17480.DAT  
Time: 24 OCT 88 - 17:48:26

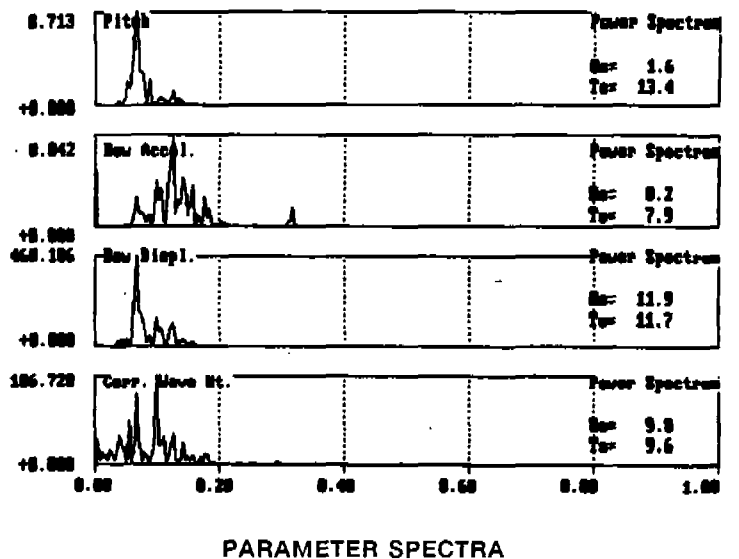
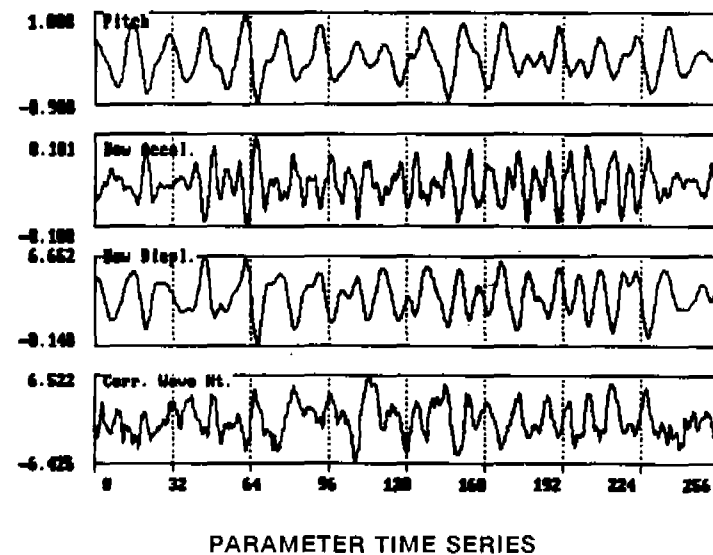
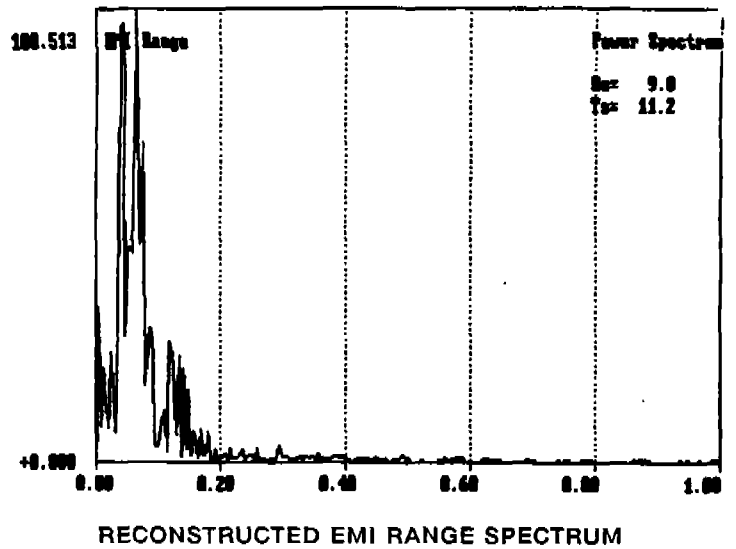
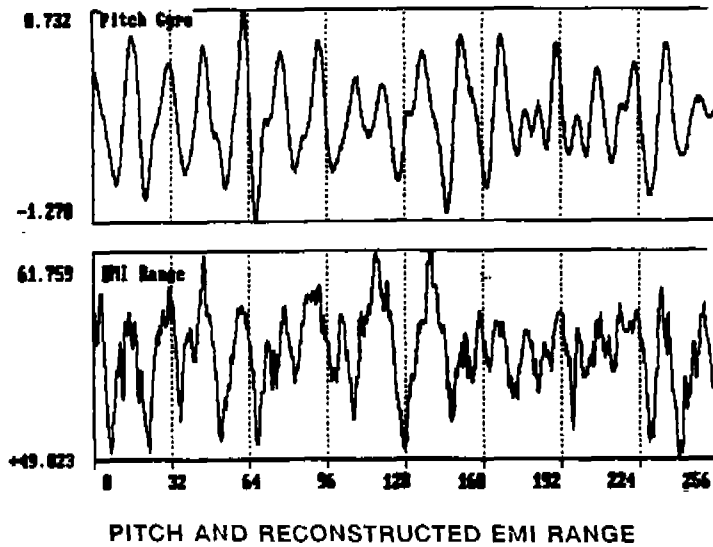
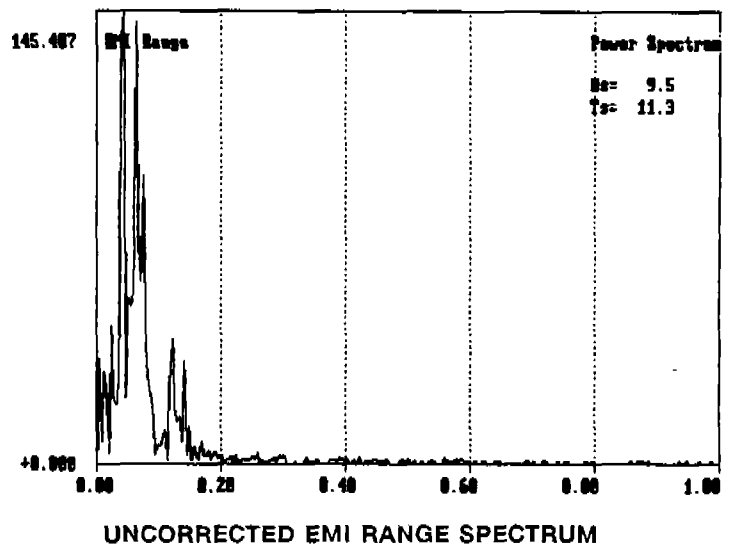
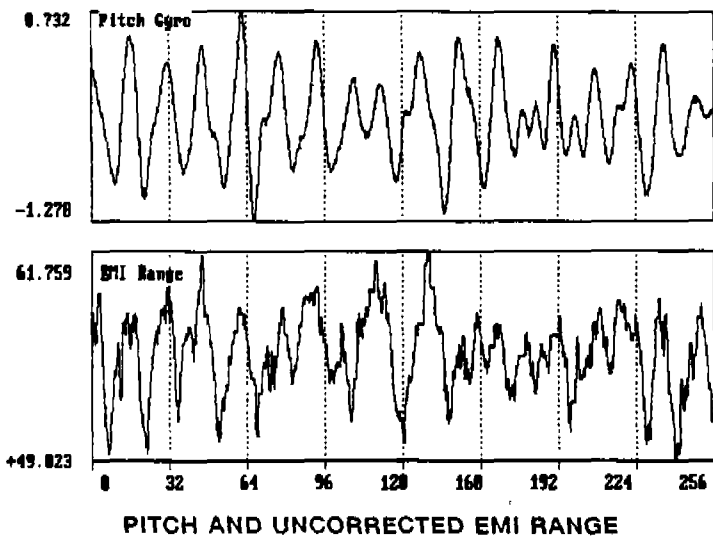
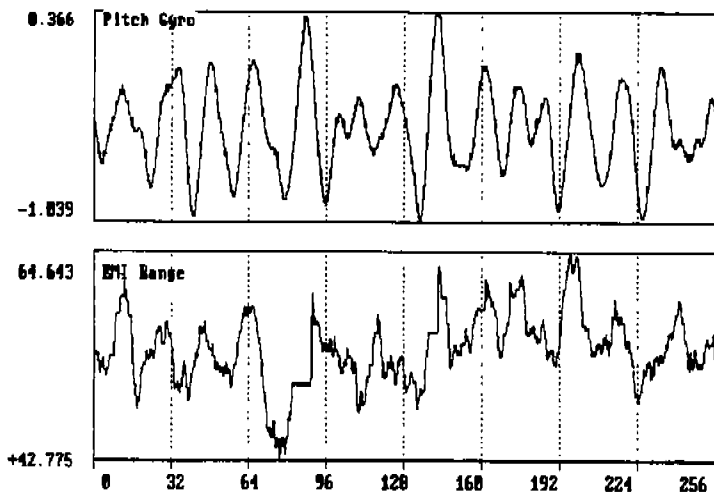
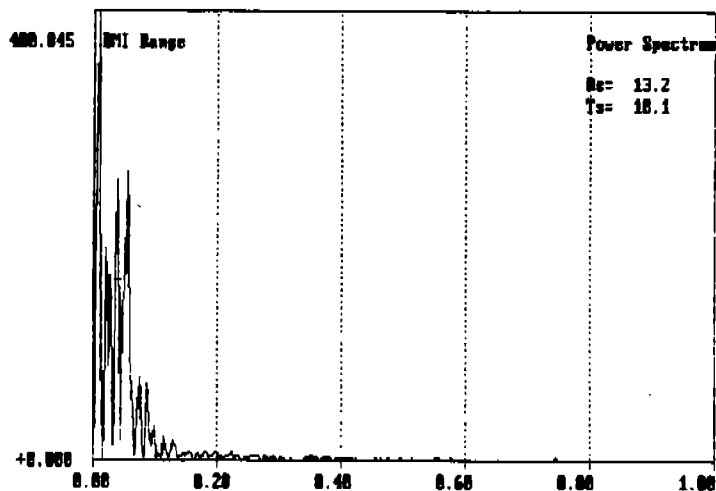


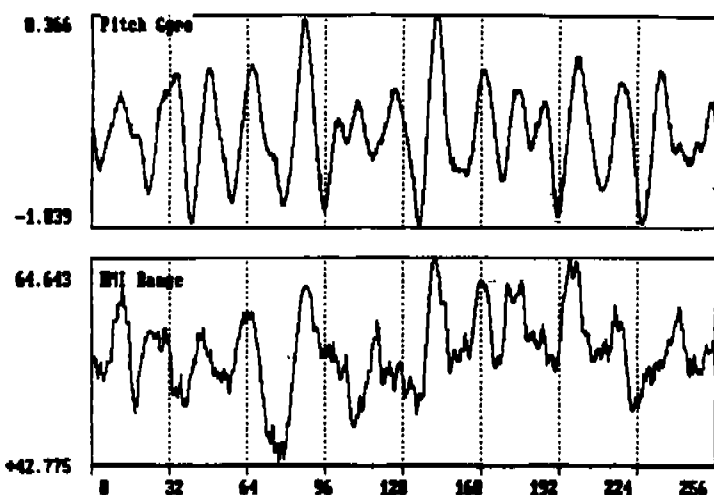
Figure 25  
SEA TRIAL DATA  
File: 12050.DAT  
Time: 21 OCT 88 - 12:05:20



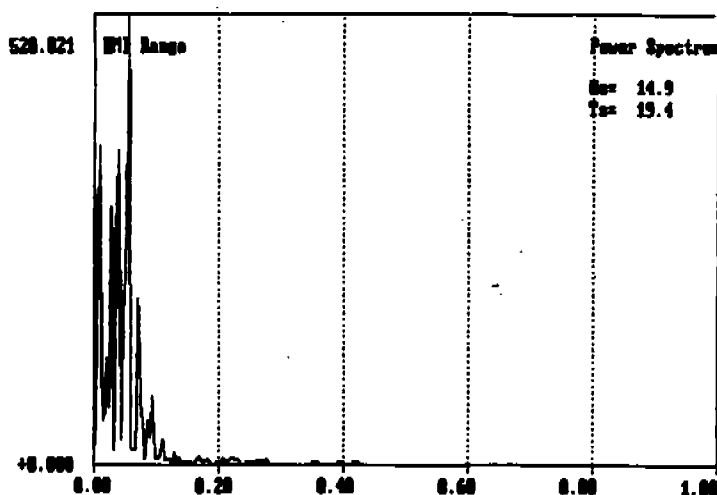
PITCH AND UNCORRECTED EMI RANGE



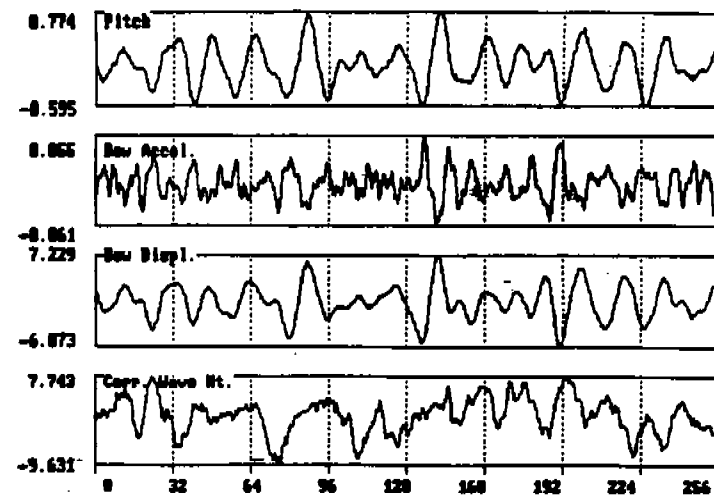
UNCORRECTED EMI RANGE SPECTRUM



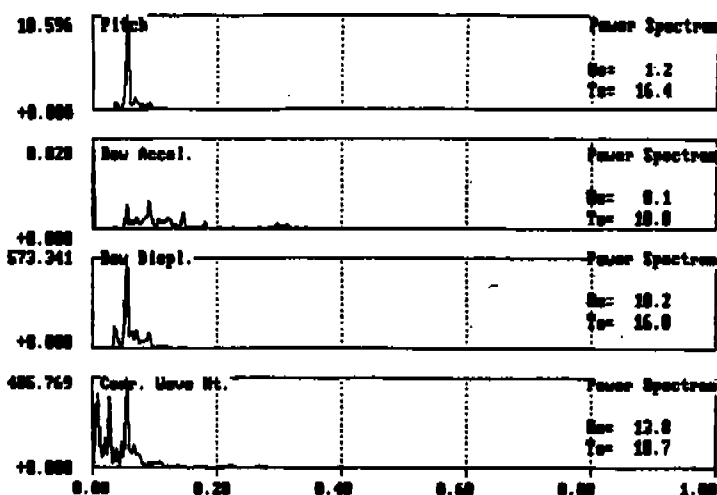
PITCH AND RECONSTRUCTED EMI RANGE



RECONSTRUCTED EMI RANGE SPECTRUM



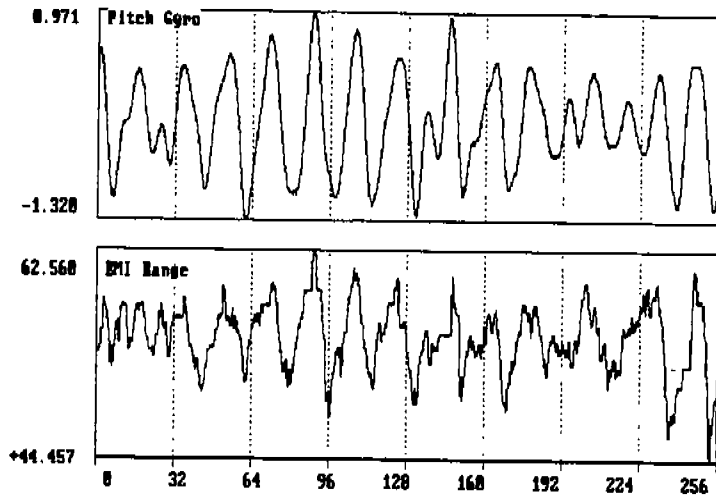
PARAMETER TIME SERIES



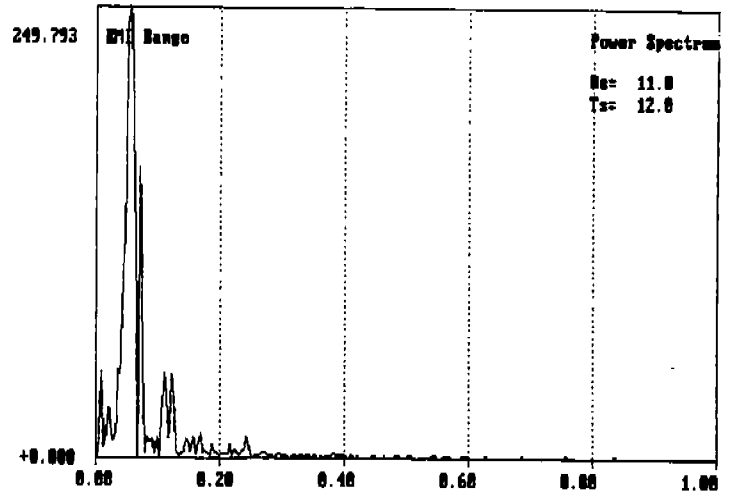
PARAMETER SPECTRA

Figure 26  
SEA TRIAL DATA

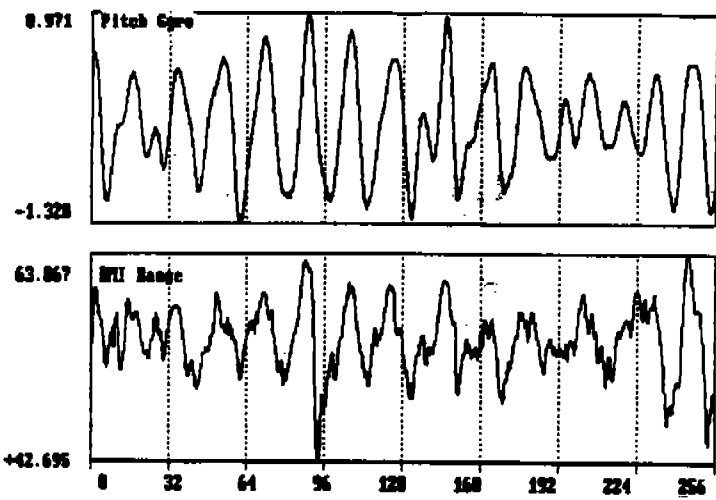
File: 12590.DAT  
Time: 22 OCT 88 - 12:59:24



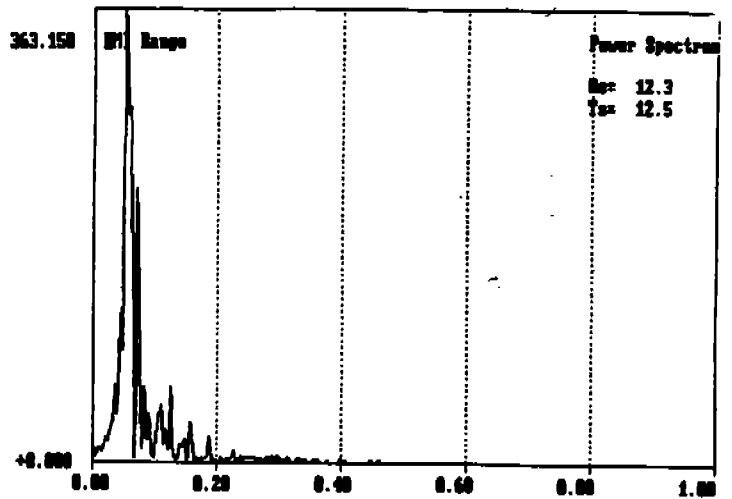
PITCH AND UNCORRECTED EMI RANGE



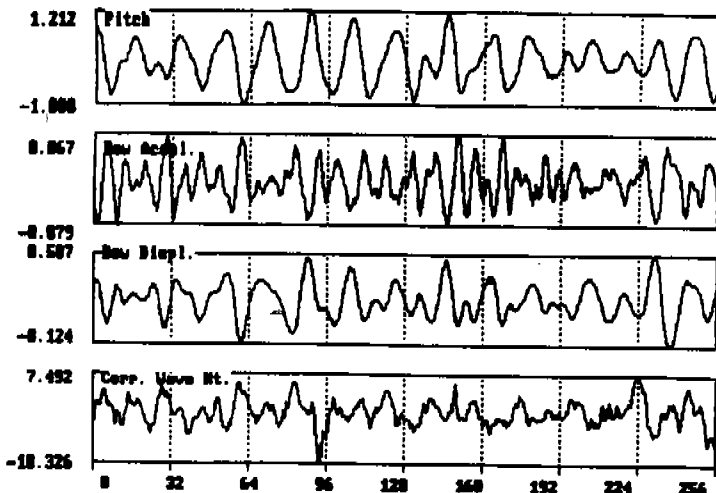
UNCORRECTED EMI RANGE SPECTRUM



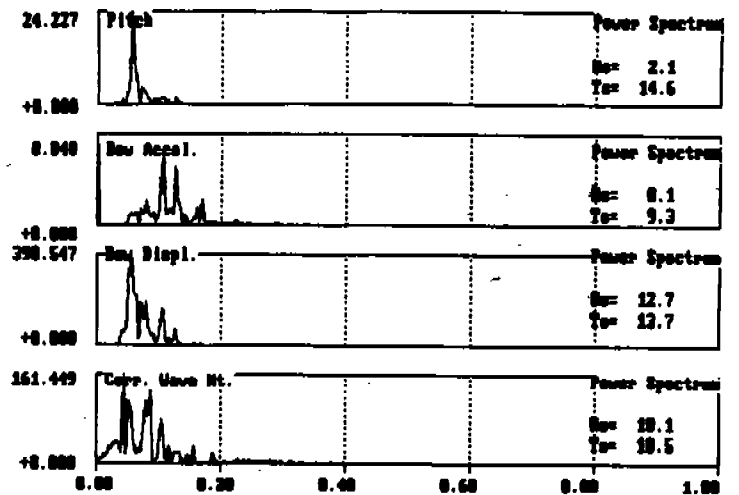
PITCH AND RECONSTRUCTED EMI RANGE



RECONSTRUCTED EMI RANGE SPECTRUM

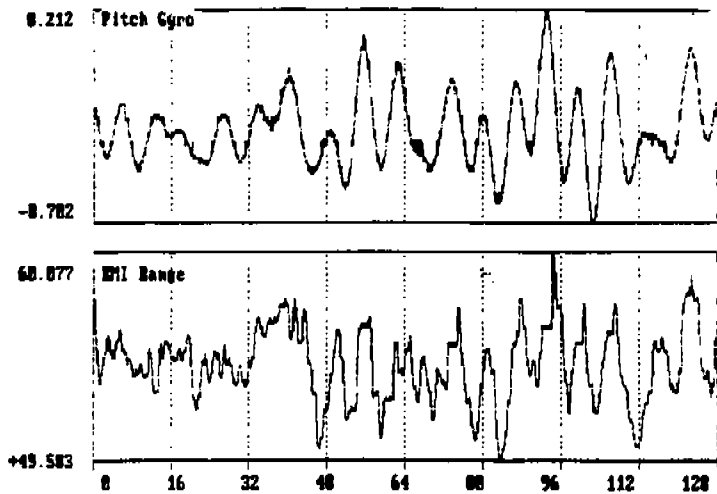


PARAMETER TIME SERIES

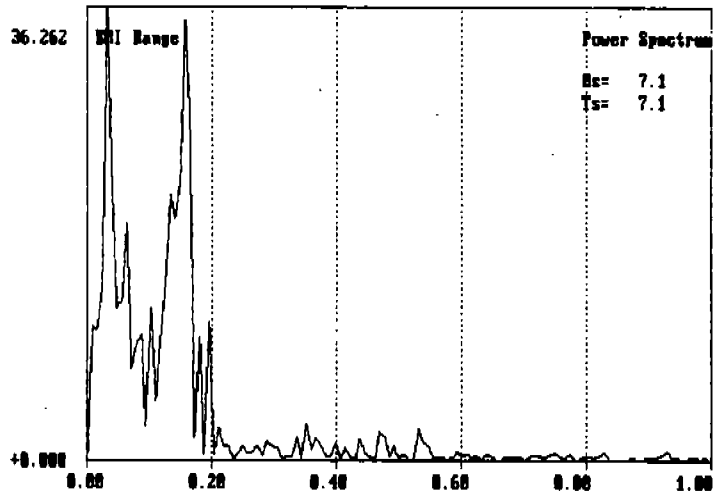


PARAMETER SPECTRA

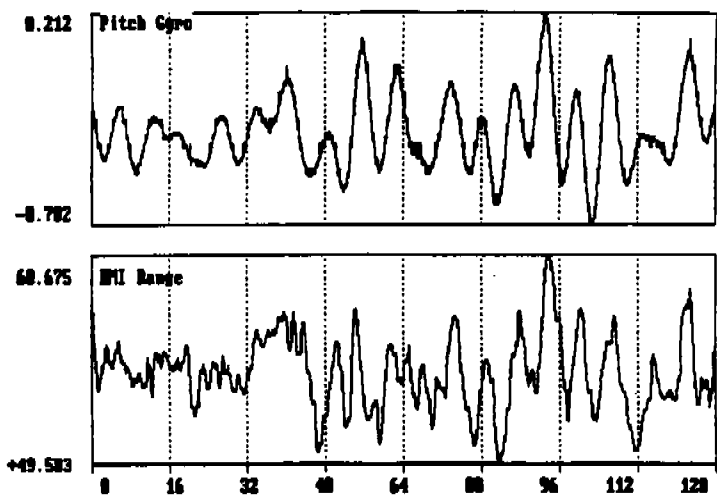
Figure 27  
SEA TRIAL DATA  
File: 17180.DAT  
Time: 21 OCT 88 - 17:18:20



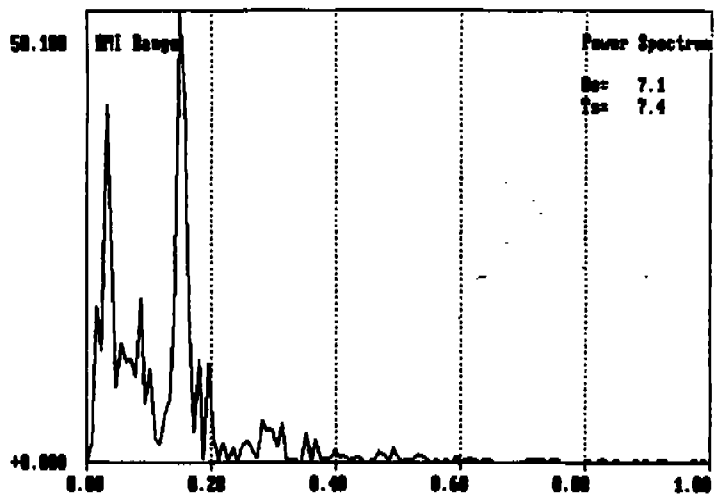
PITCH AND UNCORRECTED EMI RANGE



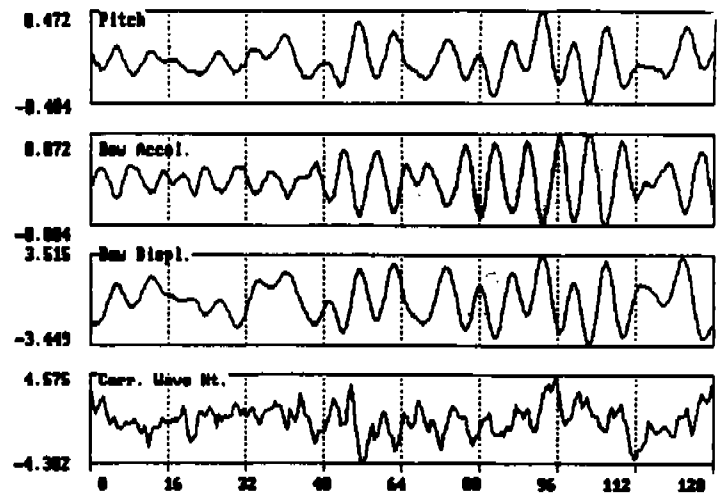
UNCORRECTED EMI RANGE SPECTRUM



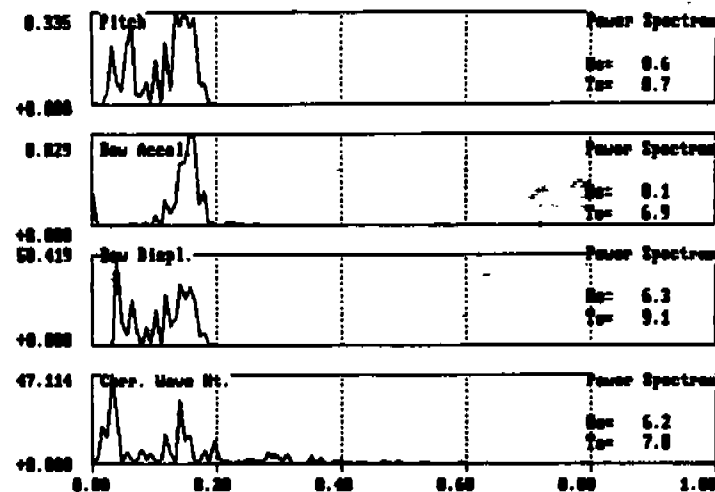
PITCH AND RECONSTRUCTED EMI RANGE



RECONSTRUCTED EMI RANGE SPECTRUM



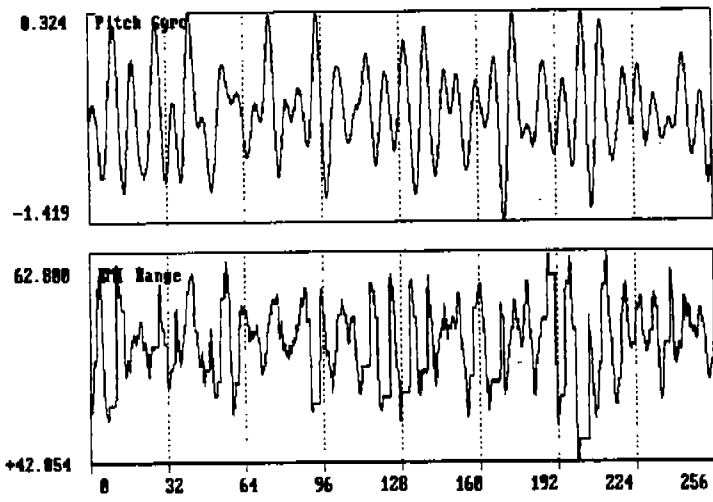
PARAMETER TIME SERIES



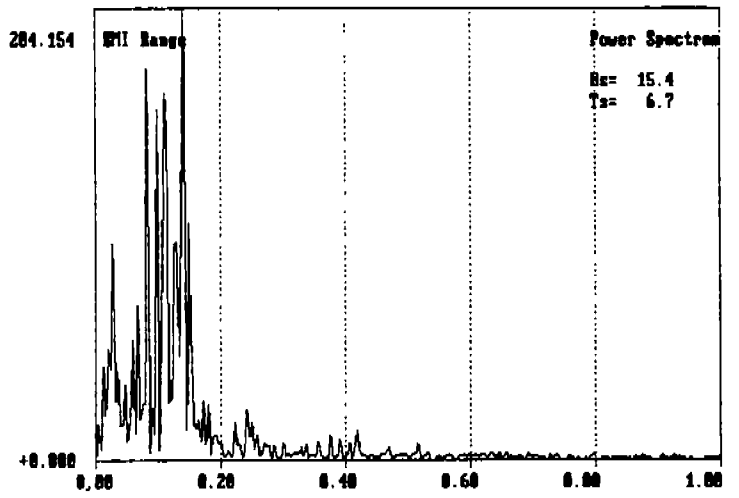
PARAMETER SPECTRA

Figure 28  
SEA TRIAL DATA

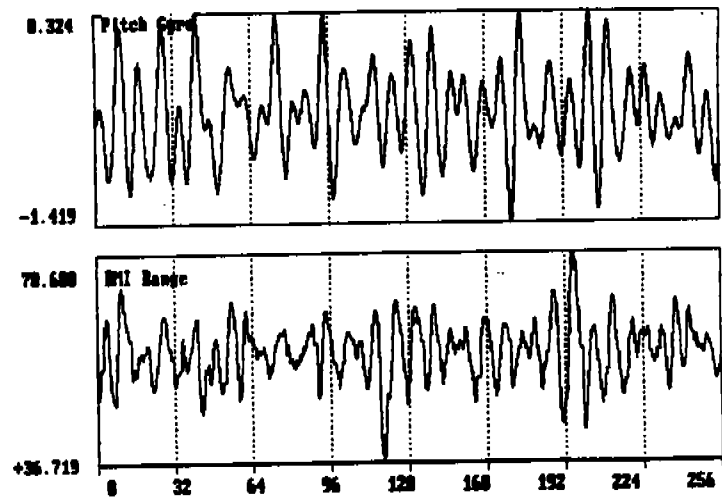
File: 134200.DAT  
Time: 24 OCT 88 - 13:44:43



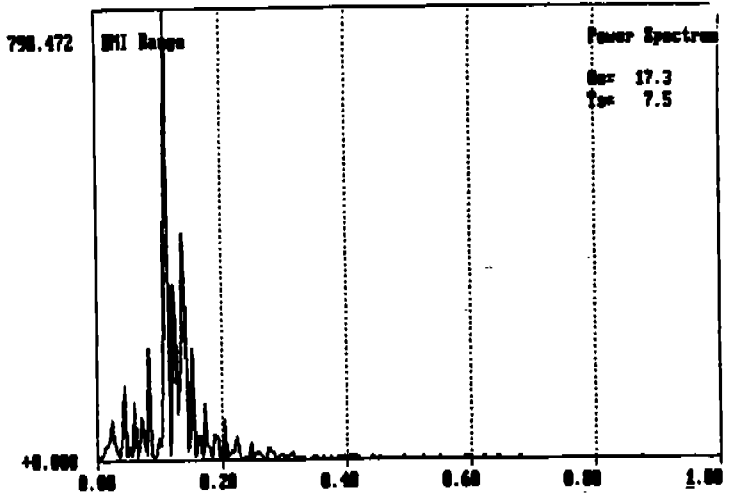
PITCH AND UNCORRECTED EMI RANGE



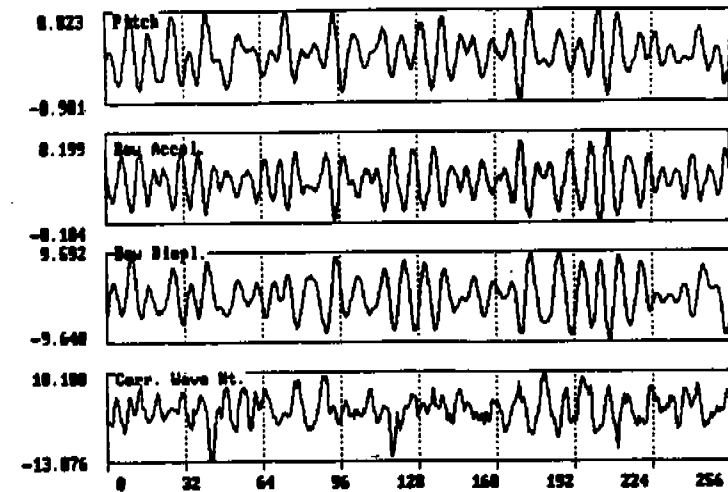
UNCORRECTED EMI RANGE SPECTRUM



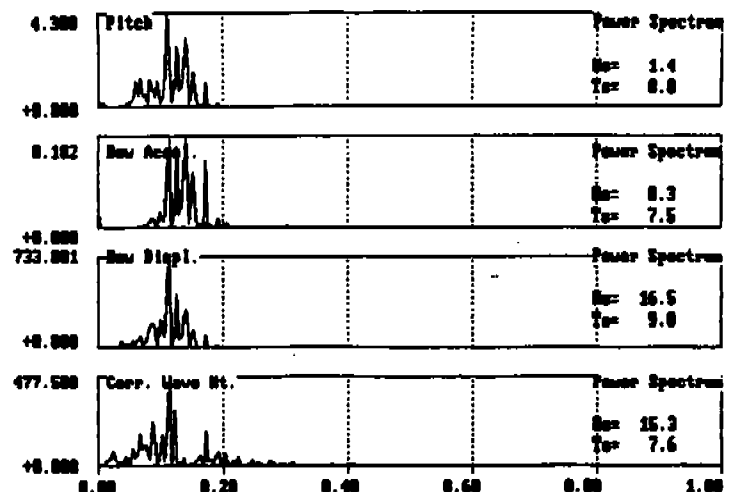
PITCH AND RECONSTRUCTED EMI RANGE



RECONSTRUCTED EMI RANGE SPECTRUM

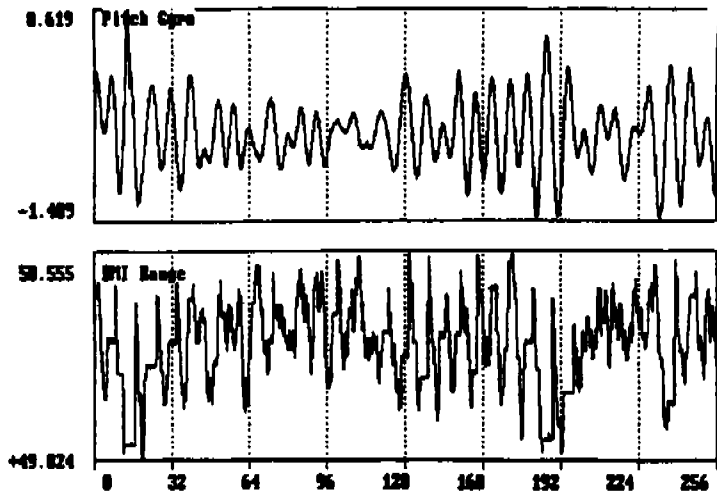


PARAMETER TIME SERIES

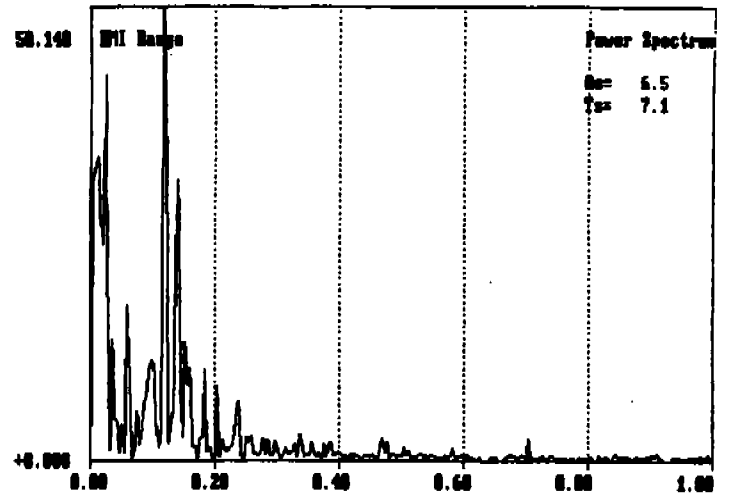


PARAMETER SPECTRA

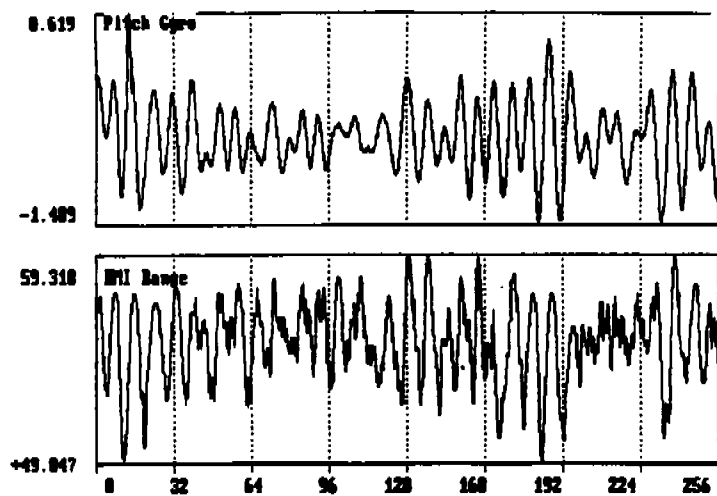
Figure 29  
SEA TRIAL DATA  
File: 14030.DAT  
Time: 20 OCT 88 - 14:03:55



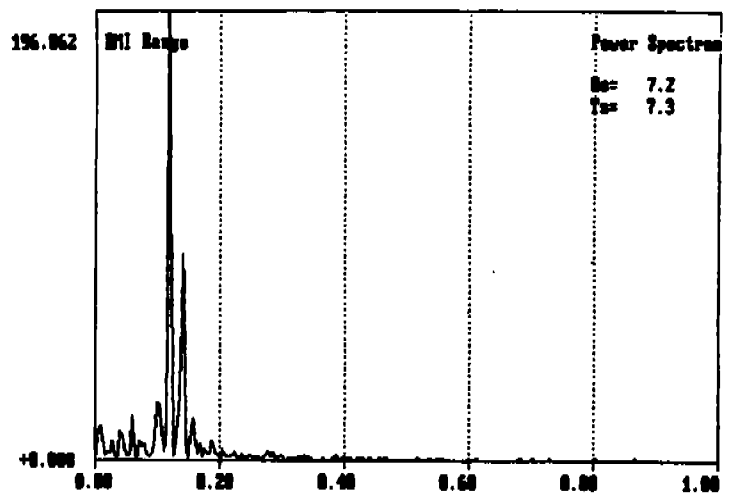
PITCH AND UNCORRECTED EMI RANGE



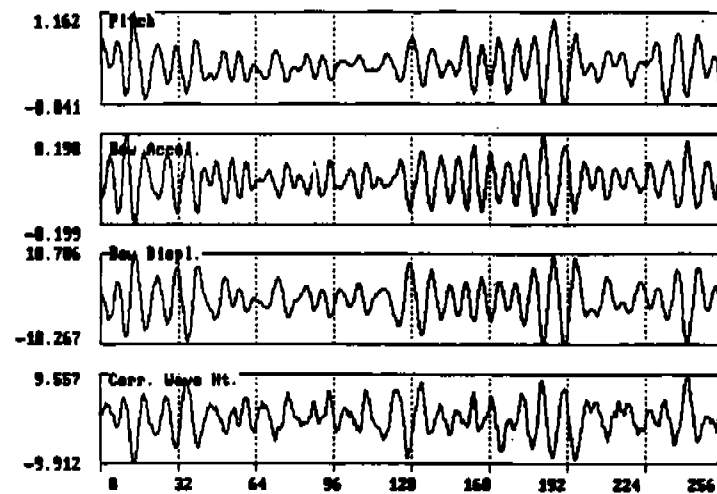
UNCORRECTED EMI RANGE SPECTRUM



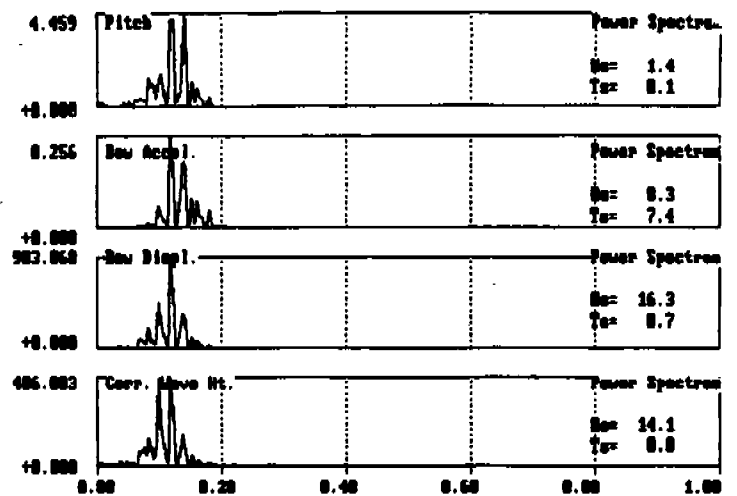
PITCH AND RECONSTRUCTED EMI RANGE



RECONSTRUCTED EMI RANGE SPECTRUM



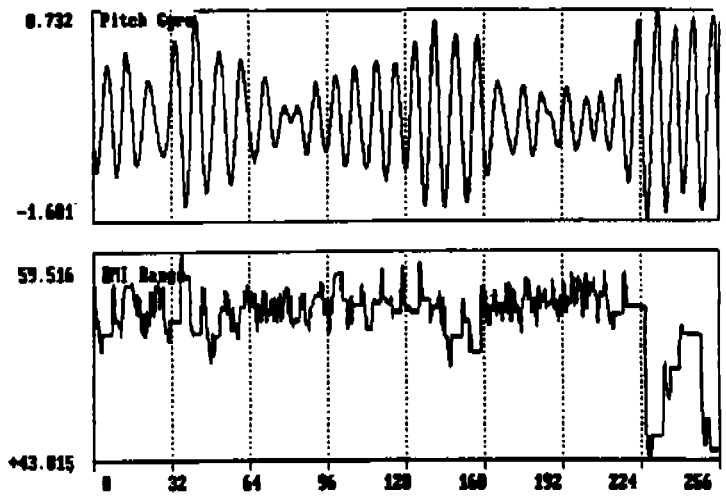
PARAMETER TIME SERIES



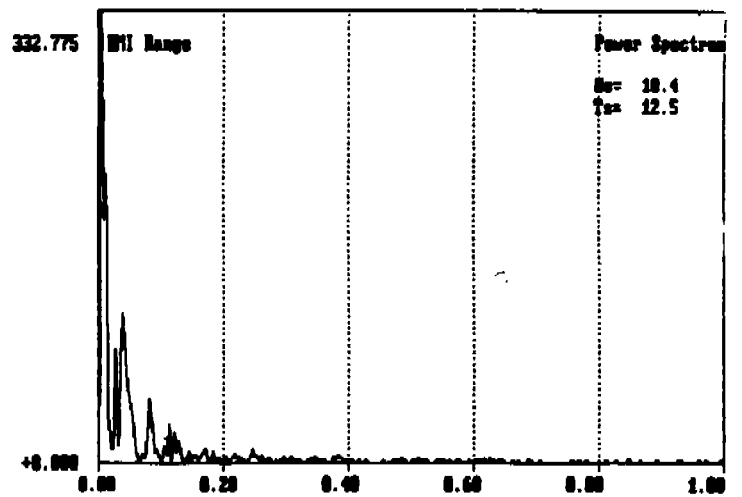
PARAMETER SPECTRA

Figure 30  
SEA TRIAL DATA

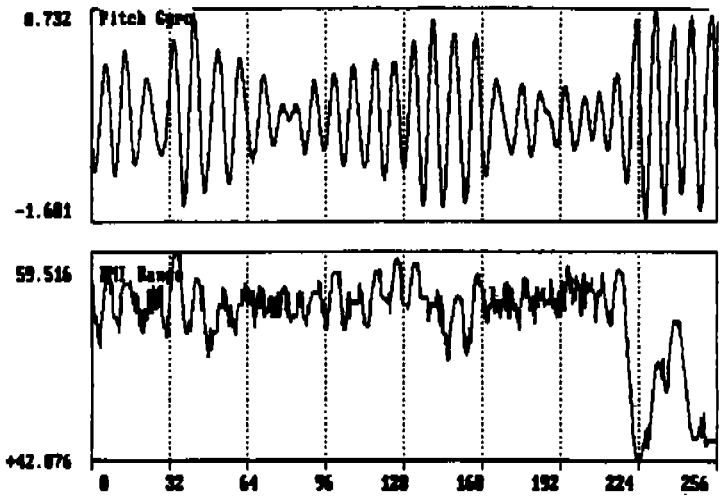
File: 083801.DAT  
Time: 20 OCT 88 - 09:15:10



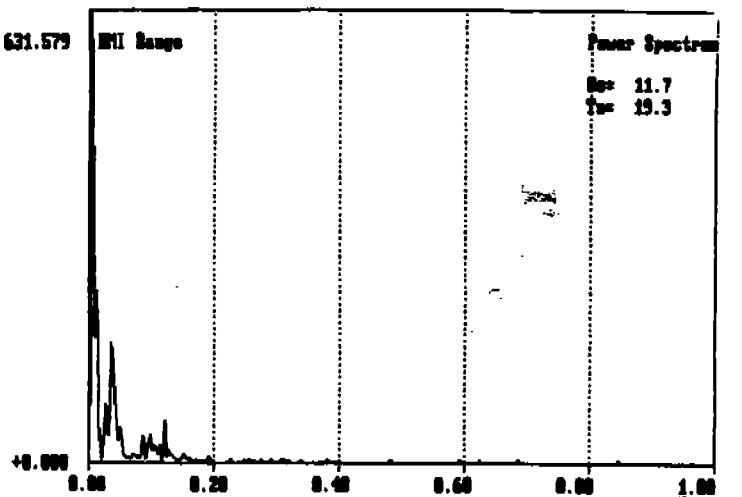
PITCH AND UNCORRECTED EMI RANGE



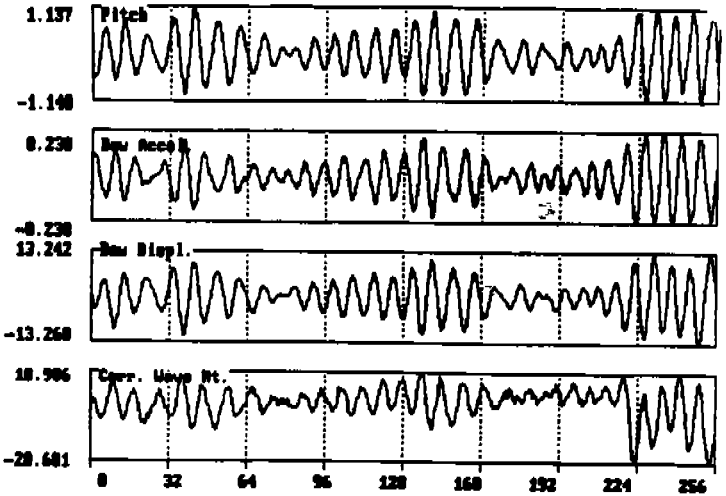
UNCORRECTED EMI RANGE SPECTRUM



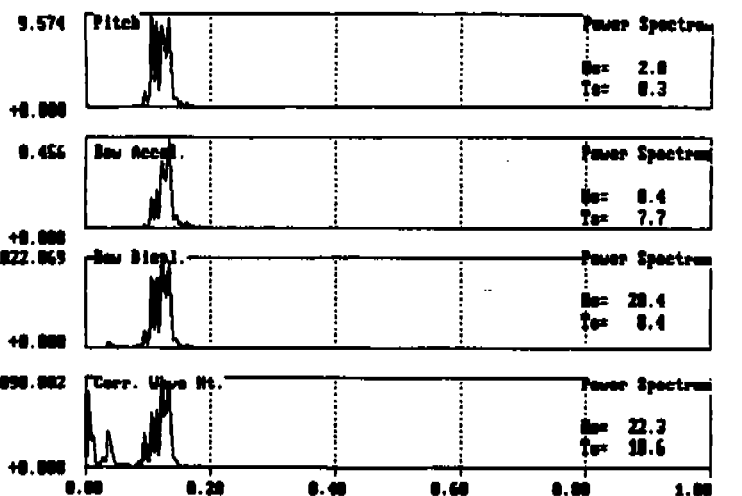
PITCH AND RECONSTRUCTED EMI RANGE



RECONSTRUCTED EMI RANGE SPECTRUM

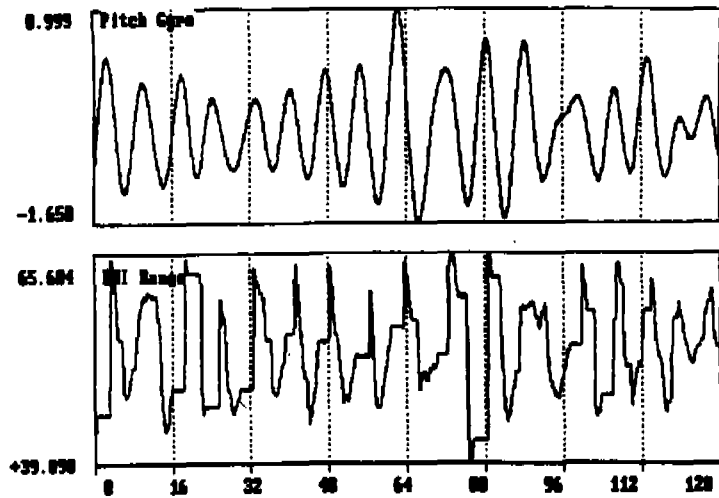


PARAMETER TIME SERIES

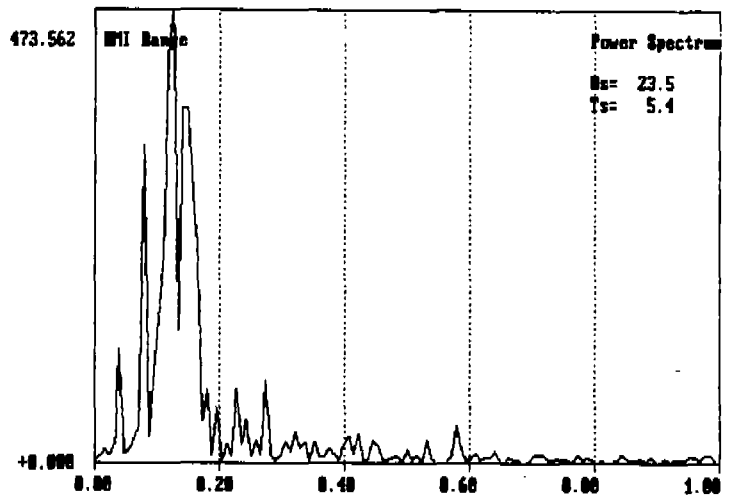


PARAMETER SPECTRA

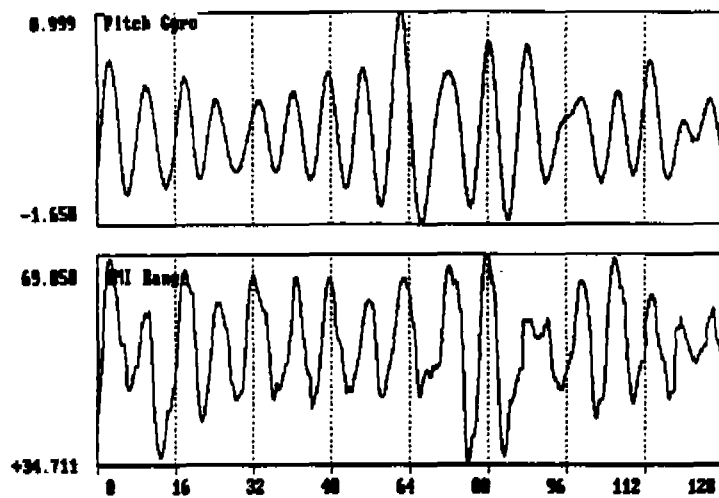
Figure 31  
SEA TRIAL DATA  
File: 08220.DAT  
Time: 19 OCT 88 - 08:22:52



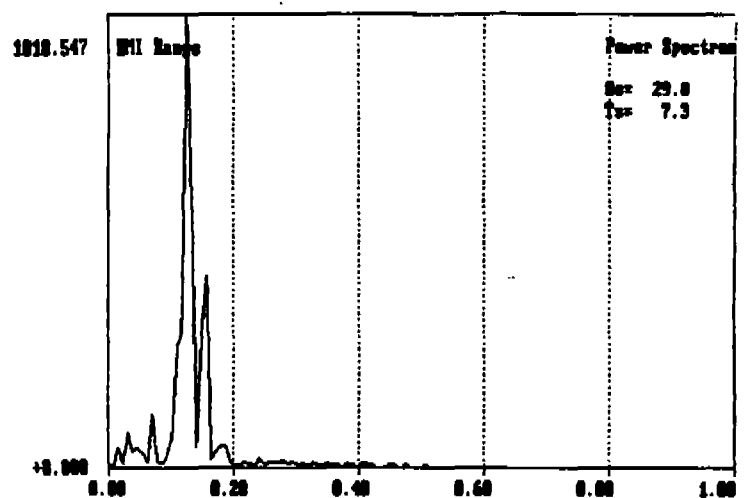
PITCH AND UNCORRECTED EMI RANGE



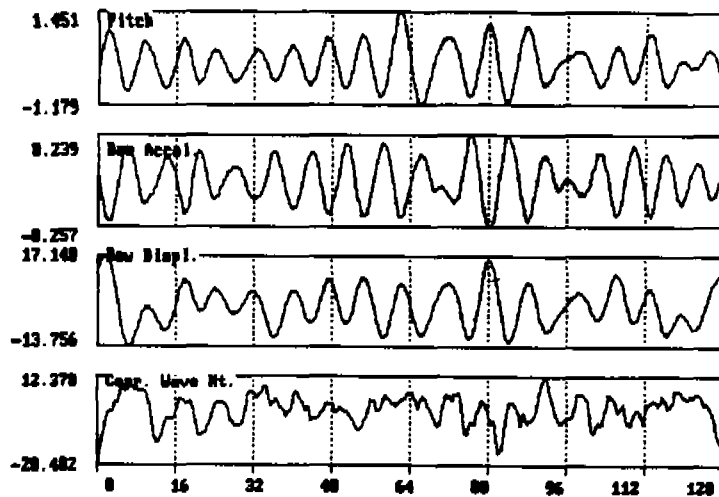
UNCORRECTED EMI RANGE SPECTRUM



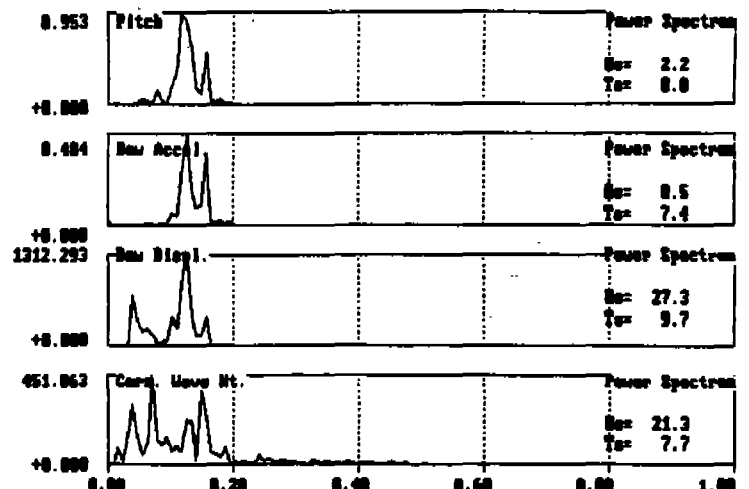
PITCH AND RECONSTRUCTED EMI RANGE



RECONSTRUCTED EMI RANGE SPECTRUM

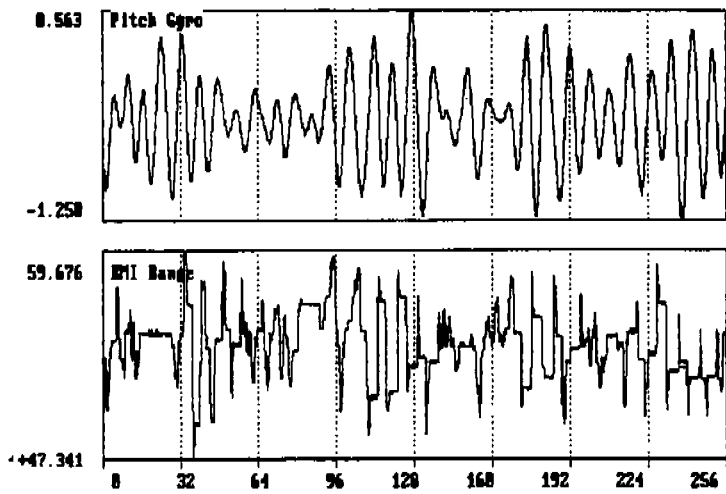


PARAMETER TIME SERIES

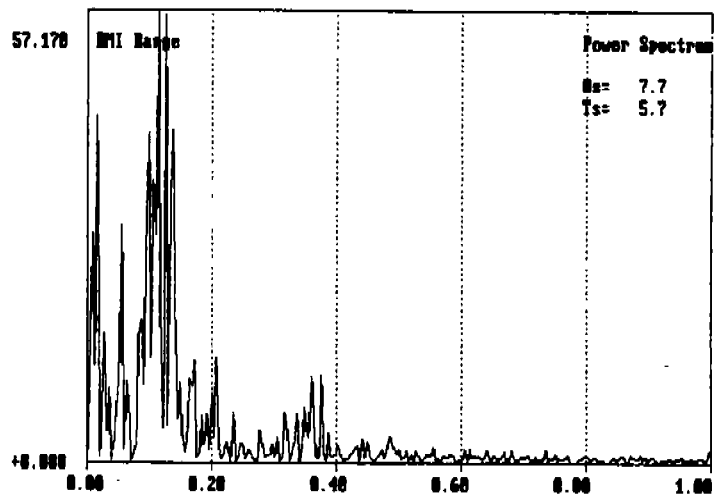


PARAMETER SPECTRA

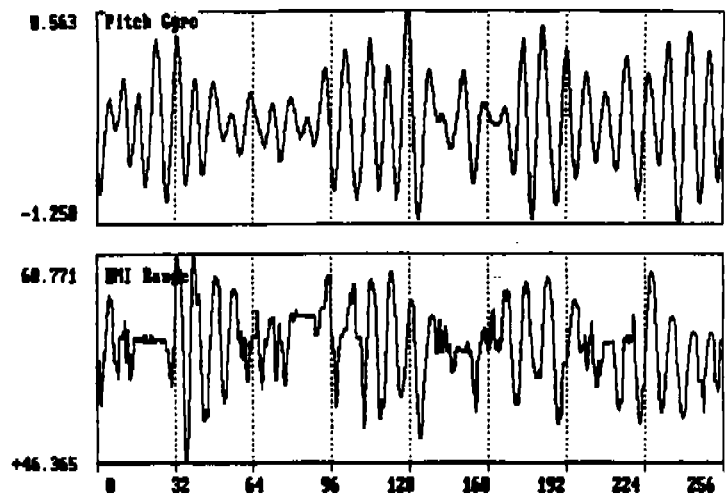
Figure 32  
SEA TRIAL DATA  
File: @16Hz0.DAT  
Time: 20 OCT 88 - 14:54:47



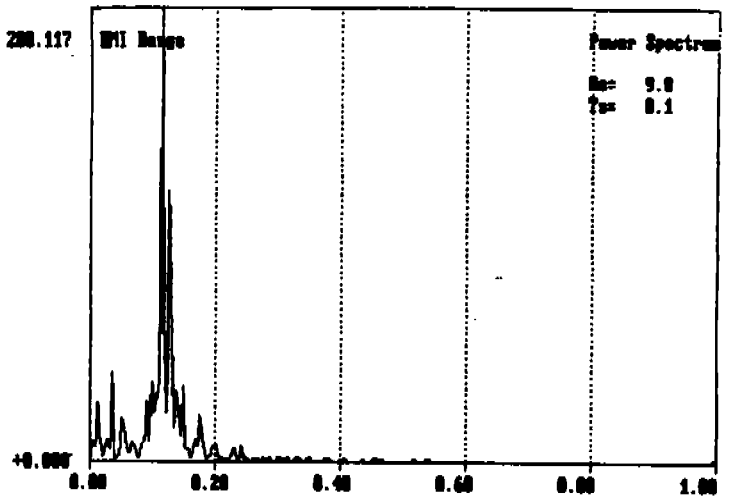
PITCH AND UNCORRECTED EMI RANGE



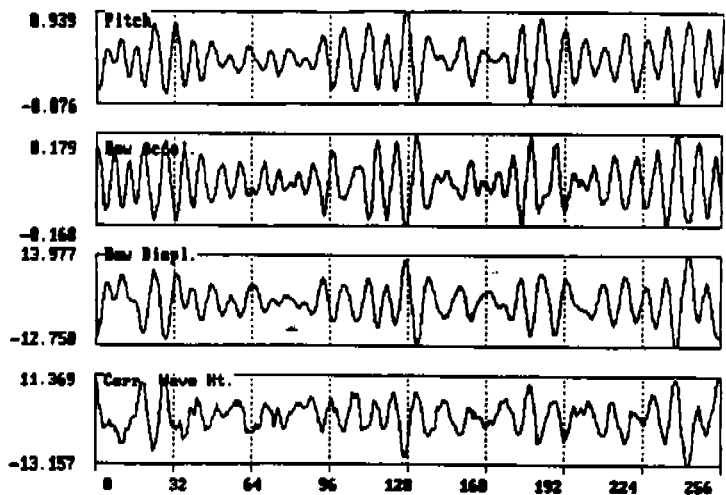
UNCORRECTED EMI RANGE SPECTRUM



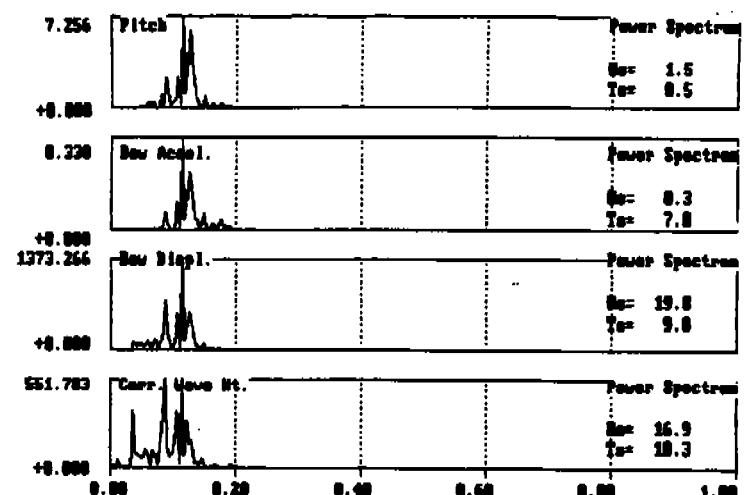
PITCH AND RECONSTRUCTED EMI RANGE



RECONSTRUCTED EMI RANGE SPECTRUM

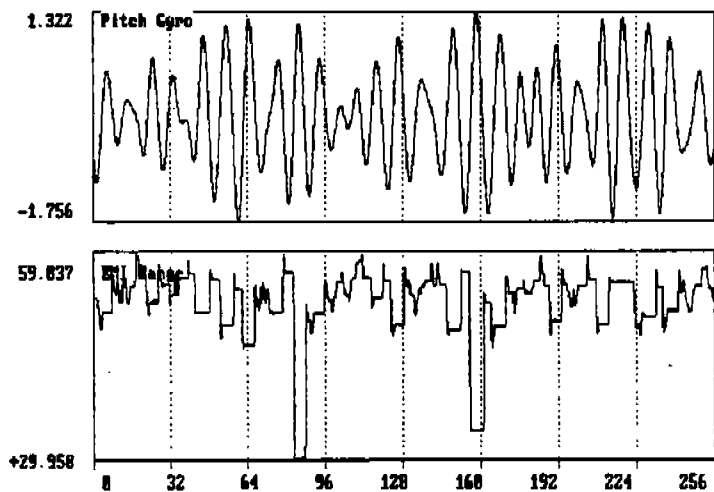


PARAMETER TIME SERIES

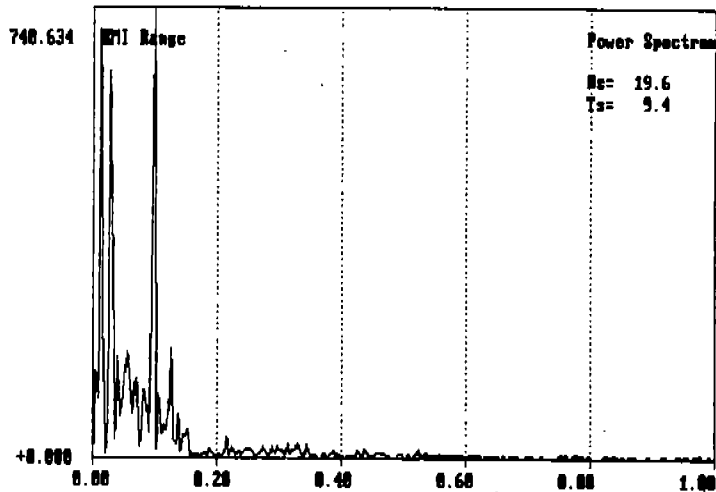


PARAMETER SPECTRA

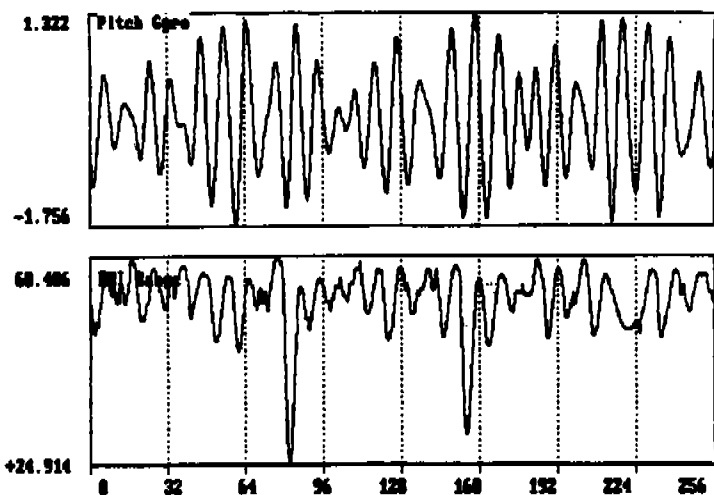
Figure 33  
SEA TRIAL DATA  
File: 08380.DAT  
Time: 20 OCT 88 -- 08:38:01



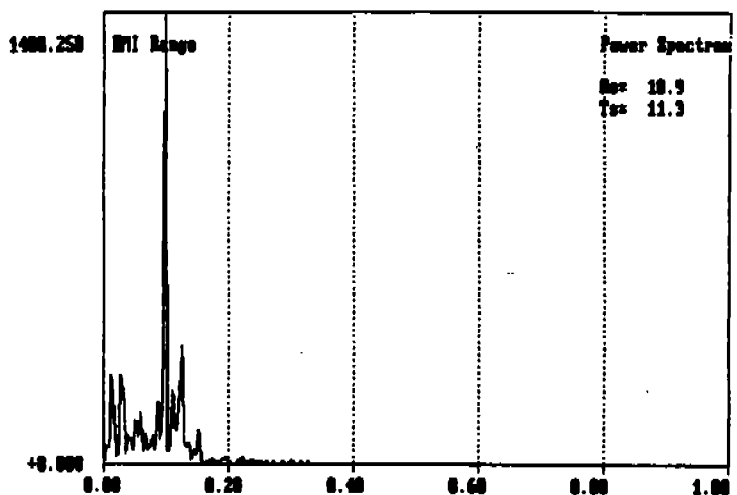
PITCH AND UNCORRECTED EMI RANGE



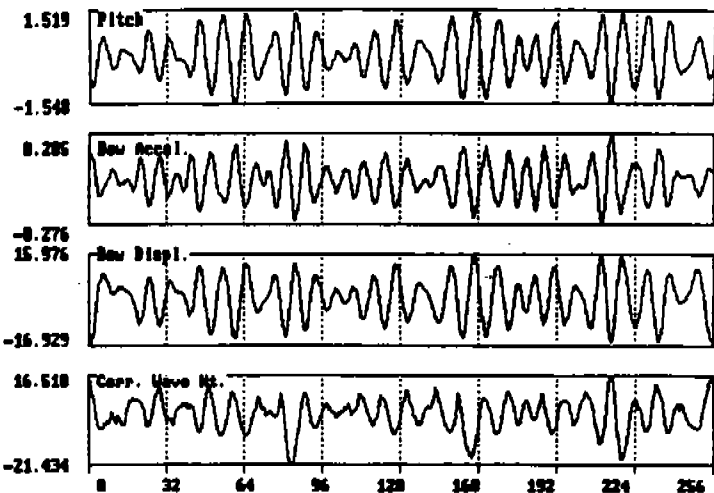
UNCORRECTED EMI RANGE SPECTRUM



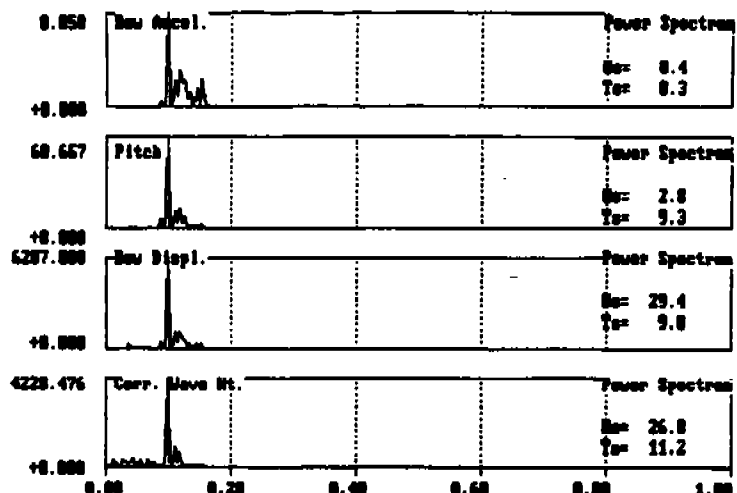
PITCH AND RECONSTRUCTED EMI RANGE



RECONSTRUCTED EMI RANGE SPECTRUM



PARAMETER TIME SERIES



PARAMETER SPECTRA

Figure 34  
SEA TRIAL DATA

File: 17550.DAT

Time: 19 OCT 88 - 17:55:31

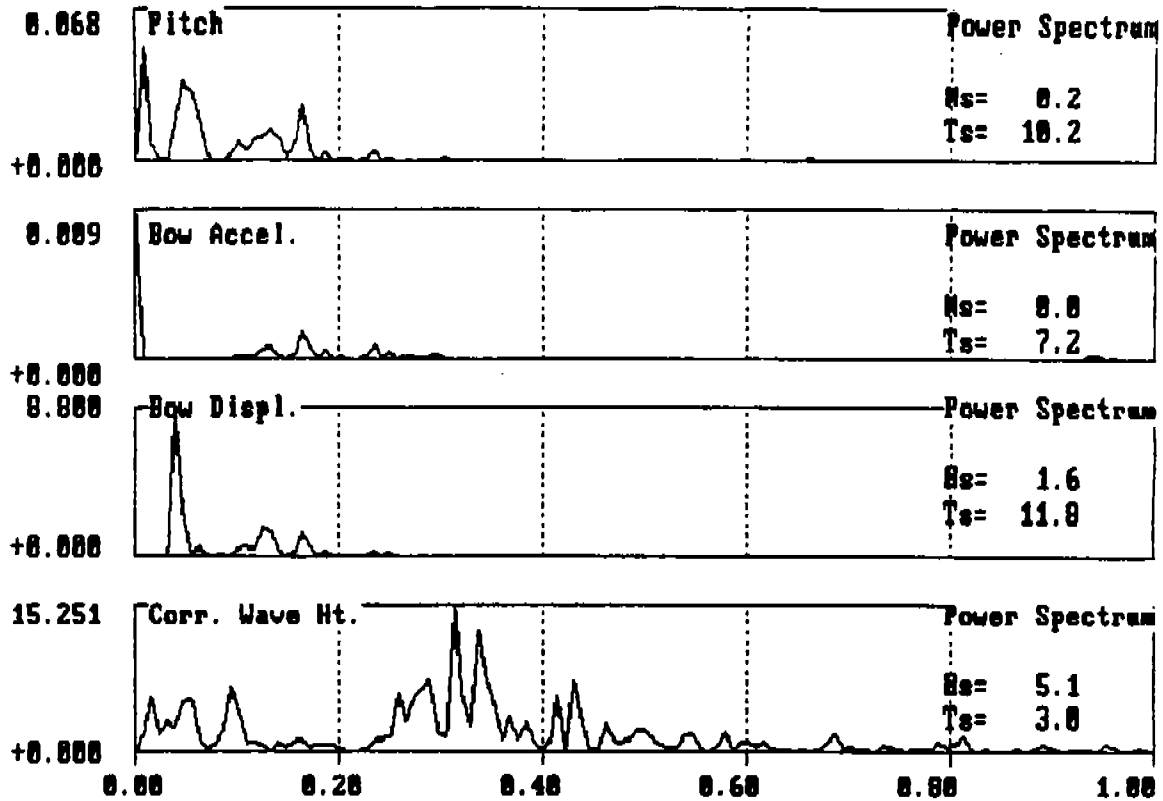
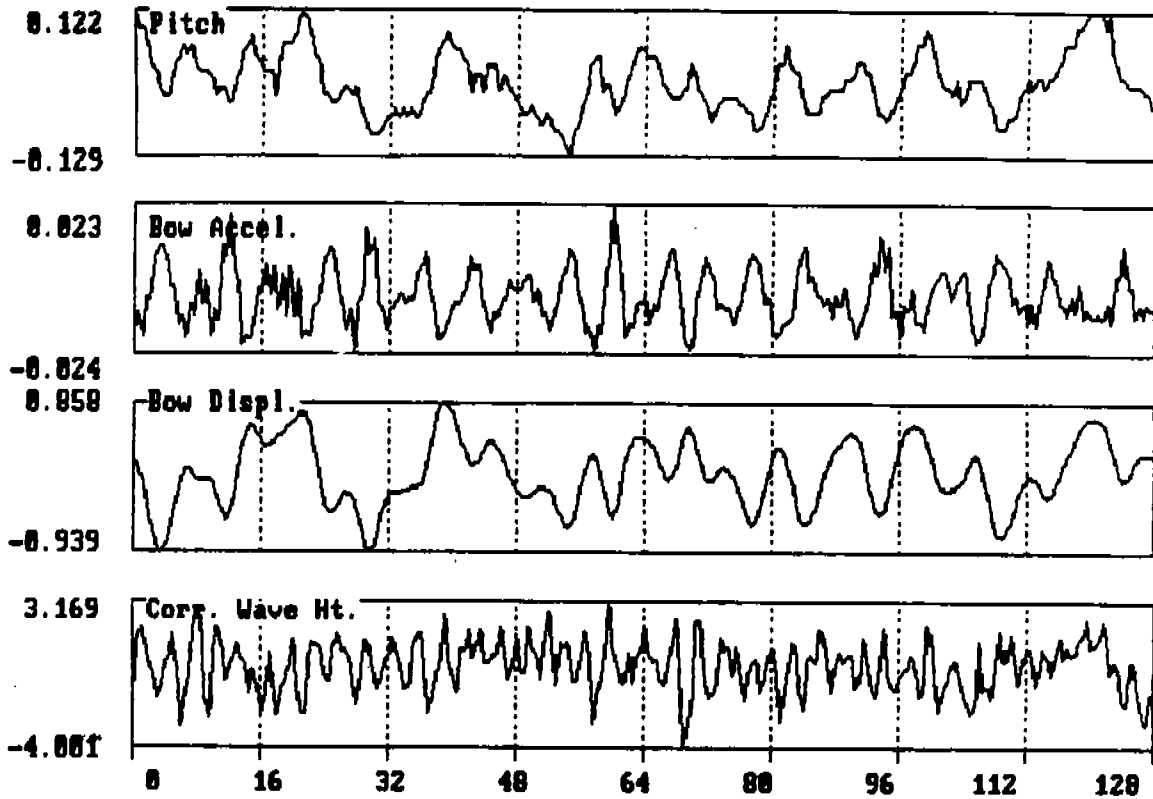


Figure 35  
 PARAMETER TIME SERIES  
 (NON-FLAT SPOT RECONSTRUCTED)

File: 131800.DAT  
 Time: 25 OCT 88 - 13:21:51

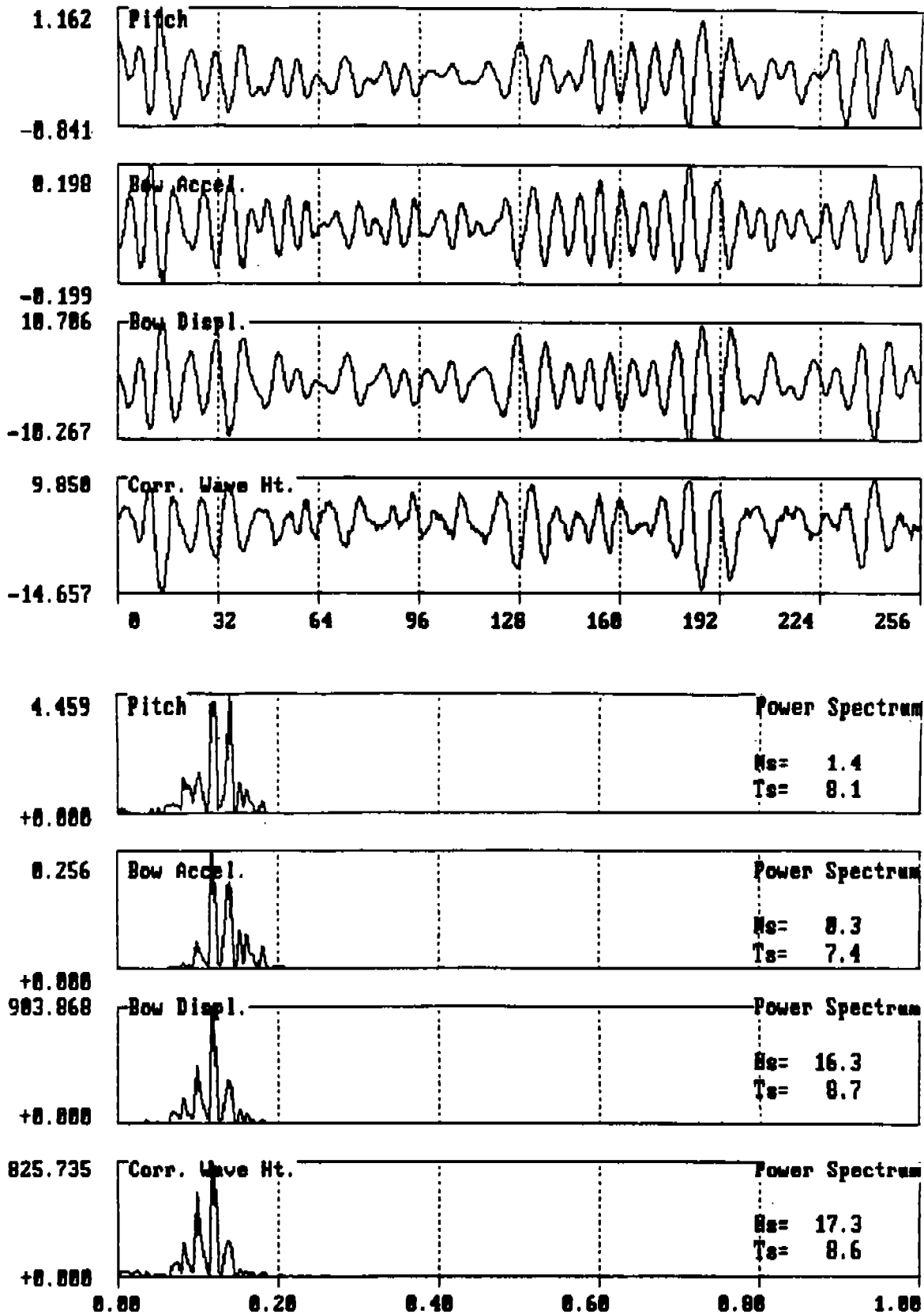


Figure 36  
 PARAMETER TIME SERIES  
 (NON-FLAT SPOT RECONSTRUCTED)

File: 083801.DAT  
 Time: 20 OCT 88 - 09:15:10

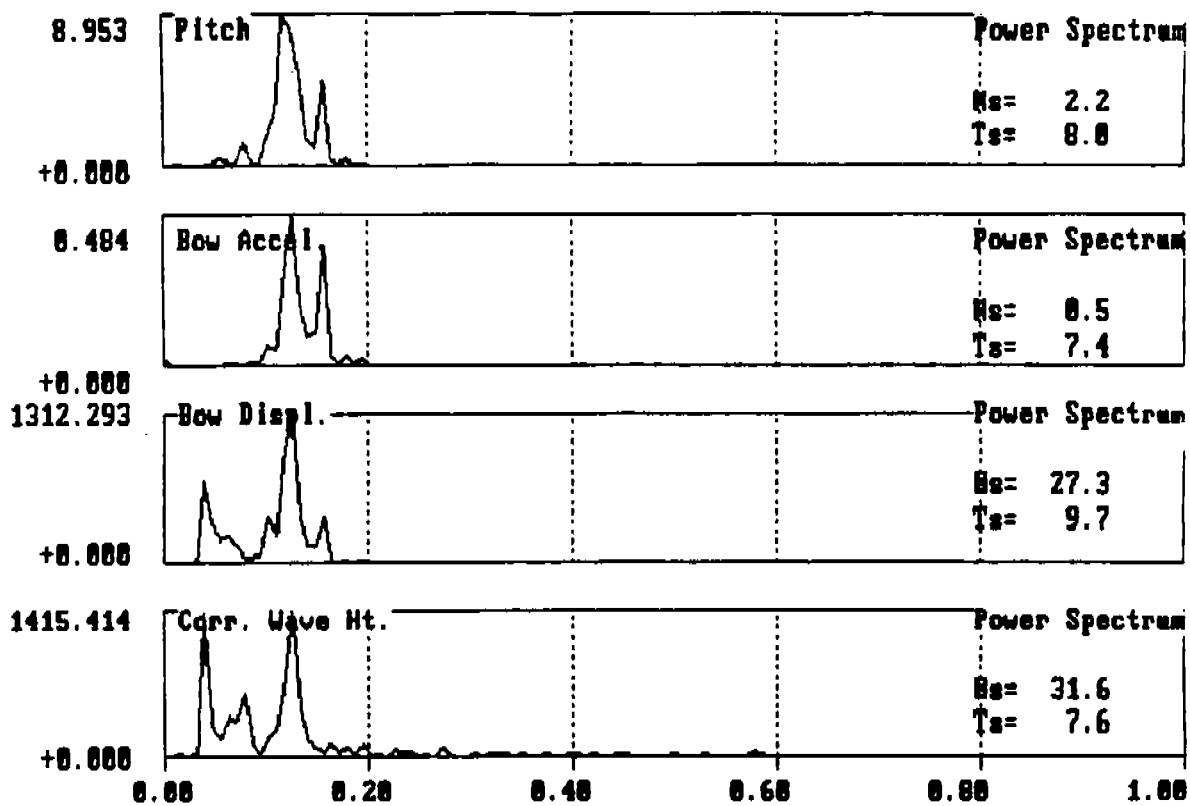
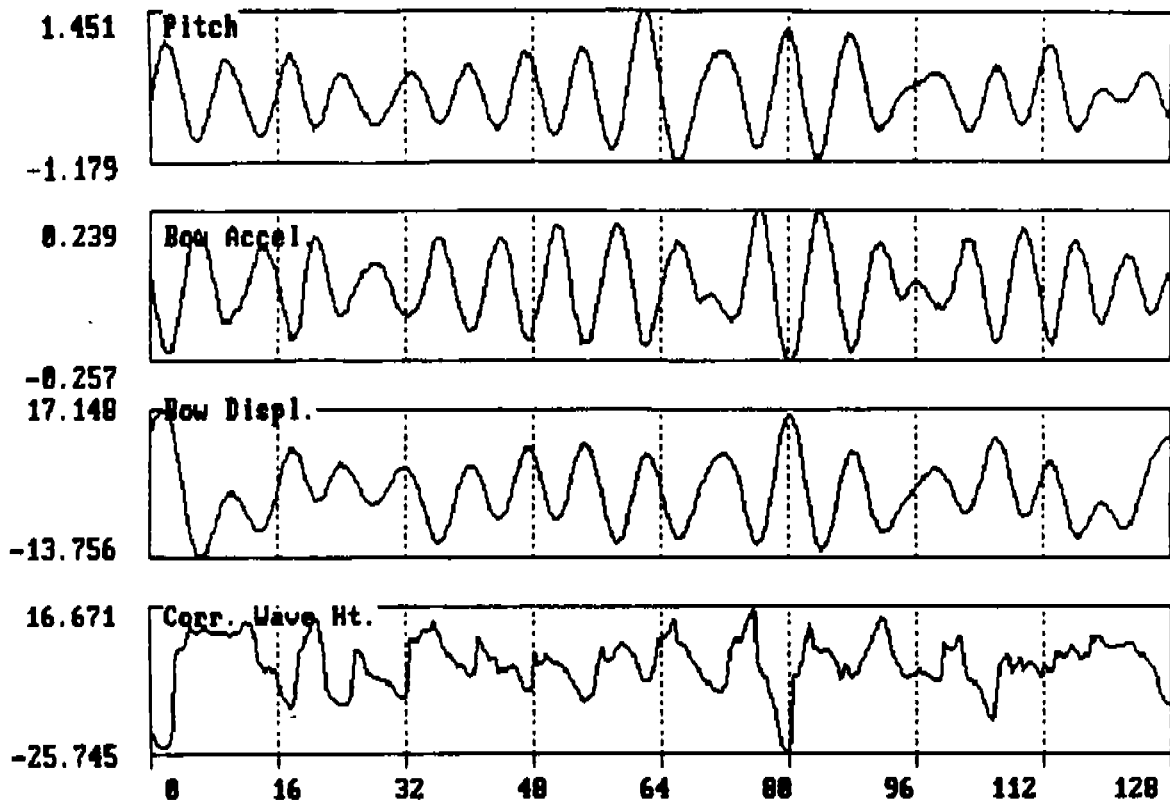


Figure 37  
 PARAMETER TIME SERIES  
 (NON-FLAT SPOT RECONSTRUCTED)

File: @16Hz0.DAT  
 Time: 20 OCT 88 - 14:54:47

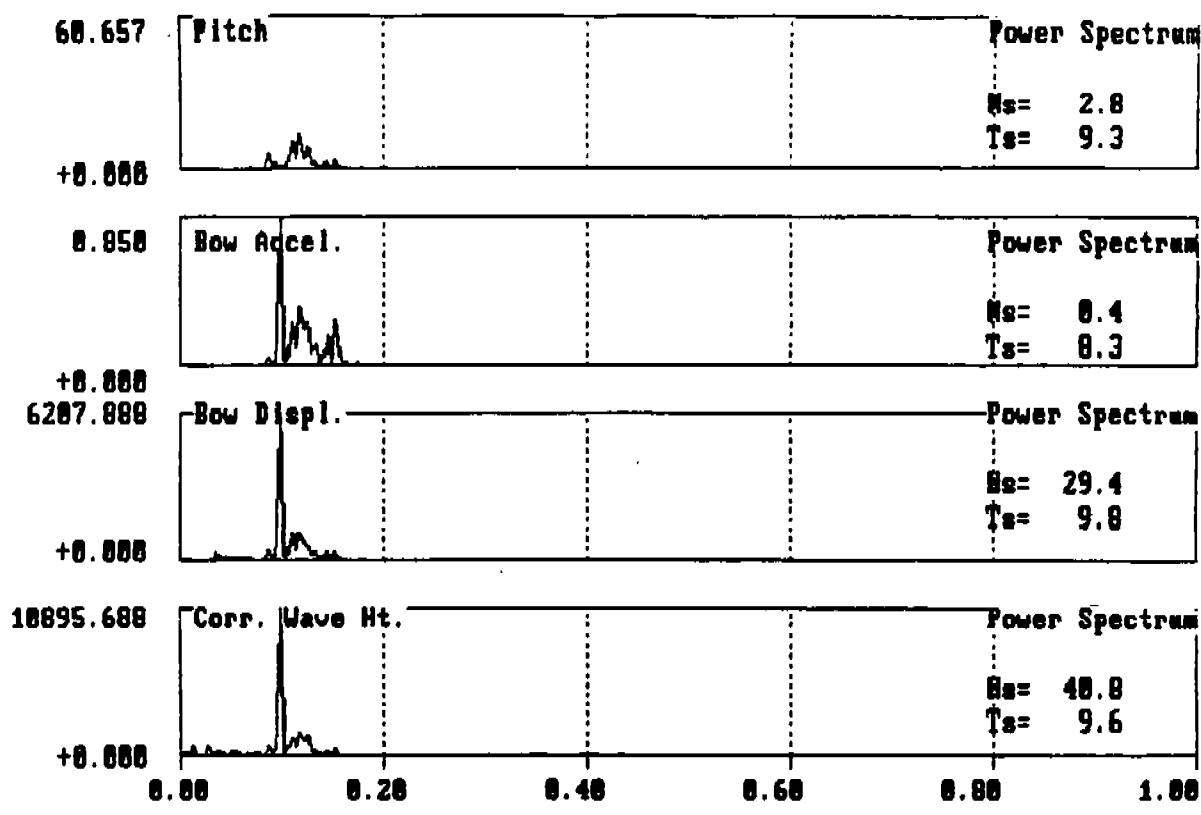
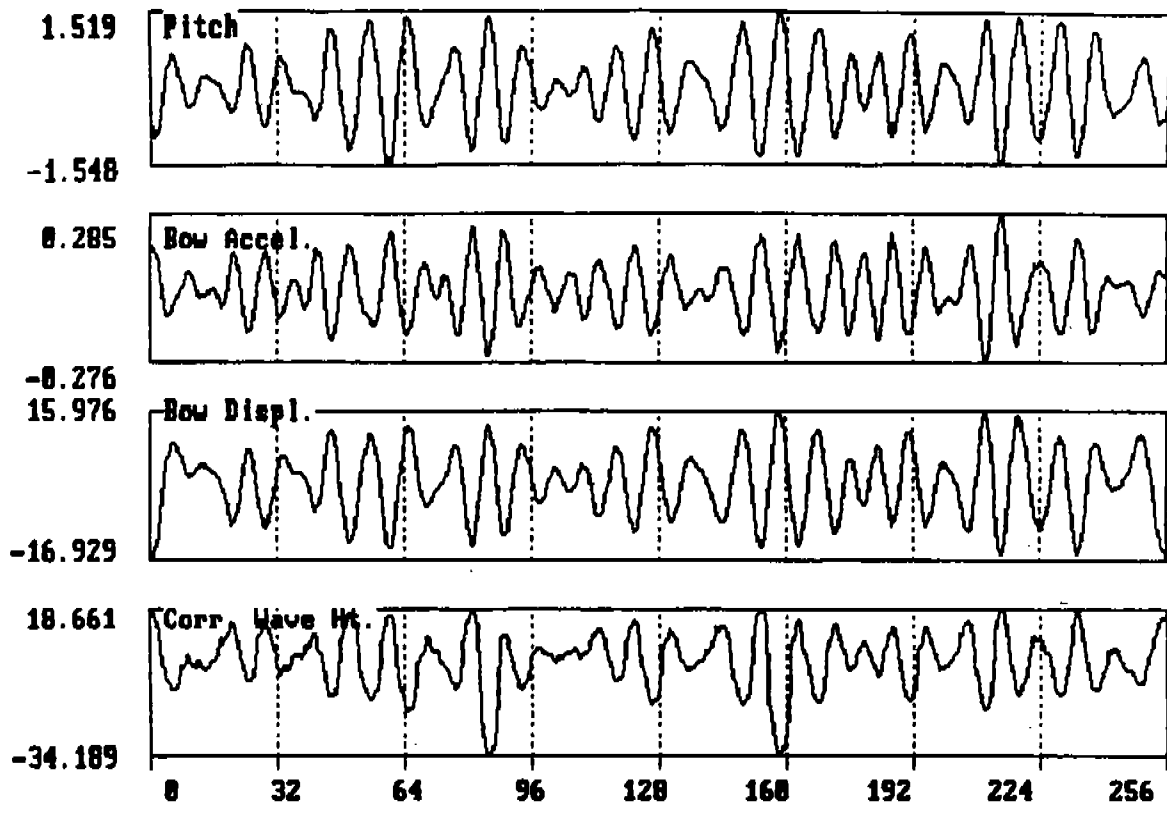


Figure 38  
 PARAMETER TIME SERIES  
 (NON FLAT SPOT RECONSTRUCTED)  
 File: 17550.DAT  
 Time: 19 OCT 88 - 17:55:31

Three possibilities have been considered for the drop out behavior of the EMI sensor: (1) infrared beam occlusion (absorption or dispersion) by "sheets of water" splashed up when the bow starts down from its uppermost position, and/or thrown up by the bulbous bow of the SL-7 when the bow starts to move upward from its lowermost position; (2) rates of change of wave range greater than the rate of change threshold (20 centimeters in 50 milliseconds or 13.1 feet/second) set within the EMI sensor electronics; and (3) a malfunction in the EMI sensor. Of the first two possibilities, beam occlusion is considered more likely than range rate threshold exceedance since even for the most extreme pitch/bow movements, the range rate of change (average rate over 1/4 of a cycle) is more than a factor of two below the 13.1 feet/ second EMI threshold.

The third possibility for the data drop outs must be considered since it can neither be verified nor ruled out by the data collected during the sea trials. It is possible that the EMI wave surface range sensor data validity "decision" logic was malfunctioning or mis-calibrated. At least one experimenter has reported that a malfunctioning EMI wave gauge (also experiencing data drop outs) was returned to the factory and then performed correctly after factory repair which included "optics realignment".

### **5.3.2 Wave Surface Range Reconstruction Algorithm**

In order to assess the impact of the wave range data drop outs on the calculated wave height spectrum and statistics, an algorithm was devised to "reconstruct" the range data during drop outs. The details of this algorithm are provided in Appendix C; the basic logic of the reconstruction process was shown in Figure 14 and outlined below.

Referring to Figure 14, the drop-out is assumed to occur near the bottom of an upward (increasing range) portion of a range cycle, or near the top of a downward (decreasing range) portion of the cycle. The reconstruction algorithm locates the point at the start of the drop out and the point (local maximum or minimum) at the end of the drop out when it is assumed that correct data is again being measured. To reconstruct the range data, the points between the start

and the midpoint of the drop out are computed by linear interpolation between the range value at the start of the drop out and the range value at the local minimum/maximum after the drop out. The points representing the "peak" of the range cycle (i.e., the points between the midpoint of the drop out and the following local minimum/maximum) are then computed by parabolic interpolation using the three points at: (1) the start of the drop out; (2) the local minimum/maximum following the drop out; and (3) the midpoint of the drop out which is assumed to have the same range value as point (2).

As can be seen by Figures 15 through 18, the reconstruction algorithm appears to perform qualitatively as expected. Comparing the uncorrected with the reconstructed data, it can be seen that the reconstructed data has reasonable magnitude and phase relationships with the non-compromised portions of the range data as well as with the pitch data. Occasionally, the parabolic interpolation of the peak portion of the range cycle appears too steep, resulting in peak over or under-shoot. This behavior can easily be remedied, for example, by adding some logic to the algorithm to limit the difference between the height of the reconstructed "peak" and the measured following local minimum/maximum.

The non-reconstructed (i.e. as measured) wave surface range data are presented in Figures 35 through 38 for comparison with the corresponding reconstructed data presented earlier in Figures 20, 30, 32 and 34. The significantly lower wave heights computed using the reconstructed wave range data are due to several factors:

1. Wave range peaks are missed; spurious large wave heights result when these missing range peaks are subtracted from the (in-phase) bow displacement values.
2. Since they "hold" the range values at the top and bottom of the wave range cycles, the drop outs cause the wave range to act as though the waves are out of phase with the bow motion; in effect the wave heights are added to the bow displacement when they should be subtracted, and vice-versa.

3. The drop outs introduce spurious low frequency energy in the wave height spectrum since this energy is "required" to produce the non-varying portions of the range record.

Except for the most severe drop out conditions, the reconstructed range data appear to eliminate the problems listed above. In the absence of "ground truth" information, the quantitative accuracy of the reconstructed data can not be ascertained; however, the results are at least reasonable and do not at all rule out the use of the reconstructed wave height data when the sea state conditions are within the limits cited below.

For some of the most severe drop out conditions, the drop out condition appears to persist for more than one expected range cycle (see Figure 5 for example). In these cases, the reconstruction algorithm will not produce a reasonable approximation to the true wave surface range and usable spectral wave height data may not be recovered. In a few other cases, the range values at which the drop outs occurred appear to be inconsistent with the range values of the rest of the data record (see Figure 34 for example); in these cases reasonable range data also can not be recovered.

#### 5.4 Overall Performance

Overall performance of the underway wave measurement system including the application of the data drop out reconstruction algorithm would be best evaluated by comparison against ground truth information. Unfortunately, with one exception, such information is essentially not available. The sole exception consists of measured data from the NOAA data buoys off the coasts of Georgia and South Carolina. The sea state was low, as the DENEbola approached the US coastline and drop outs were not a severe problem.

Table 3 compares data from the prototype shipboard wave measurement system with the data processed by NOAA buoy #41002 located at 32.2 degrees North Latitude, 75.3 degrees West longitude. On 25 October between about 11:30 and 15:00 hours, the USNS DENEbola passed approximately 120-180 nautical miles to the southeast of the buoy. Although the buoy and DENEbola were relatively distant, analysis of the comparable data recorded at NOAA Buoys 41001 (34.9N, 72.9W) and 41008 (30.7N, 81.1W) indicate relatively uniform wind conditions and wave heights increasing from the southwest (#41008) to the northeast (#41001). On this basis, Buoy #41002 data are believed to be representative but slightly higher than the conditions at DENEbola.

TABLE 3 COMPARISON WITH NOAA BUOY #41002 DATA (BUOY LOCATION: 32.2N, 75.3W)						
Time/File (25-Oct)	Position	Denebola *		Buoy Data		
		Data H(s) (ft)	T(s) (sec)	H(s) (ft)	T(dom) (sec)	T(avg) (sec)
11:32 11300	32.2N, 77.4W	5.6	3.4	5.6	6.7	5.1
11:58 11550	32.2N, 77.5W	5.0	3.3	5.6	6.7	5.1
13:21 13180	32.2N, 78.1W	5.2	3.1	6.2	7.1	5.5
14:25 14250	32.2N, 78.6W	4.5	3.6	5.6	7.1	5.1
15:09 15020	32.2N, 78.8W	5.5	3.9	5.2	7.1	5.2

\* Denebola data are wave encounter statistics. Vessel was operating at 20 + knots in head seas during this period.

The USNS DENEbola data are "encounter" spectra. For the October 25th records, the DENEbola was travelling at over 20 knots in essentially head seas; thus the encountered wave period would be lower than that measured by a stationary buoy. Correcting for this relative motion brings the wave period data into good agreement.

Additional "ground truth" information was provided in the form of visual observations made by the sea trial personnel and the comparison of recorded vessel motions. Although there appears to be some uncertainty and confusion in the visual observations of wave height, the measurements of vessel pitch and roll provide individual confirmation of the wave data through comparison with results from Navy's ship motion program. A cursory examination of SL-7 pitch and roll data derived using the SMP84 program, visually observed wave direction information and the measured wave height shows reasonable agreement to that measured on the DENEbola.

Several of the EMI wave range spectra contain a small component of very low frequency energy. Since the magnitude of this energy is relatively low, it is most noticeable in spectra obtained during low sea states. Several sources of this energy are possible, including: (1) drop out distortion; (2) "imperfect" compensation for bow displacement; and/or (3) bow wake effects. The net effect of this low frequency energy on the wave height statistics is generally small, and further evaluation has not been attempted within the scope of this report.

## 6.0 RECOMMENDATIONS

Based on the results of the October 1988 sea trials, several recommendations are warranted. These are listed below in order of estimated importance. The first two recommendations are considered critical prior to additional sea trial efforts.

1. Any future sea trials should include better ground truth information; for example, sailing in close proximity to data buoys. The ground truth information should also include wave height spectra, if possible.
2. Means should be provided to include visual recording (video camera, etc.) of the wave field "seen" by the wave range sensor. The visual information should be time-referenced to the measured data records.

3. An alternative mounting location for the wave surface range sensor, positioned away from the bow "splash/spray" area should be considered. The sensor package should be movable from the bow to this location during the sea trial. It should be noted that this off-bow position is not intended as an "operational" position but is instead intended as a temporary location to be used to investigate the effects of bow spray and waves on data drop out.
4. To resolve the uncertainties relative to the EMI performance during the sea trials, the gauge should be returned to the manufacturer with the following courses of action: (1) if the gauge is found to have been malfunctioning, it should be repaired and new sea trials conducted; and (2) the sensor should be modified to defeat or bypass the data validity "decision" logic so that unmodified data are sent to the data acquisition system. This data can then be subsequently analyzed in order to determine if drop-out severity can be reduced by improving the processing algorithms.
5. Future sea trials should use the gyro angle sensors instead of the pendulum sensors so that accurate angles are measured under all sea states.
6. A tri-axial accelerometer should be used instead of the single axis vertical accelerometer used for the USNS DENEbola sea trial. The lack of longitudinal and transverse acceleration data precluded full calculation of the true vertical acceleration component.
7. In an operational system, the existing A/D subsystem should be replaced by a system which includes a buffered memory so that data acquisition and processing can occur in parallel. In the existing system data acquisition and processing were serialized with resulting time gaps while processing was performed. Such gaps are not serious if the wave statistics are stationary, but they could compromise results obtained during transitional conditions.

8. Operational system software should include a capability to trigger data logging when a sensor threshold is exceeded so that data of interest is not lost when an operator is not monitoring the system.



## REFERENCES

1. Dalzell, J.F., Wavemeter Data Reduction Method and Initial Data for the SL-7 Containership, Report SSC 278 (SL-7), Stevens Institute of Technology, Hoboken, New Jersey, 1978.
2. Dalzell, J.F., Original Radar and Standard Tucker Wavemeter SL-7 Containership Data Reductin and Correlation Sample, 1978, Report SSC 277 (SL-7-14), Stevens Institute of Technology, Hoboken, New Jersey, 1978.
3. SL-7 Research Program Summary, Conclusions and Recommendations, Report SSC 313 (SL-7-28), Ship Structure Committee, 1981.
4. Jepsky, J., C. Petly, D. Hammond, Environmental Sensor Requirements for Shipboard Wave Height Measurements, 1981, Report NMRC 204, National Maritime Research Center, Kings Point, New York.
5. Shipboard Wave Height Sensor, Phase I Report, Report R89-20, Science Applications International Corporation, Goleta, California, 1988.
6. Infrared Wave Height Sensor Operators Manual, Report CP7358, Thorn EMI, Survey, England, 1988.



## APPENDIX A

### A.0 DATA ACQUISITION AND PROCESSING SOFTWARE

Three computer programs have been developed in the course of the wave height measurement project. These programs are coded in QuickBASIC 4.0 (Microsoft Corporation) and run within the QuickBASIC environment. Listings of these programs are provided under separate cover.

The three programs consist of:

1. **TEST-2K.BAS:** This is the real-time data acquisition and processing program used to acquire, display and log the sensor data during the sea trial. Figure \_\_\_ in the main text contains a flow chart for this program. A more detailed flow chart of the 'TRANSFORM' module which performs the double integration of acceleration to compute bow displacement is included in Table A-1. Several subroutine modules are contained within the code for this program; the function of these routines is described in A-2.
2. **EMINTERP.BAS:** This program is a version of the real-time program modified to read the raw data files stored on the disk by that program. EMINTERP is used to generate time series plots of raw data sensors and spectral plots of the EMI wave surface range sensor data records. It should NOT be used to plot any "processed" parameter data. The float spot reconstruction algorithm described in the main text and in Appendix C is included in this program (see 'INTERP' subroutine). EMINTERP was used to create the pitch and EMI sensor time series and the EMI sensor spectrum plots which appear in this report.
3. **TEMP.BAS:** This program reads the raw data files stored on the disk by the real-time program and generates time series plots of raw and/or processed data and spectral plots of all sensors and parameters EXCEPT the EMI sensor. The float spot reconstruction algorithm described in the main text and in Appendix C is included in this program ('INTERP' subroutine). TEMP was used to create the parameter time series (pitch, acceleration, bow displacement and wave height) and spectrum plots which appear in this report.

**TABLE A-1**  
**TRANSFORM FLOWCHART**

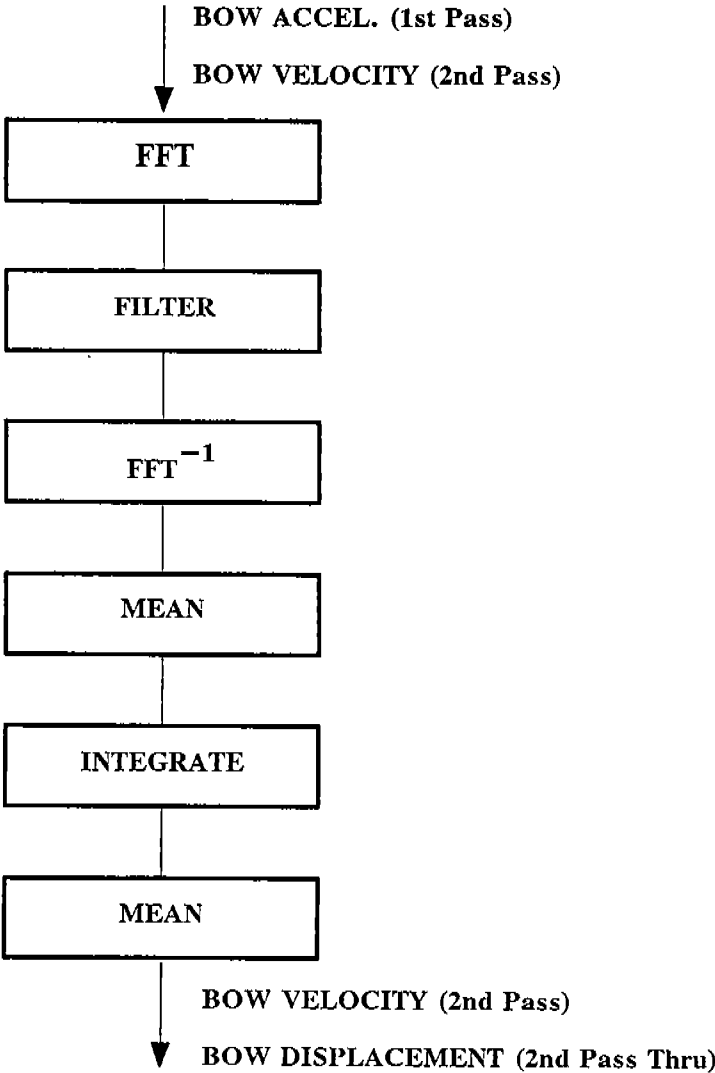


**TABLE A-2**  
**PROCESSING PROGRAM MODULES**

**CNVRT:**

Converts raw data from the A/D converter to engineering units (ft., deg., G's, etc.), scales and offsets data according to predetermined scaling and offset factors.

**TRENDS:**

Using a least-squares method, removes any unwanted trend line from the data.

**TRIG:**

Performs trigonometric correction of bow acceleration and EMI range to extract only the vertical component of those signals.

**TRANSFORM:**

This module integrates the input signal, transforming bow acceleration to velocity, and again from velocity to displacement (heave). Filtering is also accomplished in this module.

**DECIMATE:**

This module decimates all data to an effective sample rate of 2 Hz.

**EMI-DISPLACEMENT:**

This module subtracts bow heave from EMI range to calculate actual wave height.

**STATS:**

This module calculates various statistical parameters, such as max, min, period, etc. for each parameter.

**PSD:**

This module calculates Power Spectra for each input, for later display.



## APPENDIX B

### RECORDED DATA FILES

The format of the data records stored on the disk by the real time program is given in Table B-1. See subroutine 'READBACK' in the EMINTERP.BAS or TEMP.BAS listing for an example of BASIC code to read the raw sensor data back from disk.

A tabulation of data records logged during the sea trials is provided in Table B-2. NOTE: the "UP\_LIM" and "LO\_LIM" columns of this list indicated the high frequency (UP\_LIM = 1 second period) and low frequency (LO\_LIM = 10, 20 or 50 second period) limits for filtering of the acceleration FFT data during the double integration process (see Figure C-1). These values affect the processed data and spectra in the disk data but have no effect on the raw data (used for re-processing).

**TABLE B-1  
DATA FILE FORMAT (2048 POINT RECORDS)**

<p><u>HEADER</u></p> <p>DATE\$ TIME\$ FR % MAXCYCLE% NPTS% CYCLE% LOGFLAG% LLINP% ULINP% GAM% SIG%</p>	<p>10 CHARACTERS 8 CHARACTERS SAMPLE RATE MAX NO. OF CYCLES ALWAYS 0 BUT RECORDS ACTUALLY CONTAIN 2048 POINTS CURRENT CYCLE NUMBER LOGGING FLAG USED (TYPICALLY 4) LOWER FLTR LEVEL UPPER FLTR LEVEL GAMMA ANGLE (TYPICALLY 0) SIGMA ANGLE (TYPICALLY 79 DEGREES)</p>
<p><u>DATA</u></p> <p>A%(I,J)</p>	<p>RAW DATA. TYPICALLY 6 X 2K INTEGER ARRAY. I = SENSOR, J = #POINTS</p> <p><u>SENSORS:</u></p> <p>I = 1...EMI DATA I = 2...ACCELEROMETER I = 3...ROLL GYRO DATA I = 4...PITCH GYRO DATA I = 5...ROLL PENDULUM DATA I = 6...PITCH PENDULUM DATA</p>
<p>KEEP(I,J)</p>	<p>PROCESSED DATA. TYPICALLY 6 X DN% REAL ARRAY, WHERE DN% = (2K/(FR%/2)). I=PROCESSED DATA PARAMETER</p> <p><u>PARAMETERS:</u></p> <p>I = 1...WAVE HEIGHT I = 2...BOW DISPLACEMENT (HEAVE) I = 3...ROLL I = 4...PITCH I = 5...BOW VELOCITY I = 6...BOW ACCELERATION</p>
<p>PSDATA(I,J)</p>	<p>POWER SPECTRUM DATA. TYPICALLY 6 X DN% REAL ARRAY, WHERE DN% = (2K/(FR%/2)). I = POWER SPECTRA PARAMETER.</p> <p><u>PARAMETERS:</u></p> <p>I = 1...WAVE HEIGHT I = 2...BOW DISPLACEMENT (HEAVE) I = 3...ROLL I = 4...PITCH I = 5...BOW VELOCITY I = 6...BOW ACCELERATION</p>

# APPENDIX B

## SHIPBOARD WAVE HEIGHT DATA FILES SSC SEA TRIALS: 18-25 OCTOBER 1988

#	Date	Time GMT	Data ID	Sample Freq	Up_Lim	Lo_Lim
1	25-Oct	15:09:02	150200	8	1	20
2	25-Oct	15:52:30	150201	8	1	20
3	25-Oct	14:25:58	14250	8	1	20
4	25-Oct	13:21:51	131800	16	1	50
5	25-Oct	11:58:30	115500	16	1	10
6	25-Oct	12:53:01	115501	16	1	10
7	25-Oct	11:32:40	113000	16	1	20
8	24-Oct	20:01:28	20010	8	1	20
9	24-Oct	17:48:26	17480	8	1	50
10	24-Oct	18:37:35	174801	8	1	50
11	24-Oct	19:16:38	174802	8	1	50
12	24-Oct	16:57:03	165200	8	1	20
13	24-Oct	14:45:53	14450	8	1	50
14	24-Oct	15:39:26	144501	8	1	50
15	24-Oct	16:18:29	144502	8	1	50
16	24-Oct	13:44:43	134200	16	1	50
17	24-Oct	11:16:51	11160	8	1	50
18	24-Oct	12:03:27	111601	8	1	50
19	23-Oct	20:00:39	20000	8	1	20
20	23-Oct	17:03:47	165800	8	1	50
21	23-Oct	17:45:50	165801	8	1	50
22	23-Oct	18:24:54	165802	8	1	50
23	23-Oct	19:03:58	165803	8	1	50
24	23-Oct	16:22:34	16220	8	1	20
25	23-Oct	14:35:08	14350	8	1	20
26	23-Oct	15:14:19	143501	8	1	20
27	23-Oct	13:49:02	13490	8	1	20
28	22-Oct	20:16:45	201300	16	1	20
29	22-Oct	19:14:32	19140	8	1	20
30	22-Oct	18:24:09	test60	16	1	25
31	22-Oct	18:07:32	test50	16	1	25
32	22-Oct	12:59:24	12590	8	1	20
33	22-Oct	13:31:54	125901	8	1	20
34	22-Oct	14:04:14	125902	8	1	20
35	22-Oct	11:38:44	93500	16	1	20
36	22-Oct	10:30:46	10300	8	1	20

# APPENDIX B

## SHIPBOARD WAVE HEIGHT DATA FILES SSC SEA TRIALS: 18-25 OCTOBER 1988

#	Date	Time GMT	Data ID	Sample Freq	Up_Lim	Lo_Lim
37	21-Oct	19:18:48	19180	8	1	20
38	21-Oct	17:18:20	17180	8	1	20
39	21-Oct	17:57:36	171801	8	1	20
40	21-Oct	18:29:56	171802	8	1	20
41	21-Oct	14:14:20	14140	8	1	20
42	21-Oct	12:54:29	12540	8	1	20
43	21-Oct	13:26:49	125401	8	1	20
44	21-Oct	12:05:20	12050	8	1	20
45	21-Oct	11:49:53	test40	8	1	20
46	21-Oct	09:40:32	9400	8	1	20
47	20-Oct	18:27:56	18270	8	1	20
48	20-Oct	14:03:55	14030	8	1	20
49	20-Oct	10:37:44	10370	8	1	20
50	20-Oct	08:38:01	8380	8	1	20
51	20-Oct	09:15:10	83801	8	1	20
52	19-Oct	17:55:31	17550	8	1	20
53	19-Oct	10:14:40	10140	8	1	20
54	19-Oct	10:47:01	101401	8	1	20
55	19-Oct	11:19:21	101402	8	1	20
56	19-Oct	11:51:41	101403	8	1	20
57	19-Oct	08:22:52	8220	8	1	20
58	19-Oct	08:55:12	82201	8	1	20
59	18-Oct	11:51:06	11510	8	1	20
60	18-Oct	10:08:27	810030	4	1	20
61	18-Oct	09:42:36	189400	8	1	20
62	20-Oct	14:54:47	@16hz0	16	1	20
63	20-Oct	15:34:59	@16hz1	16	1	20
64	21-Oct	10:36:12	video	32	1	20

## APPENDIX C

### FLAT SPOT DETECTION/RECONSTRUCTION ALGORITHM

Refer to the main text (Sections 5.X.X and X.X.X) for a qualitative description of this algorithm. Figure C-1 presents the detailed logic flow.

**FLAT SPOT  
DETECTION**

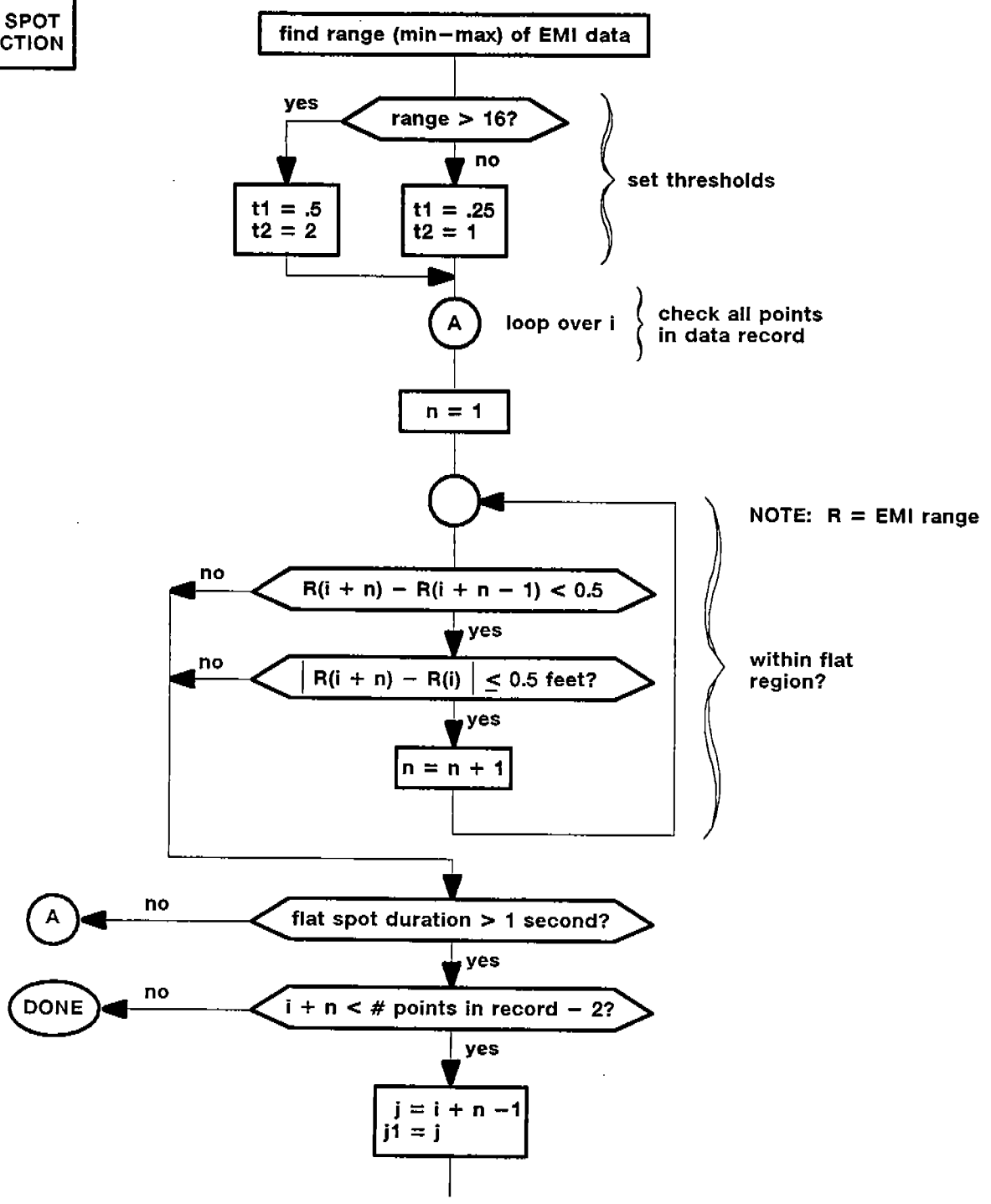


**Figure C-1**  
(sheet 1 of 3)  
**Flat Spot Detection/Reconstruction Algorithm**

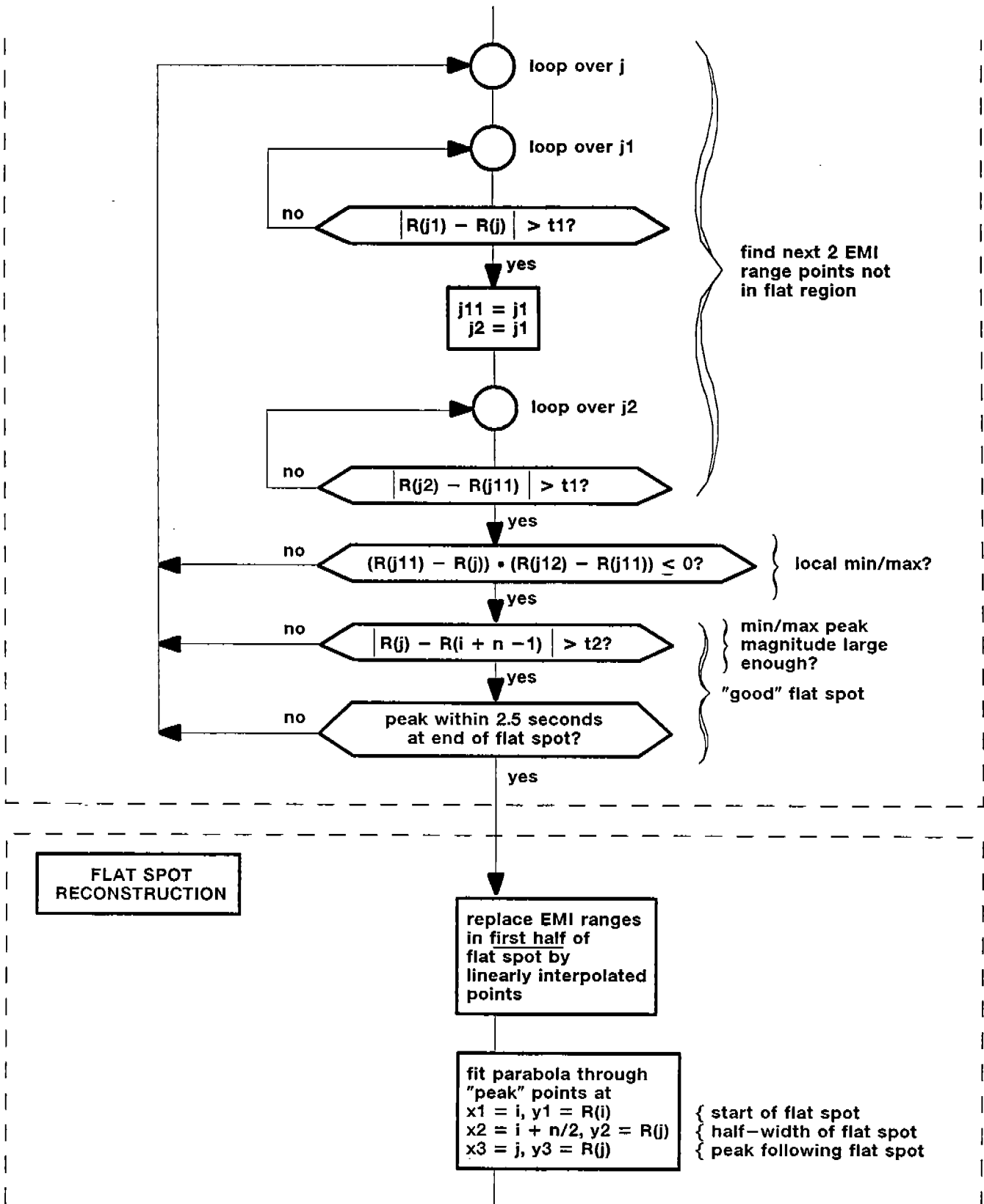
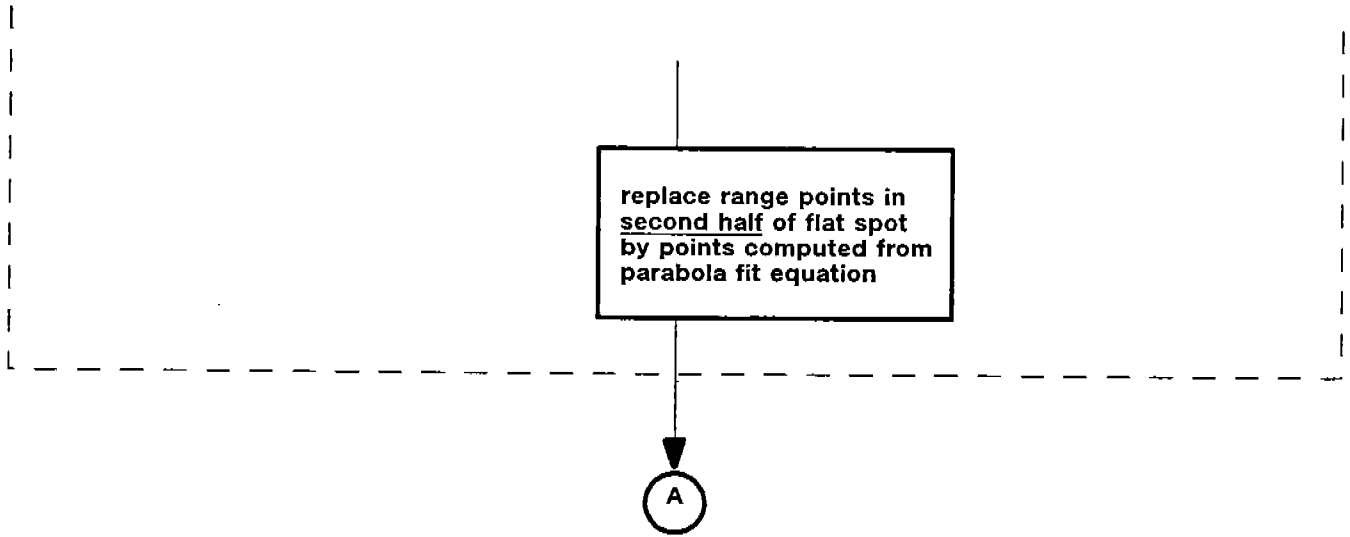


Figure C-1  
 (sheet 2 of 3)  
 Flat Spot Detection/Reconstruction Algorithm



**Figure C-1**  
**(sheet 3 of 3)**  
**Flat Spot Detection/Reconstruction Algorithm**

390172

COLLEGE OF ENGINEERING  
DEPARTMENT OF NAVAL ARCHITECTURE AND MARINE ENGINEERING  
SHIP HYDRODYNAMICS LABORATORY

VESSEL-WAVE INTERACTIONS

on an

SL-7 CLASS SHIP

by

F. H. ASHCROFT  
Principal Investigator

R. F. BECK  
Project Director

for

The Ship Structure Committee  
and  
The Society of Naval Architects and Marine Engineers

MODEL 1420

December 1990



## TABLE OF CONTENTS

List of Figures .....	i
Introduction .....	1
The Model.....	1
The Test Set-Up.....	1
The Model Tests.....	2
Results.....	3
Conclusions.....	4
Figures.....	5

## LIST OF FIGURES

- Figure 1.....Bow Lines
- Figure 2.....Stern Lines
- Figure 3.....Sketch of Heave-Pitch-Surge Dynamometer  
with wave probe holder.
- Figure 4.....Plot of Correction Factors for Transverse  
Wave Probe Location
- Figure 5.....Plot of Correction Factors from Forward  
Speed Dynamic Calibration of Wave Probes
- Figure 6.....Ratio of Near/Far versus  $\lambda/L$  at 2.2 ft/s for  
small waves
- Figure 7.....Ratio of Near/Far versus  $\omega_e$  at 2.2 ft/s for  
small waves
- Figure 8.....Ratio of Near/Far versus  $\lambda/L$  at 2.2 ft/s for  
large waves
- Figure 9.....Ratio of Near/Far versus  $\omega_e$  at 2.2 ft/s for  
large waves
- Figure 10.....Ratio of Near/Far versus  $\lambda/L$  at 3.965 ft/s for  
small waves
- Figure 11.....Ratio of Near/Far versus  $\omega_e$  at 3.965 ft/s for  
small waves
- Figure 12.....Ratio of Near/Far versus  $\lambda/L$  at 3.965 ft/s for  
large waves
- Figure 13.....Ratio of Near/Far versus  $\lambda/L$  at 3.965 ft/s for  
large waves
- Figure 14.....Ratio of Near/Far versus Time History  
Number at 3.965 ft/s for random seas

## INTRODUCTION

In 1988 a full scale laser wave probe was developed and installed on an SL-7 containership. The probe was mounted on the bow and looked forward at an angle of  $12^\circ$  forward of the vertical. The purpose of the probe was to measure the incident wave amplitude. This was accomplished by subtracting from the absolute amplitude measured by the probe the relevant ship motions. No corrections were made for the steady wave system or the unsteady radiated and diffracted waves. After reviewing the results, questions arose as to possible contamination by the steady and unsteady ship generated waves in front of the bow. To begin to investigate these questions, model tests were conducted in the Ship Hydrodynamics Laboratory using an existing model of the SL-7 and a small test matrix.

The experiments were designed for head seas only with the model free to surge, heave, and pitch. Wave amplitudes were measured in front of the model and off to one side.

## THE MODEL

An existing 1:80 scale model of an SL-7 class container ship was used for these tests. The model was rigged with a pitch gimbal located at the LCG (2.76% aft of midship). The model lines are shown in Figures 1 and 2. The model was ballasted to the scale 30 foot draft and the pitch radius of gyration was adjusted to 0.251 L.

## THE TEST SET-UP

The model was tested free to surge using the Heave-Pitch-Surge (HPS) dynamometer. The purpose of these tests was to measure the incident waves at a point close to the bow of the model simulating the laser foot print in the full scale tests. In order to maintain the relative position of the model and wave probe, measurements had to be made in the model reference frame. This requirement was met by installing a boom on the lightweight carriage of the HPS dynamometer which would hold a capacitance wire wave probe at the point in front of the model where the laser hit the smooth water line in the full scale experiment. A sketch of this set-up is given in Figure 3.

A second wave probe was located on the towing carriage 6 feet off the model centerline. This probe was located directly abeam of the mean position (with respect to surge) of the dynamometer mounted wave probe.

The HPS dynamometer allows the model freedom to both surge and drift. Obviously, if the model drifts during the test, the desired speed through the water is not achieved and the positional relationship between the wave probes is lost as well. Several runs were made to determine the correct force settings to eliminate the drift while allowing surge freedom.

## THE MODEL TESTS

The model was first run in regular head seas at speeds of 1.0 and 3.965 ft/s (corresponding to 5.30 and 21.00 knots full scale) for a range of  $\lambda/L$ 's from 0.5 - 1.4 at two constant wave heights of 0.75 inches and 1.50 inches (5.0' and 10.0' full scale). The waves were measured at a point 5.81 inches forward of the F.P. on the vessel centerline and at the second probe 6 feet off center to starboard. Testing was also done in one random sea spectra (7 time histories) at the 3.965 ft/s speed. The two parameter ITTC spectrum was used with full scale  $H_{1/3}=11.32$  feet and  $T_1=9.7$  seconds:

ITTC spectrum:

$$S(\omega) = \frac{A}{\omega} e^{-B/\omega^4}$$

where:  $A = 173 (H_{1/3})^2 / T_1^4$

$$B = 691 / T_1^4$$

During the initial testing we experienced a major mechanical failure on our wavemaker (one ball nut blew out, destroying the ball screw it was riding on). The replacement parts had a seven month delivery time causing us to miss the test window.

After the new ballscrews were installed, the wavemaker was recalibrated and a check of the transverse wave shape was performed at midtank (150 feet from the wavemaker) with probes located at tank centerline, 6 feet off, and 10 feet off center. Plots of wave height versus wave length for all three locations is given in Figures 4 a and b.

The wave probes were calibrated dynamically with forward speed. Plots of these calibrations are given in Figures 5 a and b.

The results of the cross tank and forward speed dynamic calibrations did show that the data from the model would need correction for both position and speed.

With the wavemaker repaired and probes ready, the test matrix was completed. The 3.965 ft/s data showed excellent agreement with the data taken before the wavemaker failed, however the 1 ft/s data seemed inconsistent. Calculation showed that this speed was below the group velocity of the hull transversely generated/reflected waves which meant that the low speed data was contaminated due to wall reflections.

We determined that a model forward speed of 2.2 ft/s (11.65 knots full scale) would assure contamination free results at all  $\lambda/L$ 's. The regular wave test matrix was then rerun at 2.2 ft/s and the 1 ft/s data discarded.

The data was acquired and analyzed using Tektronix 4052 computers with software which allows processing of signals in both time and frequency domains. The data samples were 1024 points typically scanned at a rate of 25 Hz. The input signal was digitally filtered with a cut-off frequency of 6.4 Hz. This allows good reconstruction of signals of less than 2 Hz which are typically found in seakeeping model tests. Time and frequency domain results were both used in the analysis of the data with comparisons also being made of the first harmonics in the frequency domain. The results show good agreement between domains.

## RESULTS

The final data is presented in graphic form in terms of wave height ratios (near height/far height) versus both  $\lambda/L$  and frequency of encounter (regular waves only). All regular wave data has been corrected for forward speed effects and transverse location. It can be seen from the graphs that the height of the waves in the near field is effected by the presence of the hull. In most cases the near field wave amplitude is less than the far field amplitude. At 2.2 ft/s in the small waves there is a near field attenuation from 25% at the lower frequencies of encounter (4.5 rad/s) decreasing to about 10% at the higher frequencies (8.6 rad/s). For this speed in the large waves the attenuation is humped with 12% at 4.5 rad/s, 1-2% attenuation at 6 rad/s, and 12% at 8.6 rad/s. For the 3.965 ft/s forward speed and small wave amplitudes there is about 12% attenuation at 5.2 rad/s, 0% at 7.5 rad/s, plus 8% at 9.5 rad/s, and plus 2% at 10.6 rad/s. For the large waves at this speed, the curve again has a hump with 8% attenuation at 5.2 rad/s, plus 1% at 7 rad/s, going back to an attenuation of 6% at 10.5 rad/s. Plots of the regular wave data corrected for both forward speed and tank location are given in Figures 6 through 13.

The results of these tests show distinctly different shapes between the small and large wave graphs at both speeds. The height ratios for small waves increase with increasing frequency of encounter while the large wave ratios show a distinct hump just below the middle of the frequency of encounter range. This is clearly shown for the 2.2 ft/s speed comparing Figures 7 and 9 and for the 3.965 ft/s speed comparing Figures 11 and 13. In a linear system the wave amplitude ratios should be independent of incident wave amplitude. The fact that they are not indicates the presence of nonlinear behavior. To properly quantify the nonlinearities, many more incident wave amplitudes would have to be investigated. As shown in Figures 6-13 some repeat runs were made. At 3.965 ft/s and large incident wave amplitude, the tests were run twice for each  $\lambda/L$ . These results indicate that absolute repeatability on any given run was in the range of  $\pm 5\%$ . Random repeat points for the other conditions were also within this band. Since the differences between the large and small incident waves is greater than the repeatability band, the nonlinear behavior is probably real and not due to experimental error.

The causes of the nonlinear behavior are not known but may be related to a hydraulic jump-like wave visually observed in front on the model during the test runs. This jump-like wave may also have an influence on the full scale laser measurements. When the model pitched up a small hydraulic jump-like wave was propagated forward towards the wave probe wire. This small wavelet never appeared to reach the probe and moved back towards the bow on the down pitch. The small wavelet is probably caused by the proximity of the bulb to the free surface on the up pitch. The small wavelet came within one inch of the wave probe wire but may have had an influence which was not visible. Since small waves are very subject to scale effects, it is not known whether or not the wave would reach the laser footprint in full scale.

In the random sea the model was run only at the 3.965 ft/s forward speed and only one sea state was tested. The transverse correction is wave length dependent and we did not consider it practical to correct the random sea data for transverse position, however, the forward speed correction was applied. The final data plot for the random sea test is given as a ratio of near to far mean and significant wave height (corrected for forward speed) versus time history number and is given in Figure 14. There is some variation in the attenuation among the time histories which is to be expected due to the random nature of the process. The attenuation ranges from 1-10% and does not appear to favor either the ratio of mean or significant heights.

### CONCLUSIONS

The wave heights measured at the laser footprint are affected by the presence of the hull. Over most of the frequency range in the regular wave tests, the near field waves are attenuated due to the presence of the ship. Typical attenuation is less than 10%. The irregular wave tests also show an attenuation in the range of 5 - 10% on significant wave height.

It appears that this attenuation is somewhat wave amplitude dependent. At both the high and low speeds the near field/far field ratios change slightly for the small or large wave amplitudes with the small waves generally showing more attenuation than the large incident waves. Since the nonlinearities are small, more testing must be done varying wave amplitude and more repeatability runs are required to determine precisely the nature of the variation with the incident wave.

The University of Michigan  
**SHIP HYDRODYNAMICS LABORATORY**  
 Department of Naval Architecture  
 and Marine Engineering  
 Ann Arbor, Michigan 48109

MODEL 1420 (SL-7)

1-19-91

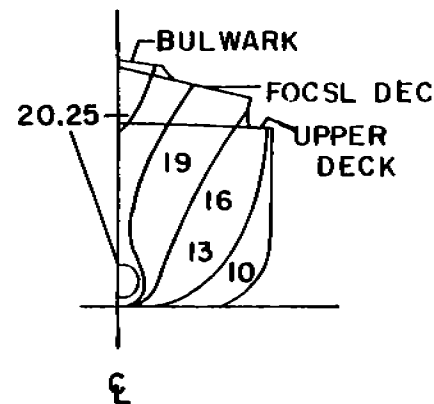
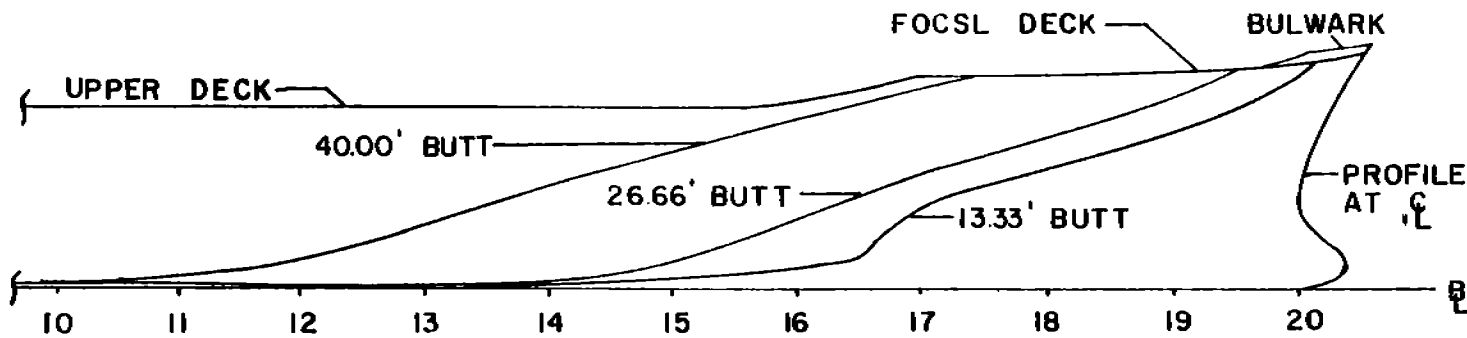
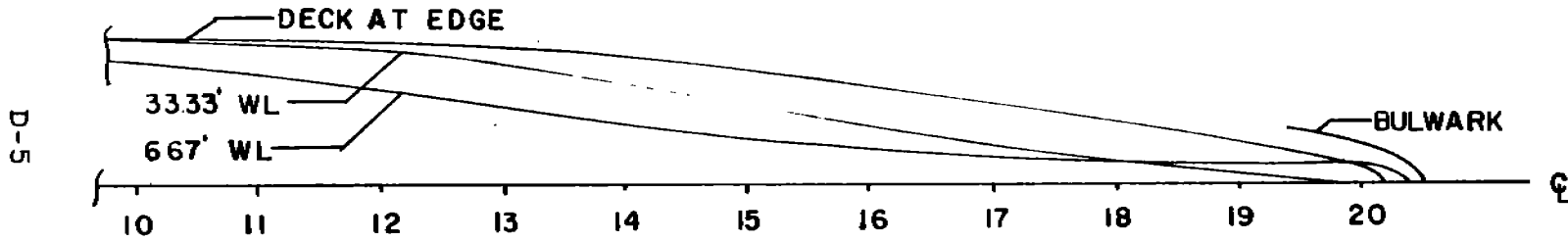


Figure 1.

The University of Michigan  
**SHIP HYDRODYNAMICS LABORATORY**  
 Department of Naval Architecture  
 and Marine Engineering  
 Ann Arbor, Michigan 48109

MODEL 1420 (SL-7)  
 1-19-91

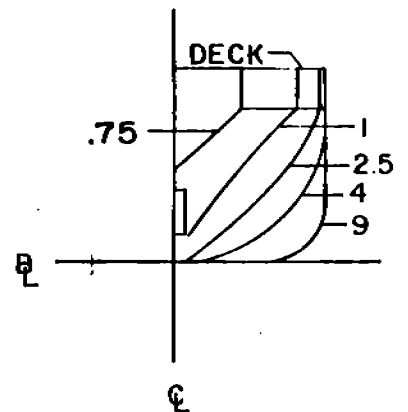
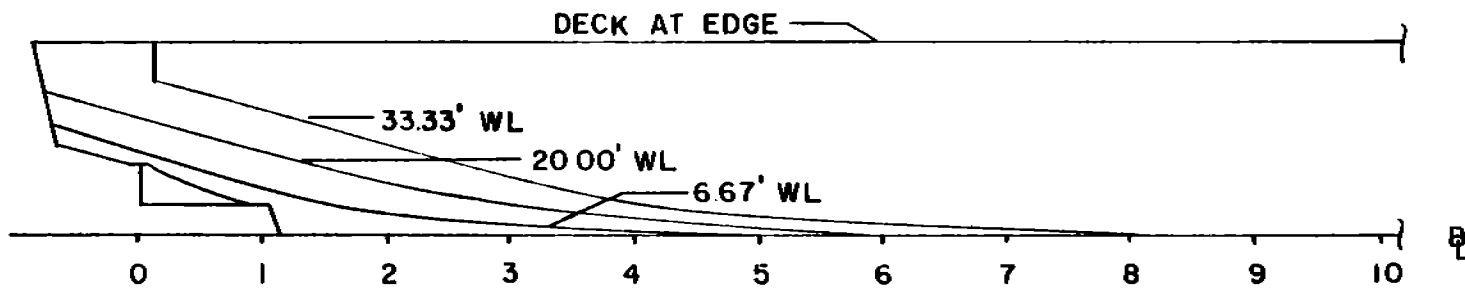
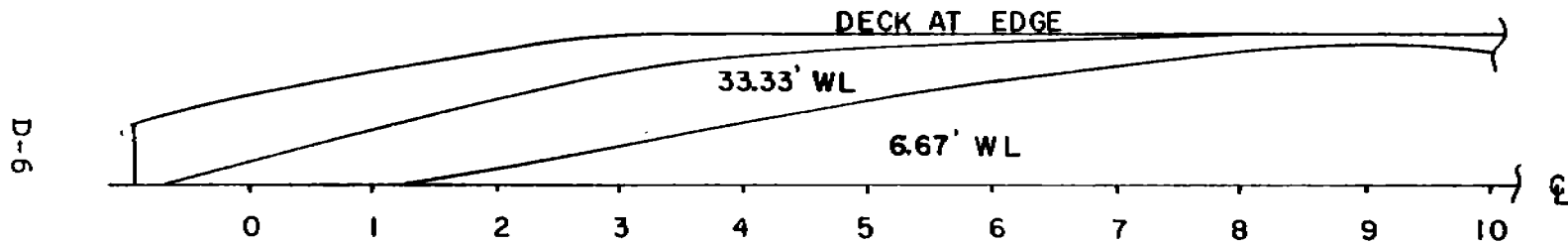


Figure 2

Heave-Pitch-Surge Dynamometer  
with Wave Probe Attachment

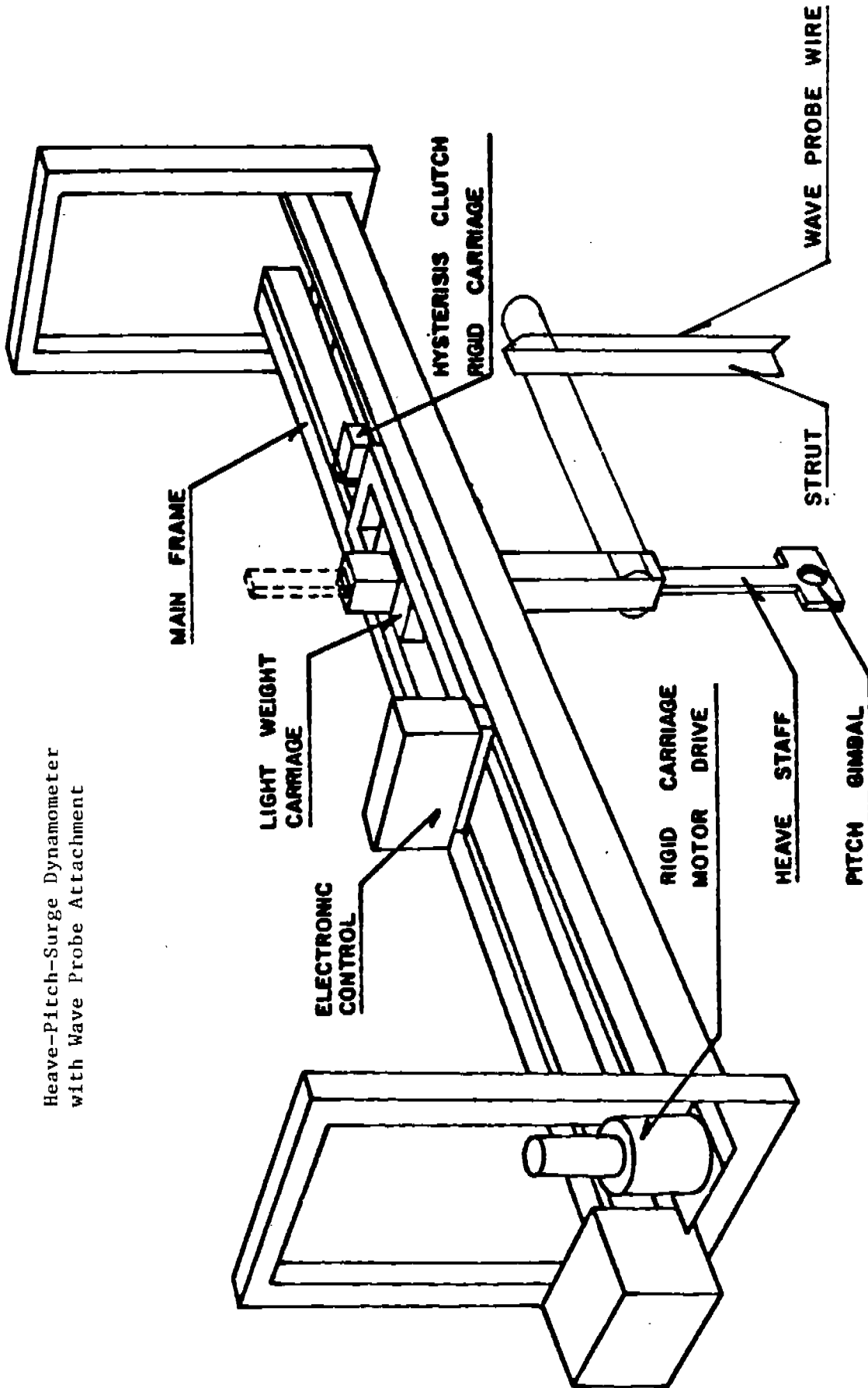
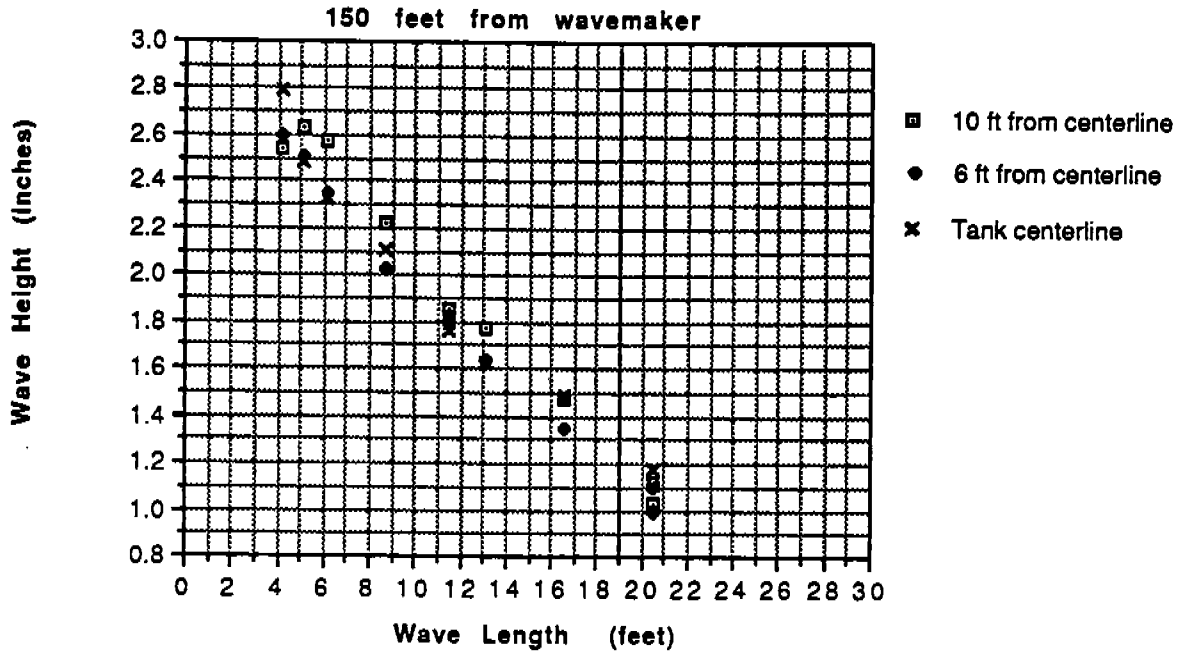


Figure 3

**Figure 4a**

**Transverse Variation in Significant Wave Height  
for Constant Stroke (-20 dB attenuator)**



**Figure 4b**

**Transverse Variation in Significant Wave Height  
at Constant Stroke (-40db attenuator)**

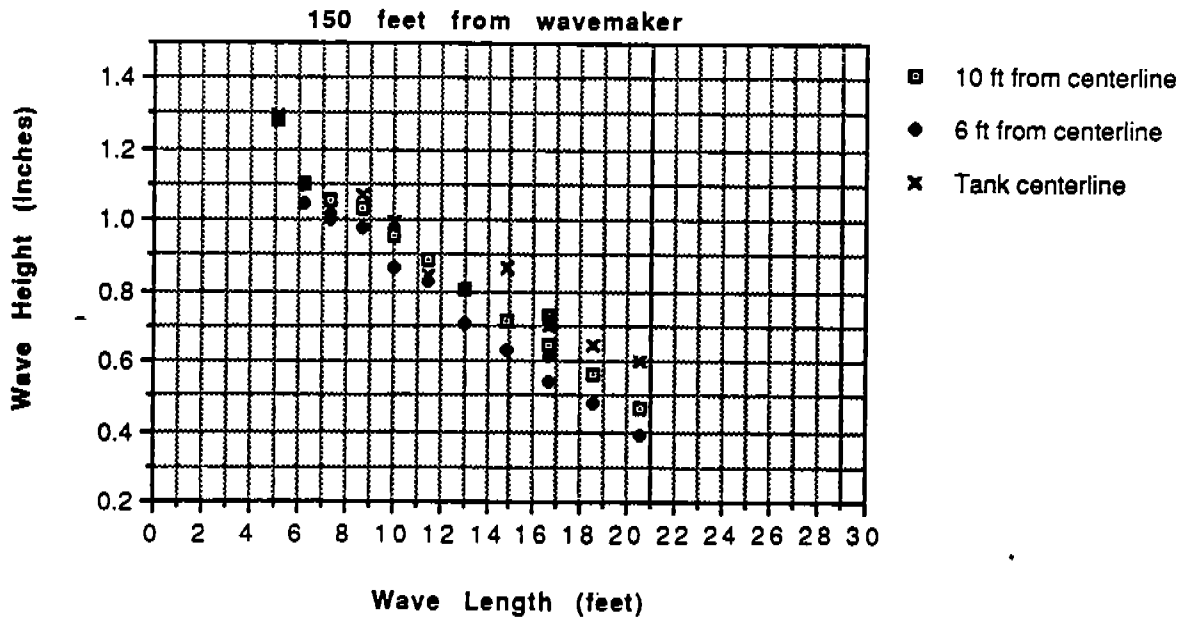


**Figure 5a**

**Forward Speed: 2.2 ft/s**

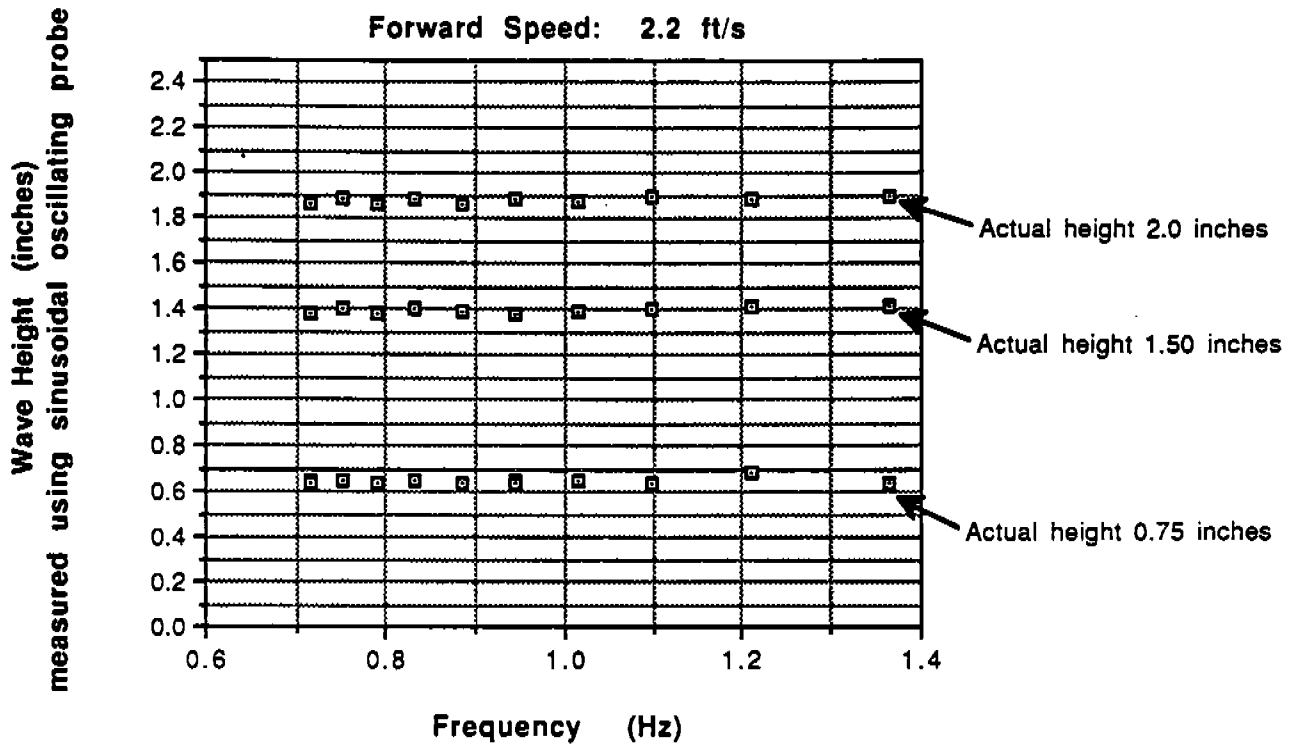


**Figure 5b**

**Forward Speed: 3.965 ft/s**

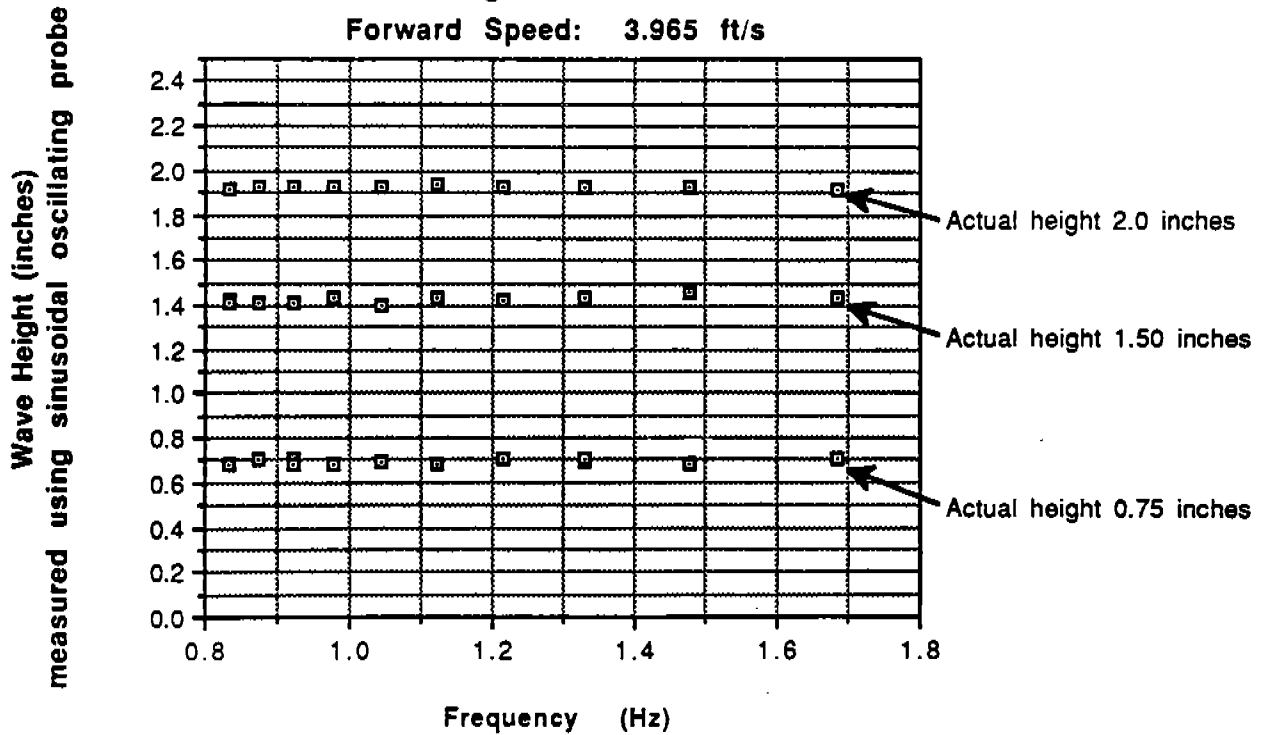


**Figure 6**  
**2.2 ft/s with Small Waves**

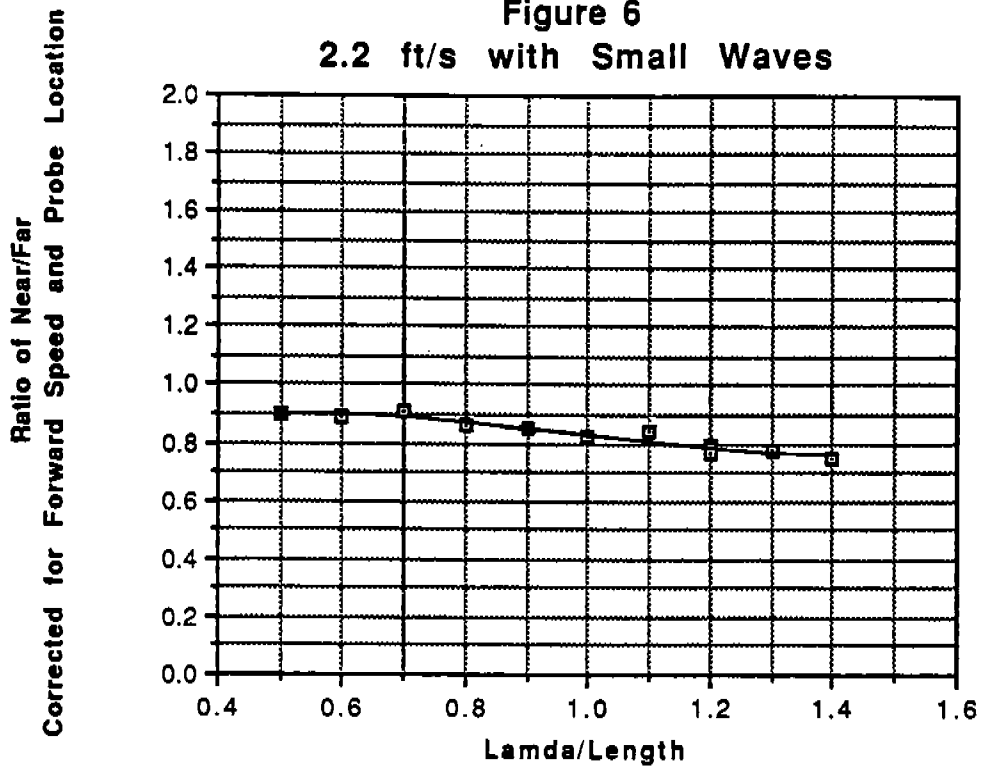
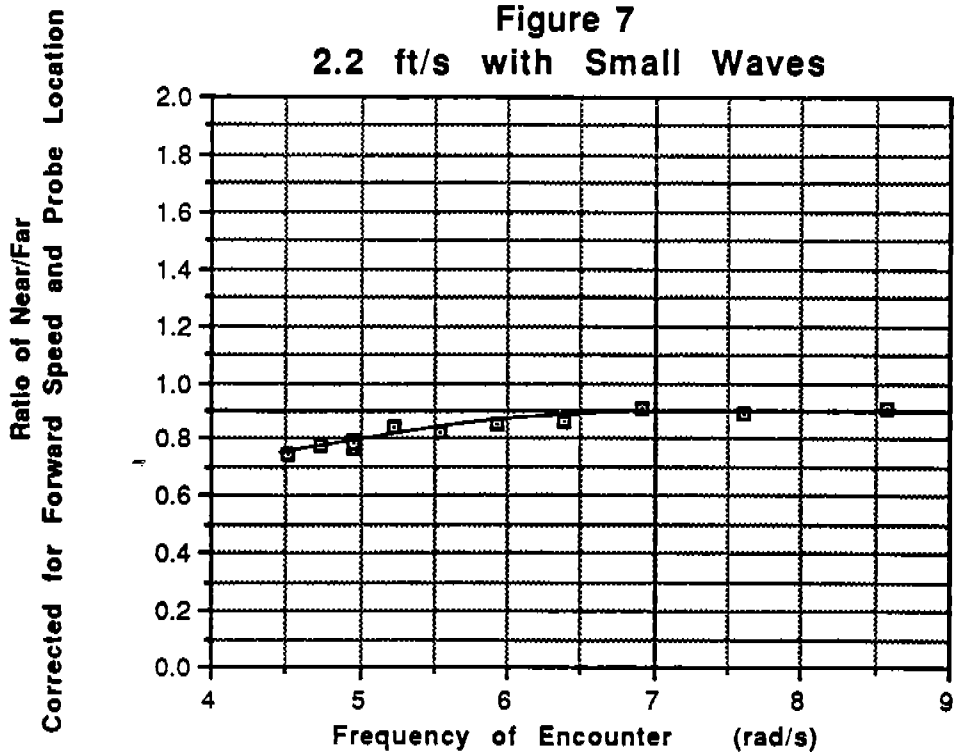
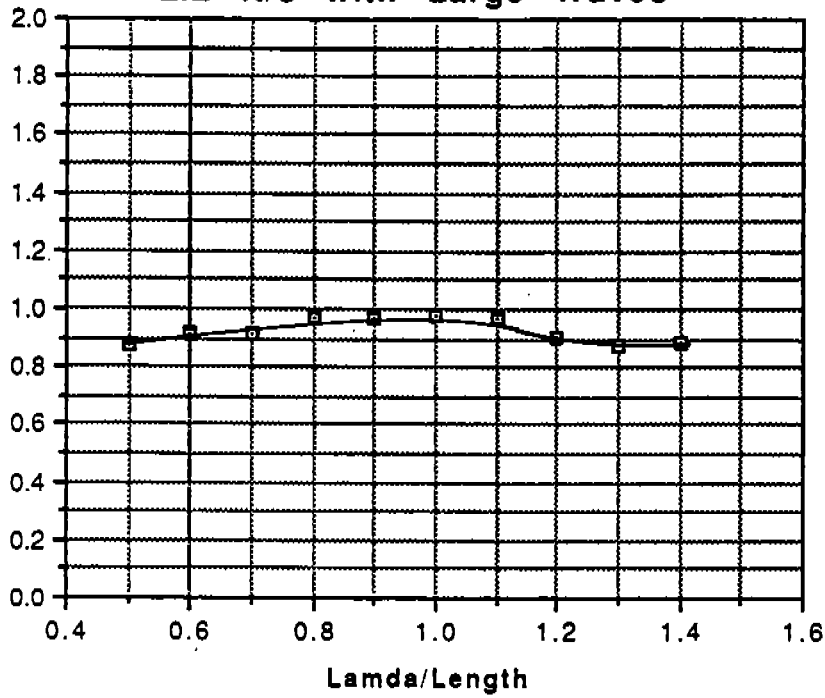


**Figure 7**  
**2.2 ft/s with Small Waves**



Ratio of Near/Far  
Corrected for Forward Speed and Probe Location

Figure 8  
2.2 ft/s with Large Waves



Ratio of Near/Far  
Corrected for Forward Speed and Probe Location

Figure 9  
2.2 ft/s with Large Waves

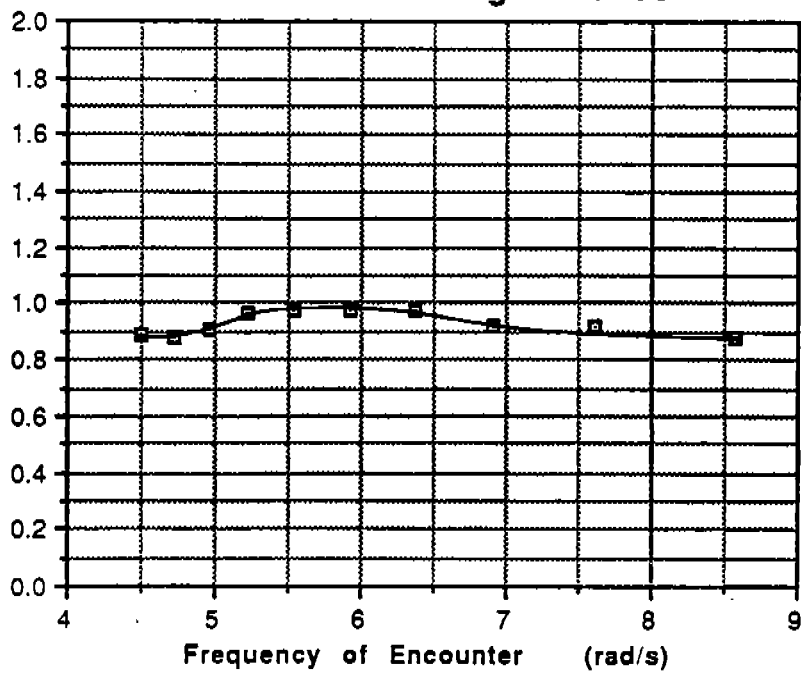


Figure 10  
3.965 ft/s with Small Waves

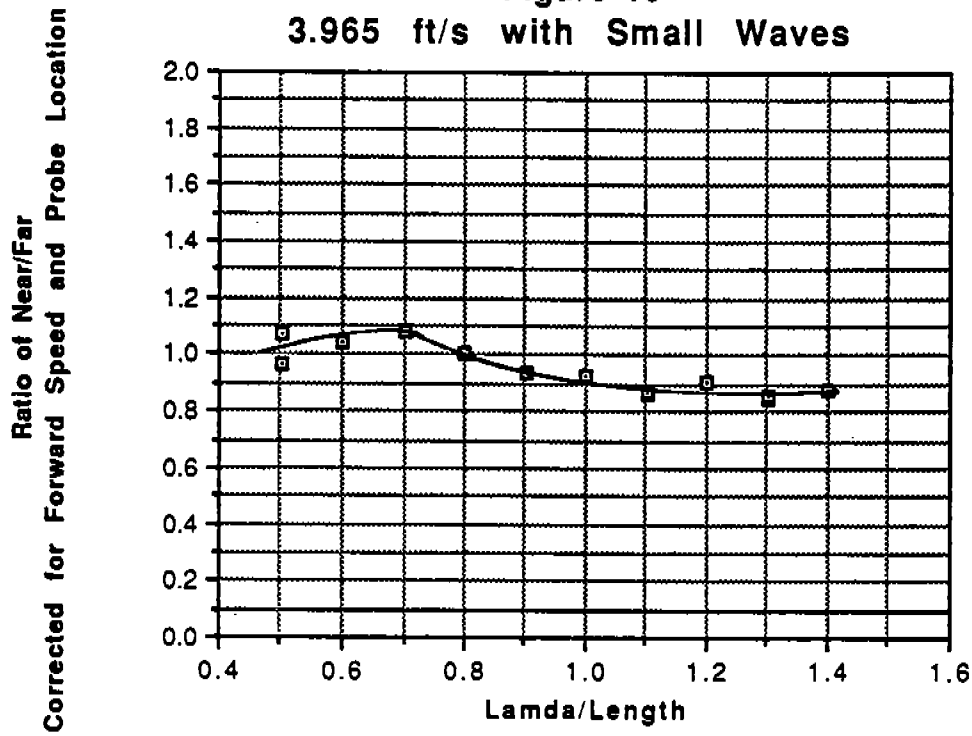
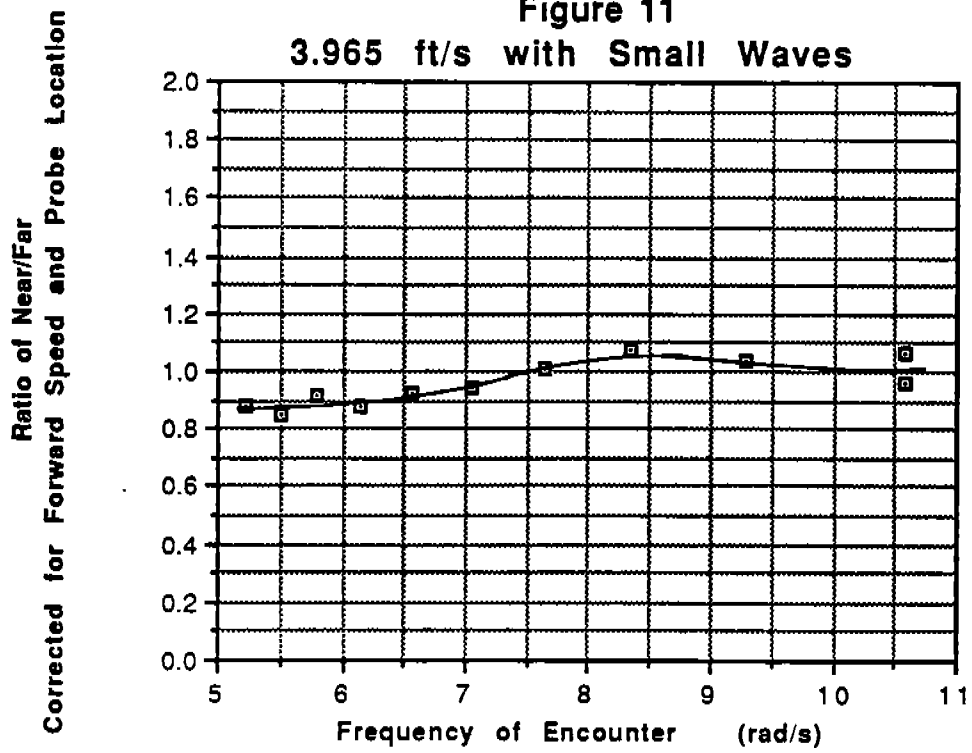
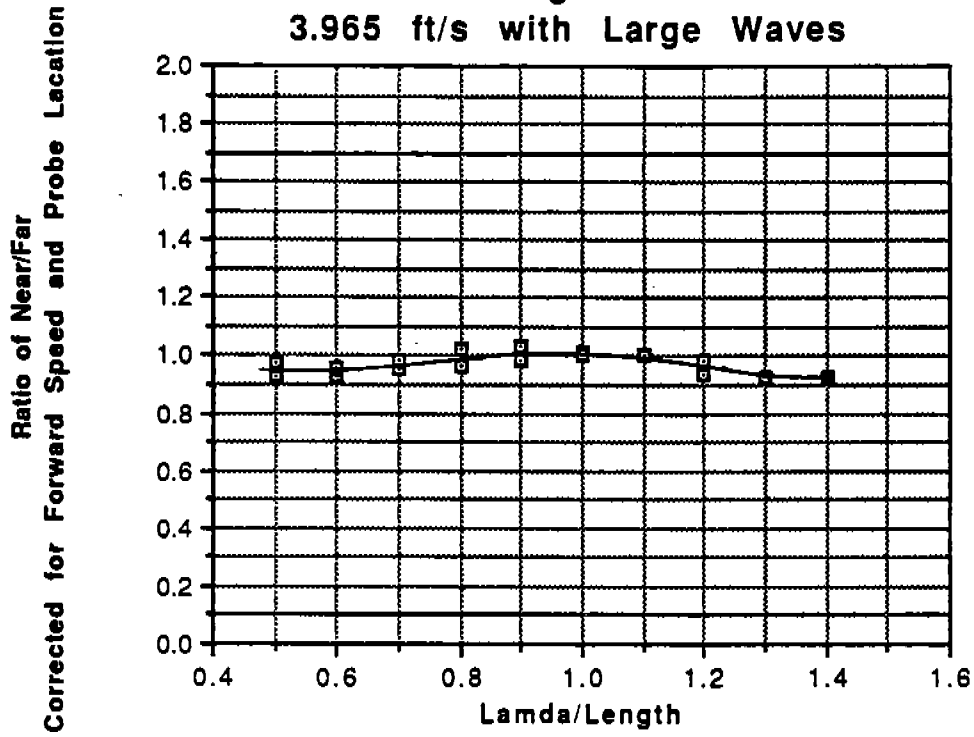


Figure 11  
3.965 ft/s with Small Waves



**Figure 12**  
**3.965 ft/s with Large Waves**



**Figure 13**  
**3.965 ft/s with Large Waves**

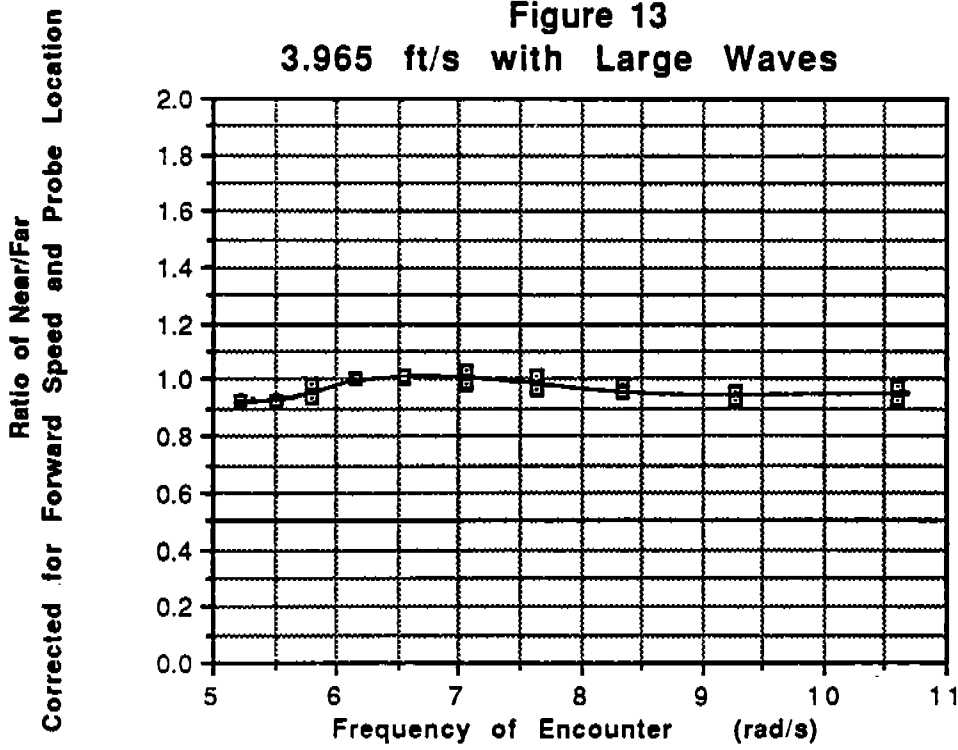
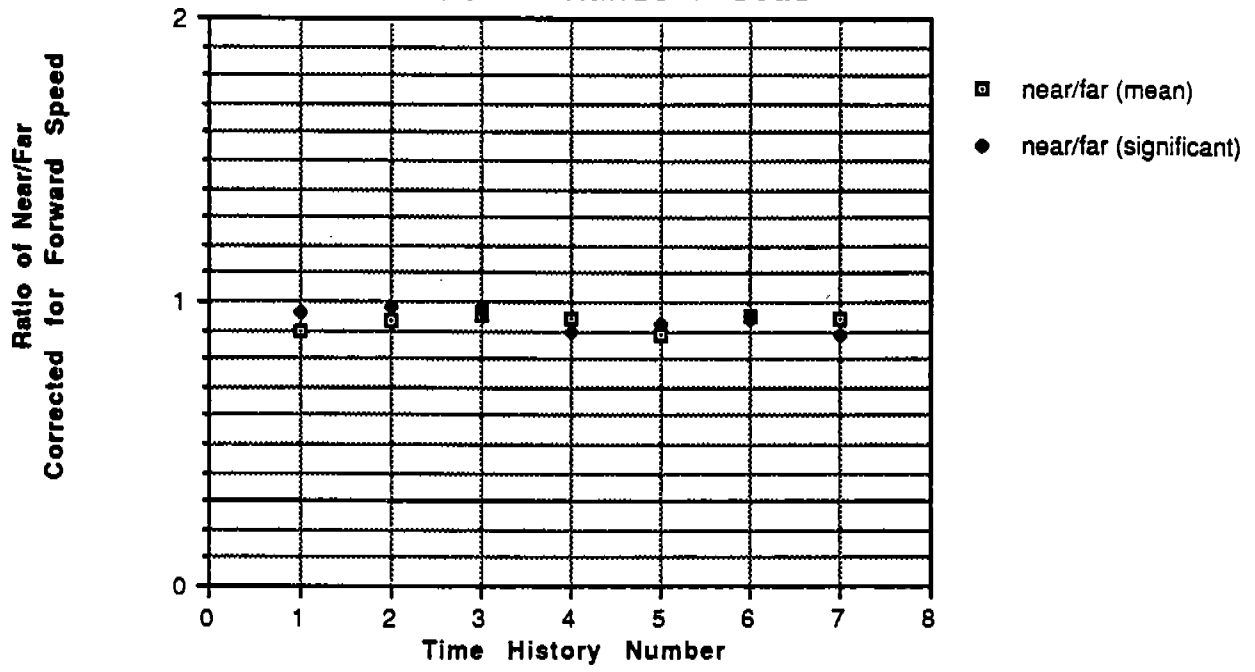


Figure 14  
3.965 ft/s in Random Seas



COMMITTEE ON MARINE STRUCTURES

Commission on Engineering and Technical Systems

National Academy of Sciences - National Research Council

The COMMITTEE ON MARINE STRUCTURES has technical cognizance over the interagency Ship Structure Committee's research program.

Stanley G. Stiansen (Chairman), Riverhead, NY  
Mark Y. Berman, Amoco Production Company, Tulsa, OK  
Peter A. Gale, Webb Institute of Naval Architecture, Glen Cove, NY  
Rolf D. Glasfeld, General Dynamics Corporation, Groton, CT  
William H. Hartt, Florida Atlantic University, Boca Raton, FL  
Paul H. Wirsching, University of Arizona, Tucson, AZ  
Alexander B. Stavovy, National Research Council, Washington, DC  
Michael K. Parmelee, Secretary, Ship Structure Committee,  
Washington, DC

LOADS WORK GROUP

Paul H. Wirsching (Chairman), University of Arizona, Tucson, AZ  
Subrata K. Chakrabarti, Chicago Bridge and Iron Company, Plainfield, IL  
Keith D. Hjelmstad, University of Illinois, Urbana, IL  
Hsien Yun Jan, Martech Incorporated, Neshanic Station, NJ  
Jack Y. K. Lou, Texas A & M University, College Station, TX  
Naresh Maniar, M. Rosenblatt & Son, Incorporated, New York, NY  
Solomon C. S. Yim, Oregon State University, Corvallis, OR

MATERIALS WORK GROUP

William H. Hartt (Chairman), Florida Atlantic University, Boca Raton, FL  
Fereshteh Ebrahimi, University of Florida, Gainesville, FL  
Santiago Ibarra, Jr., Amoco Corporation, Naperville, IL  
Paul A. Lagace, Massachusetts Institute of Technology, Cambridge, MA  
John Landes, University of Tennessee, Knoxville, TN  
Mamdouh M. Salama, Conoco Incorporated, Ponca City, OK  
James M. Sawhill, Jr., Newport News Shipbuilding, Newport News, VA

SHIP STRUCTURE COMMITTEE PUBLICATIONS

- SSC-338 Fatigue Prediction Analysis Validation from SL-7 Hatch Corner Strain Data by Jen-Wen Chiou and Yung-Kuang Chen 1985
- SSC-339 Ice Loads and Ship Response to Ice - A Second Season by C. Daley, J. W. St. John, R. Brown, J. Meyer, and I. Glen 1990
- SSC-340 Ice Forces and Ship Response to Ice - Consolidation Report by C. Daley, J. W. St. John, R. Brown, and I. Glen 1990
- SSC-341 Global Ice Forces and Ship Response to Ice by P. Minnick, J. W. St. John, B. Cowper, and M. Edgecomb 1990
- SSC-342 Global Ice Forces and Ship Response to Ice - Analysis of Ice Ramming Forces by Yung-Kuang Chen, Alfred L. Tunik, and Albert P-Y Chen 1990
- SSC-343 Global Ice Forces and Ship Response to Ice - A Second Season by P. Minnick and J. W. St. John 1990
- SSC-346 Fatigue Characterization of Fabricated Ship Details - Phase 2 by K. K. Park and F. V. Lawrence, Jr. 1988
- SSC-349 Development of a Generalized Onboard Response Monitoring System (Phase I) by F. W. DeBord, Jr. and B. Hennessy 1987
- SSC-350 Ship Vibration Design Guide by Edward F. Noonan 1989
- SSC-351 An Introduction to Structural Reliability Theory by Alaa E. Mansour 1990
- SSC-355 Relation of Inspection Findings to Fatigue Reliability by M. Shinozuka 1989
- SSC-356 Fatigue Performance Under Multiaxial Load by Karl A. Stambaugh, Paul R. Van Mater, Jr., and William H. Munse 1990
- SSC-358 Structural Behavior After Fatigue by Brian N. Leis 1987
- SSC-360 Use of Fiber Reinforced Plastic in Marine Structures by Eric Greene 1990
- SSC-361 Hull Strapping of Ships by Nedret S. Basar and Roderick B. Hulla 1990
- None Ship Structure Committee Publications - A Special Bibliography 1983